REPORT DOCUMENTATION PAGE

AFRL-SR-AR-TR-03-0105

20030508 100

1. REPORT DATE (DD-MM-YYYY)	2. REPORT TYPE	(From - To)
03-28-03	Final Report	7-25-98 to 12-21-03

4. TITLE AND SUBTITLE
Pulsed Laser Deposition of Carbide Coatings for Rolling and Sliding Contact Applications

5a. CONTRACT NUMBER

5b. GRANT NUMBER
F499620-98-1-0499

5c. PROGRAM ELEMENT NUMBI

6. AUTHOR(S)
James E. Krzanowski, Todd S. Gross, Carmela C. Amato-Wierda and Olof Echt

5d. PROJECT NUMBER

5e. TASK NUMBER

5f. WORK UNIT NUMBER

7. PERFORMING ORGANIZATION NAME(S) AND ADDRESS(ES)

University of New Hampshire
Durham, NH 03824

Systran, Inc.
4126 Linden Ave.
Dayton, OH 45432

8. PERFORMING ORGANIZATIO NUMBER

9. SPONSORING / MONITORING AGENCY NAME(S) AND ADDRESS(ES)
AF Office of Scientific Res.
AFOSR/NL
4015 Wilson Blvd., Rm 713
Arlington, VA 22203-1954

10. SPONSOR/MONITOR'S ACRONYM(S)
AFOSR

11. SPONSOR/MONITOR'S REPORT NUMBER(S)

12. DISTRIBUTION / AVAILABILITY STATEMENT
Distribution Statement A: Approved for public release; distribution is unlimited

13. SUPPLEMENTARY NOTES
LtCol Paul C. Trulove, Ph. D., Program Manager, Surface and Interfacial Science

14. ABSTRACT

In this research program several new concepts were investigated for improving the mechanical and tribological properties of coatings intended for applications subject to repeated rolling and sliding contacts. The investigation of these new concepts was carried out within four primary thrust areas: 1) alloying carbides to enhance coating hardness; 2) depositing composite carbide-silver coatings for reduced friction in vacuum environments; 3) evaluating carbide-metal nacreous structures for improving coating toughness; and 4) CVD methods for nano-structured composite carbide coatings. Major findings can be summarized as follows: In carbide coatings, it was found that additions of silicon can provide a useful and practical route towards improving coating hardness. This is due to the disordering effect of silicon when present in transition metal carbides. Investigation of composite carbide-silver coatings demonstrated their potential as low-friction coatings in vacuum environments. In these coatings, phase separation between carbide and silver allows the silver to act as a solid lubricant, while the carbide matrix improves wear resistance over silver alone. The research on carbide-metal nacreous structured films demonstrated the potential for these structures to provide improved coating toughness. These results were obtained with a newly developed reciprocating nano-scratch test method that allows testing of a coating independent of its adhesion to the substrate. Research on chemical vapor deposition (CVD) of TiC-based coatings evaluated three areas of thermal CVD were investigated and one plasma method.

15. SUBJECT TERMS
Hard Coatings; Thin Films; Wear, Tribology; Carbides

16. SECURITY CLASSIFICATION OF: Unclassified			17. LIMITATION OF ABSTRACT	18. NUMBER OF PAGES	19a. NAME OF RESPONSIBLE PERSON
a. REPORT	b. ABSTRACT	c. THIS PAGE	UL		James E. Krzanowski
					19b. TELEPHONE NUMBER (Include area code) 603-862-2315

Final Report: Pulsed Laser Deposition of Carbide Coatings for Rolling and Sliding Applications, AFOSR Grant No. F49620-98-1-0499

Table of Contents

Pulsed Laser Deposition of Carbide Coatings for Rolling and Sliding Contact Applications

AFOSR Grant No. F49620-98-1-0499

I. Executive Summary

In this research program we investigated several new concepts for improving the mechanical and tribological properties of coatings intended for applications subject to repeated rolling and sliding contacts. The investigation of these new concepts was carried out within four primary thrust areas: 1) alloying carbides to enhance coating hardness; 2) depositing composite carbide-silver coatings for reduced friction in vacuum environments; 3) evaluating carbide-metal nacreous structures for improving coating toughness; and 4) CVD methods for nano-structured composite carbide coatings.

Both mixed transition metal and metal-metalloid carbide coatings were investigated as routes to enhancing the hardness of carbide coatings. Coatings within the Ti-Mo-C and Ti-W-C systems were deposited by sputter deposition and their structural, tribological and mechanical properties were evaluated. Structural characterization of these coatings revealed that mostly solid solutions had formed, and little property enhancement was found. However, systems with silicon additions to transition metal carbides, namely Ti-Si-C and W-Si-C, showed that significant hardness enhancements can be realized over transition metal carbides. While the hardness levels themselves were not exceptional (up to ~30 GPa), it was found that the compositional modification of adding Si can substitute for the higher temperatures or substrate bias levels often needed to obtain optimal hardness levels, a result which is of significant practical utility. The mechanisms by which Si enhances hardness levels in transition metal carbide coatings was also investigated, and it was found that microstructural modifications at the nanometers scale were responsible the observed effects.

The research on carbide-silver composite coatings led to several important findings. First, when a carbide material, such as TiC, is co-deposited with silver (by either sputtering or pulsed-laser deposition), phase separation is always observed and separate carbide and silver phases form. This is critical, because it allows the silver in the coating to act as a solid lubricant. Second, the tribological evaluation the coatings tested in vacuum environments showed that a significant reduction in friction can be obtained in comparison to coatings of carbides alone. There is an optimal amount of silver that minimizes friction and wear, typically in the 15-25% range. Our studies showed that the microstructures formed in these coatings are dependent not only on typical deposition parameters such as temperature and substrate bias, but also on the actual amount of silver in the coatings. This was due to a concentration-dependent diffusivity effect. Overall, results obtained here indicate that carbide-silver composite coatings are promising candidates for applications requiring reduced friction and wear in vacuum environments.

In the third thrust area, research was conducted to evaluate whether increasing film toughness could enhance the wear resistance of TiC-based films. Toughness enhancement was to be achieved by creating TiC-X multilayer films where the X represents a metal layer. Numerous methods for measuring film toughness were examined. A reciprocating nanoscratch technique was also developed as our primary method to evaluate the wear resistance of the film independently of adhesion to the substrate. We also used standard pin-on-disk wear tests performed at the Air Force Materials Lab for selected films. After investigating numerous methods for fabricating test specimens, the method of sputter deposition was selected and Cr was chosen for the interlayer metal. The results showed that a number of the deposited films had higher nanoscratch resistance than monolithic TiC films as determined from the rate of penetration for reciprocating scratching. The films that had the highest nanoscratch resistance were comprised of 160 nm thick TiC layers with thin (5-10 nm) Cr interlayers. In summary, we have shown that the use of thin (<10 mm) interlayers of Cr can significantly improve the wear resistance compared to monolithic TiC. Further research must performed before we can state that this is a practical approach that will provide a significant enough improvement to justify the additional complication of multilayer deposition.

In the chemical vapor deposition (CVD) research thrust, three areas of thermal CVD were investigated and one plasma method was explored. Unlike sputtering methods or PLD where the process starts with purified materials and delivery of the material and subsequent properties are of primary interest, in CVD the first step is to develop a chemical system that will produce the desired material. Reaction conditions can then be varied to develop an understanding of the products and properties that result. The first area of investigation was a thermal CVD method to produce hard titanium carbide coatings by CVD. A series of studies were carried out to produce films of the type Ti-M-Y (M=W; Y=C, N). Atomic layer deposition (a variation of the conventional CVD method) with an organometallic precursor was used to deposit TiC and TiN films. Finally plasma studies were performed to explore the reactor species present during the production of hard films in a parallel plate plasma reactor.

The results obtained in our program have been widely disseminated to the scientific community. Thus far we have published 10 peer-reviewed journal publications, and 11 conference proceeding publications, with one journal publication in review and several in preparation. In addition, there were 23 presentations at conferences, and four graduate dissertations. The participants of the program included 3 post-doctoral associates and 5 graduate students.

II. Description of Research Accomplishments

The details of the research accomplishments generated in this program are described in this section. Four main areas of research are described: 1) Nano-structured hard coatings; 2) Solid lubricant composite coatings; 3) Mechanical properties of multilayers; and 4) CVD of composite carbide coatings.

II.1. Understanding the Effects of Nano-structure on the Mechanical and Tribological Properties of Composite Carbide Coatings

Hard coatings have found widespread use in applications requiring improved wear resistance, lower friction and high hardness. These applications include tool bits, bearings, gears, and a host of specialized mechanical components. The successful application of these coatings has driven research and development on a new class of "super-hard" coatings that derive their exceptional properties from the nano-scale microstructure created during coating deposition. However, there is much controversy over to what extent the super-hardness exhibited in these coatings can be attributed to the nanoscale structure, vs. attributing it to high residual stresses, chemical bonding effects, deposition artifacts, or simply incorrect hardness measurement methods. Furthermore, the extent to which the performance of a coating in a wear-intensive application can be related to hardness is another critical issue. In this component of the hard coatings research program, we have focused on understanding the relationships between coating microstructure and mechanical and tribological properties in carbide-based coating materials.

The first series of coatings that we examined were mixtures of transition metal carbides[1]. For these experiments, Ti-Mo-C and Ti-W-C films were deposited by co-sputtering from carbide targets in order to examine phase formation, microstructure and mechanical properties. A series of Ti-Mo-C films were deposited with compositions ranging from TiC to Mo_2C. XRD analysis showed that multiphase Ti-Mo-C films, containing the (Ti,Mo)C, Mo_2C and Mo_3C_2 phases were only obtained in highly Mo-rich films. TEM analysis showed a higher defect content in single-phase alloy Ti-Mo-C films in comparison to TiC alone. The hardness for most Ti-Mo-C films was in the range of 8-10 GPa, but even lower values were obtained in the multiphase films. Ti-W-C films deposited by co-sputtering of TiC and WC formed only (Ti,W)C solid solutions. XPS analysis of peak positions showed that the W $4f_{7/2}$ binding energy decreased with increasing the W content. The hardness of most of the Ti-W-C coatings was in the range of 15-17 GPa, however, a sample with 40% W had a hardness of 29 GPa. TEM analysis of this sample revealed an extremely small grain size (~ 5 nm) and a higher film density. The high hardness of this specimen is attributed to Hall-Petch strengthening. Therefore, while most films did not exhibit a superhardness effect, the sample with 40% W, a

[1] S.H. Koutzaki, J.E. Krzanowski, and J.J. Nainaparampril, "Phase Formation and Microstructure in Sputter-Deposited Ti-Mo-C and Ti-W-C Thin Films," Met. and Mat. Trans. A., v. 33A, pp. 1579-1588 (2002).

hardness of 29 GPa and a grain size of 5 nm did lend credence to the idea that nano-structured films could exhibit elevated hardness levels.

One method of achieving a nano-structured grain size is to force co-deposition of insoluble compounds. In the TiC-SiC system, TiC and SiC are insoluble due to the nature of bonding in each of these compounds: in TiC, carbon atoms occupy the octahedral sites and bonding is mostly metallic, whereas in SiC carbon atoms are tetrahedrally bonded and bonding is mostly covalent. We therefore proceeded to conduct and in-depth investigation of Ti-Si-C films[2,3]. First attempts were made by depositing films by rf-cosputtering. We examined Ti-Si-C films with a nominal $(Ti_{1-x}Si_x)C$ stoichiometry and with $x \leq 0.31$. It was found that the nano-indentation hardness increased with Si content, and the maximum hardness achieved was nearly twice that of sputter-deposited TiC. We further analyzed these films using high-resolution TEM, XPS and X-ray diffraction. Since cubic SiC has an X-ray pattern almost identical to that of TiC, the extent of phase separation could not be determined by that method. However, XRD did demonstrate a general disordering of the films with increasing SiC content. In addition, a mottled structure was observed in high-resolution TEM images of the Si-containing films, confirming microstructural effects due to the Si additions.

Further studies were conducted where TiC and Ti-Si-C films were deposited by pulsed laser deposition (PLD)[4]. Conditions for these experiments included substrate temperatures ranging from room temperature to 600°C. X-ray diffraction, X-ray photoelectron spectroscopy, and electron microscopy were employed for structural and compositional evaluation of the films, and nano-indentation hardness testing and pin-on-disc wear tests were used to evaluate the mechanical and tribological properties. All the TiC films were highly crystalline except the one deposited at room temperature, whereas for the Ti-Si-C films the degree of crystallinity increased with temperature, ranging from amorphous for the room temperature deposit to about 50% crystalline at 600°C. The hardness of the TiC films was relatively constant with deposition temperature at about 25 GPa, whereas the hardness of the Ti-Si-C films increased with deposition temperature from 11 to 32 GPa. The temperature dependence of the hardness is attributed to the degree of crystallinity and the extent of phase separation in the Ti-Si-C films. The wear test data showed good results for all films, up to the tested limit of 10,000 cycles at 1 N load.

While the Ti-Si-C films deposited by sputtering and PLD showed promising hardness levels, the friction coefficients for these films were only similar to TiC or SiC alone. It was believed that a small fraction of excess carbon (beyond the stoichiometric level) could promote lower friction coefficients. In addition, experiments

---

[2] J.E. Krzanowski and S.H. Koutzaki, "Mechanical Properties of Sputter-Deposited Ti-Si-C Films," J. American Ceramic Society, v. 84 pp. 672-674 (2001).

[3] S.H. Koutzaki, J.E. Krzanowski, and J.J. Nainaparampril, "Structure and Mechanical Properties of Ti-Si-C Coatings Deposited by Magnetron Sputter Deposition," J. Vac. Sci. Tech. A, v. 19, pp. 1912-1918 (2001).

[4] A.R. Phani and J.E. Krzanowski, "Structure and Mechanical Properties of TiC and Ti-Si-C Films Deposited by Pulsed Laser Deposition," J. Vac. Sci. Tech. A, v. 19, pp. 2252-2258 (2001).

in the literature pointed to experiments where an excess of an amorphous phase (10-20%) resulted in a dramatic increase in hardness and toughness. Therefore, we sought to deposit TiC and Ti-Si-C films with super-stoichiometric levels of carbon[5]. The most reasonable technique for these experiments was the hybrid sputtering/PLD method. The magnetron sputtering – pulsed laser deposition (MSPLD) method was used to deposit Ti-C and Ti-Si-C films with both sub- and super-stoichiometric levels of carbon. The structure and composition of the films were analyzed by transmission electron microscopy, x-ray diffraction and x-ray photo-electron spectroscopy. The mechanical properties were determined by nano-indentation and the tribological properties by pin-on-disc testing. Films deposited with sub- and near stoichiometric levels of carbon had good crystallinity and strong (111) texture. However, films deposited under similar conditions but with a substrate bias resulted in super-stoichiometric carbon levels and nano-crystalline or near-amorphous structures. The hardness of these super-stoichiometric films was generally lower than the sub-stoichiometric films, but they also exhibited significantly better wear life. The laser power used in the MSPLD process was also found to influence hardness, where increased laser power led to higher hardness levels. Using these results, an effort was made to deposit a film with optimal mechanical and tribological properties by depositing a Ti_4Si-C film with -150V bias, maximum laser power (700 mJ/pulse) at a temperature of 400°C. This film contained 55% carbon, had a hardness of 28 GPa, and ran for greater than 10^6 cycles on the pin-on-disc test.

Success with the Ti-Si-C system led us to examine other ternary carbide systems containing SiC. We did a series of experiments on Hf-Si-C films deposited by co-sputtering[6]. The difficulty with these films was that the Si appeared to be preferentially etched away during deposition, leaving little Si in the films. Because of this problem, we turned instead to the W-Si-C system. A study was conducted in which we investigated the mechanical properties of WC-SiC thin films deposited by dual RF magnetron sputtering[7]. The films were characterized by x-ray photoelectron spectroscopy (XPS), x-ray diffraction (XRD) and transmission electron microscopy (TEM) to evaluate the details of the microstructure and degree of amorphization. In these experiments, we examined the entire range of WC to SiC compositions. The results indicated that small additions of SiC (< 25%) significantly increased the hardness compared to a pure WC film, but higher SiC contents did not strongly affect hardness. XRD studies show the SiC had a disordering effect. TEM results showed that WC films had coarse porous structure, but films with a low silicon carbide content (~10 to 25 at. %) had a denser nanocrystalline structure. Samples with greater than 25% SiC were amorphous. The initial hardness increase at lower SiC contents correlated well with the observed densification, but the transition to an amorphous structure did not strongly affect

---

[5] A.R. Phani, J.J. Nainaparampil, and J.E. Krzanowski, "The Effects of Substrate Temperature and Bias on the Structural, Mechanical and Tribological Properties of TiC Films Deposited by Magnetron Sputtering Pulsed Laser Deposition," in Surface Engineering 2001: Fundamentals and Applications, Materials Research Society Symposium Proceedings, vol. 697, pp. 409-424 (2002).

[6] J.E. Krzanowski, J.L. Endrino and S.H. Koutzaki, "Determining the Limit of Hardness in Ternary Carbide Thin Films," in Surface Engineering 2001: Fundamentals and Applications, Materials Research Society Symposium Proceedings, vol. 697, pp. 9-14 (2002).

[7] Jose L. Endrino and J.E. Krzanowski, "Nanostructure and Mechanical Properties of W-Si-C Thin Films," Journal of Materials Research, v. 17, pp. 3163-3167 (2002).

hardness. These results highlight a very important point about studying nanostructure effects. Namely, the variation in structure size (micron to nanometer) is often accompanied by changes in other film properties, and those properties can also effect hardness. In the present case, the film density changed as we altered the grain size within the films. Another important result from this study was that Si additions brought about this densification in the films. This result could have important consequences in the search for improved coatings for tribological applications.

II.2. Coatings for Reduced Friction in Vacuum Environments

One type of coating application that is particularly challenging is that of lubrication in a vacuum environment. There are numerous types of solid lubricant coatings available. Carbon films can be lubricious provided water vapor is present, which prohibits its use in vacuum. MoS_2 is a good solid lubricant for vacuum environments, but has limited use in air. Soft metals such as gold, silver and lead are often used as solid lubricant materials. However, when used as coatings, their wear life can be limited. In our work, we have examined the concept of using a composite coating consisting of a hard phase (for wear) and a soft metal (for lubrication). The hard phases we have examined are WC, HfC, SiC and TiC, whereas the soft lubricant used was silver.

The first series of experiments was conducted by sputtering films of TiC or WC along with Ag[8]. Our first objective was to determine whether phase separation would occur in the deposited film, giving us the desired phases of a carbide along with Ag. Thin films of WC-Ag and TiC-Ag were deposited by magnetron sputtering. X-ray diffraction was used to determine structural properties, and energy dispersive x-ray analysis was used to determine the relative atomic content of silver in the films. Pin on disk friction tests were performed to obtain the coefficient of friction in vacuum. The deposited films showed a structure containing separate carbide/silver phases, as was desired for providing both high wear resistance and low friction. Pin-on-disk tribological tests were also conducted in vacuum environments. The tribological test results show a significant decrease in the friction coefficient for both TiC-Ag and WC-Ag, to a minimum value of 0.2, with increasing silver content. This first study therefore validated the concept of carbide/silver thin films and their application as tribological coatings in vacuum environments.

After conducting this study, it was recognized the magnetron sputtering-pulsed laser deposition method could be a suitable method for depositing carbide-silver coatings. Therefore, composite titanium carbide-silver films were co-deposited by magnetron sputtering of Ag and pulsed laser deposition (MSPLD) of TiC[9]. The deposited films

---

[8] J. Endrino, J.J. Nainaparampril and J.E. Krzanowski, "Magnetron Sputter Deposition of WC-Ag and TiC-Ag Coatings and their Frictional Properties in Vacuum Environments," Scripta Mat., v 74, pp. 613-618 (2002).

[9] Jose L. Endrino, Jose J. Nainaprampil, and James E. Krzanowski, "Microstructure and Vacuum Tribology Studies of TiC-Ag Composite Coatings Deposited by Pulsed Laser Deposition," Surface Coatings and Technology, vol. 157, p. 95-101 (2002)

were characterized by x-ray diffraction (XRD), transmission electron microscopy (TEM) and x-ray photoelectron spectroscopy (XPS). The silver content in the films ranged from 6 to 46 atomic %. Structural characterization of the films revealed that Ag had a nano-crystalline structure when dispersed in the film, but larger crystallites of Ag (~50-100 nm) also formed on the surface. Films with higher Ag contents showed evidence of higher diffusion rates, leading to a coarser structure and more surface coverage. Pin-on-disk friction tests were performed under vacuum to observe the friction and wear behavior of these films. Friction was lower with higher Ag content, but the wear was higher; the optimal Ag concentration was found to be 15% where the friction coefficient was 0.2. SEM images from the surface of the films and wear tracks were obtained to understand the morphology of this type of composite ceramic coating, and revealed Ag layers in the wear track elongated in the direction of wear.

Based on these results, we demonstrated the significance of silver as a friction reducing agent in vacuum environments. However, while these coatings performed well in vacuum, we sought to develop a true multifunctional coating that would perform well in both air and vacuum. The concept was therefore to add carbon (as graphite or amorphous carbon) thereby providing lubrication in air. To deposit these films, we used a Ti/Ag alloy target for sputtering and a deposited carbon simultaneously by PLD[10]. Energy disperse spectroscopy (EDS) was used to determine the elemental composition, and x-ray diffraction (XRD) and cross-sectional scanning electron microscopy (XSEM) to examine the structure of the films. Hardness and reduced modulus measurements were acquired using the nano-indentation technique. The pin-on-disk friction test was used to study the friction behavior of the deposited samples in high vacuum and ambient conditions. Variations in the laser energy and the power of the sputtering gun yielded a set of samples with carbon content that ranged from 15.0 to 95.6 percent. The hardest samples with the highest reduced modulus were those with a moderate carbon content and that were shown to form a titanium carbide phase. Tribological results indicated that there is an optimum composition of a TiC/C/Ag coating (~25 at.% carbon) at which a good friction coefficient was obtained in both air (0.23) and vacuum (0.41), and did not fail within the 10,000 cycles of the pin-on-disk test. An important result from this study was that some crystallinity in the carbide phase is necessary to maintain good hardness and wear resistance. The second conclusion was that the excess carbon must be kept to a minimum; otherwise frictional behavior in vacuum will be poor, even if silver is present.

Additional work was carried out examining coatings of Ag and other carbides besides TiC, namely SiC and HfC. Microstructurally, these two carbides behaved quite differently. For HfC-Ag, the silver phase form large agglomerates within the film, while in the SiC-Ag, the silver formed small particles. We then examined films of HfC and SiC lightly decorated with silver, and examination of the surface in the SEM showed the islands of Ag were much finer for the SiC than the HfC. This indicated that the silver has a much higher surface diffusivity on HfC in comparison to SiC, which is then reflected in the structures of the composite films. Vacuum tribology studies showed that the SiC-Ag

[10] J.L. Endrino, J.J. Nainaparampil, and J.E. Krzanowski, "Structural and Tribological Properties of TiC/C/Ag Coatings in Vacuum and Ambient Environments," in Surface Engineering 2001: Fundamentals and Applications, Materials Research Society Symposium Proceedings, vol. 697, pp. 273-278 (2002).

films performed slightly better, with a minimum friction coefficient of 0.15 at 36% Ag, whereas for HfC-Ag the minimum was 0.2 at 24% Ag.

Additional research on coatings for low-friction applications was conducted in the area of MoS_2-metal coatings. MoS_2 coatings work well in vacuum but not in humid environments. The addition of a metal to the coating has been reported in the literature to improve the performance of MoS_2 in air, which could be important for dry machining applications. In our study, we examined multilayers of MoS_2 with Ti, Cr, C and TiC[11]. These films were deposited by PLD as sequential alternating layers. Examination of the films by XRD showed that for the MoS_2-Ti, Cr and TiC films, multilayer films did not form, indicating complete interdiffusion of the layers. However, multilayers did form in MoS_2-C films. The films were tested in air (45% R/H) using a pin-on-disk test. We found that, in comparison to MoS_2 alone, the films with added Cr, Ti and TiC all performed dramatically better, with friction coefficients as low as 0.15. In a second study, films of MoS_2-Al were examined. Again, the performance of the films in air was significantly improved by the addition of Al. Therefore, while metal additives to MoS_2 can significantly improve the performance of the coatings in air, and it seems to be almost independent of the metal added. There are many unanswered questions still remaining in this area, such as where are the metal atoms within the MoS_2 structure, and what are the mechanisms by which the metal additives provide the observed performance enhancements.

II.3. Mechanical Properties of Multilayer Coatings

The focus of this portion of the project was to evaluate whether the wear resistance of TiC-based films could be enhanced by increasing the film toughness. Toughness enhancement was to be achieved by creating TiC-X multilayer films where the X represents a metal layer. The expected mechanisms of toughness enhancement were:

- Interruption of the columnar microstructure of monolithic TiC films eliminates an easy crack path.
- Interruption of the columnar microstructure should result in refinement of the TiC microstructure within the TiC layers.
- The metal interlayer should blunt cracks propagating from the surface to the interface.
- Failure would have to be initiated at each TiC layer thereby increasing the work of failure.

We evaluated the several methods of measuring film toughness so that we could show whether increased film toughness results in enhanced wear resistance:

- Cube corner diamond nanoindentation normal to the film.
- Cube corner diamond nanoindentation of film cross sections.

[11] A.R. Phani, J.J. Nainaparampil, and J.E. Krzanowski, "Structural and Tribological Properties of Molybdenum Disulfide/ Metal Multilayered Films Deposited by Pulsed Laser Deposition," accepted for the 2002 MRS Fall Meeting Conference Proceedings.

- Microindentation normal to the film on brittle and ductile substrates.
- Measurement of crack density under ball indents.

While none of these methods were able to produce quantitative estimates of film toughness for films in the 1 micrometer thickness range, we developed a reciprocating nanoscratch technique as our primary method to evaluate the wear resistance of the film independently of adhesion to the substrate. While this technique could not generate a single number to characterize toughness or wear resistance of the film, it did provide quantitative information to compare the performance of different films. We also used standard pin-on-disk wear tests performed at the Air Force Materials Lab for selected films.

We chose Cr for the metal interlayer for the following reasons:

- The BCC crystal structure of Cr is different from NaCl (FCC) TiC. This was to ensure incoherent interfaces and interrupt columnar grain growth.
- The coefficient of thermal expansion (CTE) of TiC and Cr are approximately the same (6.9 ppm/K vs 6.2 ppm/K) to minimize thermal mismatch strains.
- Ti is a stronger carbide former than Cr, so the interface would remain distinct and the Cr would not convert to carbide.

We chose to consider different hard layer to soft layer thickness ratios ranging from a TiC:Cr ratio of 0.5 to 0.93 (see Table 1). The high TiC:Cr ratio structures were chosen to mimic organic nacreous structures. All results were compared to monolithic TiC films.

Table 1

TiC Layer (nm)	Cr Layer (nm)	TiC Volume Fraction	Overall Thickness (nm)	Hardness (GPa)	
160	40	0.79	1210	23.2	
160	20	0.86	1110	30.2	
160	*10*	*0.91*	*1060*	*29.7*	*
160	*5*	*0.93*	*1035*	*32.0*	*
91	91	0.52	1051	15.7	
80	5	0.90	980	26.5	
48	48	0.50	1058	14.1	
40	*10*	*0.77*	*1090*	*21.5*	*
40	5	0.85	990	23.7	
24	*24*	*0.49*	*1034*	*18.3*	*
1000	0	1.0	1050	19.0	

The films indicated by an asterisk in Table 1 had higher nanoscratch resistance than monolithic TiC films as determined from the rate of penetration for reciprocating

scratching. The films that had the highest nanoscratch resistance were comprised of 160 nm thick TiC layers with thin (5-10 nm) Cr interlayers.

The nanoscratch resistance decreased with decreasing TiC layer thickness for the films with the 5 nm interlayers. However, the nanoscratch resistance was approximately the same for two films with 10 nm interlayer thickness at the extremes of TiC thickness (160 nm and 40 nm).

Films that had interlayer thicknesses of 20 nm or greater did not perform well at all with the exception of the film with 24 nm Ti C and Cr layers which exhibited higher nanoscratch resistance than monolithic TiC.

We observed fracture surfaces of film cross sections. The presence of the metal interlayers did cause crack deflection in some of the films but not all of them. The metal interlayer did not prevent a columnar character to the fracture and from this we conclude that it did not interrupt the columnar microstructure. It is conceivable that a metal interlayer with a weaker interface would cause more crack deflection.

We have shown that the use of thin (<10 mm) interlayers of Cr can significantly improve the wear resistance compared to monolithic TiC. Further research must performed before we can state that this is a practical approach that will provide a significant enough improvement to justify the additional complication of multilayer deposition.

II.4. CVD Methods for Composite Carbide Coatings

In carrying out the chemical vapor deposition (CVD) of TiC-based composite hard coatings, three areas of thermal CVD were investigated and one plasma method was explored. Unlike sputtering methods or PLD where the process starts with purified materials and delivery of the material and subsequent properties are of primary interest, in CVD the first step is to develop a chemical system that will produce the desired material. Reaction conditions can then be varied to develop an understanding of the products and properties that result. The first area of investigation was a thermal CVD method to produce hard titanium carbide coatings by CVD. A series of studies were carried out to produce films of the type Ti-M-Y (M=W; Y=C, N). Atomic layer deposition (a variation of the conventional CVD method) with an organometallic precursor was used to deposit TiC and TiN films. Finally plasma studies were performed to explore the reactor species present during the production of hard films in a parallel plate plasma reactor.

Titanium Carbide generation by factorial design

TiC is frequently deposited by chemical vapor deposition (CVD). The advantages of CVD include high deposition rates, compositional control, and uniform, large-scale depositions. The most extensively studied CVD precursor system for TiC utilizes $TiCl_4$, CH_4, and H_2. A factorial design of experiments was used to study the influence of process variables on the chemical vapor deposition of titanium carbide using $TiCl_4$, CH_4,

H_2, and Ar. Factorial design of experiments is a proven method for simplifying the identification of the most critical processing variables in complex chemical processes. It reduces the number of experiments required and determines the influence of interactions among process variables on the final film properties. A factorial design experiment was created to investigate the process parameter space of the $TiCl_4/CH_4/H_2$ precursor system in terms of: (1) reaction temperature, (2) C:Ti in the reactant gas flow, (3) H:Ti in the reactant gas flow, (4) total reactor pressure, and (5) total mass flow of reactants. The film properties studied were: (1) titanium content, (2) carbon content, (3) deposition rate, (4) crystallite size, (5) preferred orientation, and (6) microstructure. The titanium content in the film was most influenced by the H:Ti ratio and the interaction between C:Ti/total mass flow. Carbon content was most influenced by the interaction between C:Ti/H:Ti/pressure. A five-way interaction between all variables was also found to be highly significant to carbon content. Deposition rate was found to be affected by only two terms, the interaction between temperature/H:Ti/total mass flow and H:Ti/total mass flow. Crystallite size was most influenced by H:Ti ratio in the reactant gas phase. Preferred orientation of the titanium carbide films was most influenced by the interaction of H:Ti/temperature/total mass flow. Microstructure was influenced by temperature, C:Ti in the reactant gas, and the interaction between C:Ti/total mass flow. This factorial design illustrated the importance of studying interactions between process variables in understanding how process parameters affect the chemical vapor deposition of titanium carbide and suggested ways to improve the quality of produced films.

CVD of composite films

The formation of novel hard coatings is of increasing interest in industrial applications in order to respond to the increasing demand for high performance materials. Composite films deposited by chemical vapor deposition (CVD) are a potential way to make thin films with a higher hardness and stability against oxidation at higher temperature. Composite films deposited by chemical vapor deposition (CVD) are a potential way to make thin films with a higher hardness and stability against oxidation at higher temperature. Ti-W-C thin films were deposited on stainless steel substrates (440C) by chemical vapor deposition (CVD) in a horizontal hot-wall reactor from a $TiCl_4$-$W(CO)_6$-CH_4-H_2-Ar gaseous mixture, at 1323 K and at pressures ranging from 0.13 – 20.00 kPa. The structure of the Ti-W-C thin films was characterized using X-ray diffraction (XRD). The lattice constant of the Ti-W-C films shifts from that of TiC to WC_{1-x} with increasing W concentration in the thin films. A morphological analysis was carried out using scanning electron microscopy (SEM). It was found that the surface morphology varied with the W concentration and total flow. Compositional studies and binding characteristics in the Ti-W-C films were investigated by X-ray photoelectron spectroscopy (XPS). The associated hardness measured by nano-indentation ranged from 23 – 32 GPa. The surface morphology depends on the W at.% and the total flow. The presence of a WC phase is indicated in films with higher W contents. According to preliminary results, the hardness of the Ti-W-C films ranges from 28 to 32GPa with increasing W up to 10 at.%.

Chemical vapor deposition (CVD) of tungsten nitride films was investigated on Si wafer substrate. The tungsten nitride films were deposited by CVD using the precursor of

tungsten hexacarbonyl ($W(CO)_6$) with ammonia (NH_3). Film composition, microstructure and growth rates were examined for deposition temperature at 500°C. The film was preliminarily identified as β-W_2N and the deposition rate was about 8 nm/min. The electrical properties of the films depends on the W concentration.

Atomic Layer Deposition of TiC/TiN Films

Atomic layer deposition (ALD) was used to generate a series of TiC and TiN thin films, as well as TiC/TiN multilayers. Atomic layer deposition involves the sequential delivery of reactant precursors to provide surface-limiting reaction conditions. The organometallic precursor, tetrakis-dimethylamidotitanium ($Ti(NMe_2)_4$, was used in an attempt to produce coatings at temperatures as low as 400 °C. However, the hardness of the ALD-produced films never exceeded that of conventional CVD- produced films.

Plasma Enhanced Chemical Vapor Deposition

Molecular beam mass spectrometry (MBMS) has been used to analyze the gas phase of Ar, Ar+$TiCl_4$ and Ar +$TiCl_4$ + NH_3 and CH_4 plasmas. The gas phase composition was analyzed as a function of pressure and plasma power. The results show that an increase in plasma power increases the concentration of dissociated and ionized species in the plasma phase. Higher plasma power increased the intensity of ions from $TiCl_4$ and Ar up until 100 W and then ion intensity starts to level off with increasing rf power. The Ar ion intensity increases with total reactor pressure up to 66.6 Pa and then ion intensity was found to decrease with pressure. In the case of the reaction of $TiCl_4$ and NH_3,a single peak in the mass spectrum at m/e = 80 is observed, possibly corresponding to $Ti(NH_2)_2^+$.

III. Publications

III.1. List of Publications in Peer-Reviewed Journals

1. Jose L. Endrino and J.E. Krzanowski, "Nanostructure and Mechanical Properties of W-Si-C Thin Films," Journal of Materials Research, v. 17, pp. 3163-3167 (2002).

2. Jose L. Endrino, Jose J. Nainaparampil, and James E. Krzanowski, "Microstructure and Vacuum Tribology Studies of TiC-Ag Composite Coatings Deposited by Pulsed Laser Deposition," Surface Coatings and Technology, vol. 157, p. 95-101 (2002)

3. A.R. Phani, J.E. Krzanowski and J.J. Nainaparampril, "Structural and Mechanical Properties of TiC/Ti and TiC/B4C Multilayers Deposited by Pulsed Laser Deposition," J. Mater. Res, v. 17, no. 6, pp. 1390-1398 (2002)

4. J. Endrino, J.J. Nainaparampril and J.E. Krzanowski, "Magnetron Sputter Deposition of WC-Ag and TiC-Ag Coatings and their Frictional Properties in Vacuum Environments," Scripta Mat., v 74, pp. 613-618 (2002).

5. S.H. Koutzaki, J.E. Krzanowski, and J.J. Nainaparampril, "Phase Formation and Microstructure in Sputter-Deposited Ti-Mo-C and Ti-W-C Thin Films," Met. and Mat. Trans. A., v. 33A, pp. 1579-1588 (2002).

6. S.H. Koutzaki, J.E. Krzanowski, and J.J. Nainaparampril, "Structure and Mechanical Properties of Ti-Si-C Coatings Deposited by Magnetron Sputter Deposition," J. Vac. Sci. Tech. A, v. 19, pp. 1912-1918 (2001).

7. A.R. Phani and J.E. Krzanowski, "Structure and Mechanical Properties of TiC and Ti-Si-C Films Deposited by Pulsed Laser Deposition," J. Vac. Sci. Tech. A, v. 19, pp. 2252-2258 (2001).

8. A.R. Phani and J.E. Krzanowski, "Preferential Growth of Ti and TiN Films on Si (111) Deposited by Pulsed Laser Deposition," Applied Surface Science, v. 6917, pp. 1-6 (2001).

9. J.E. Krzanowski and S.H. Koutzaki, "Mechanical Properties of Sputter-Deposited Ti-Si-C Films," J. American Ceramic Society, v. 84 pp. 672-674 (2001).

10. H. X. Ji, C. C. Amato-Wierda, "Chemical Vapor Deposition of Ti-W-C Thin Films," Surface and Coatings and Technologies, v. 148, pp. 262-267 (2001).

III.2. Conference Proceedings

1. J.E. Krzanowski, J.L. Endrino and K. Hirschman, "Novel Composite Coatings with 3D Coating Architectures for Tribological Applications Fabricated using Semiconductor

Patterning Processes," accepted for publication in the Fall 2002 Materials Research Society Conference Proceedings, Surface Engineering Symposium.

2. A.R. Phani, J.E. Krzanowski, and J.J. Nainaparampil, "Structural and Tribological Properties of Molybdenum Disulfide/Metal Multilayer Films Deposited by Pulsed Laser Deposition," accepted for publication in the Fall 2002 Materials Research Society Conference Proceedings, Surface Engineering Symposium.

3. J.L. Endrino, J.J. Nainaparampil, and J.E. Krzanowski, "Microstructure Development and Mechanisms of Lubrication in Magnetron Sputtered HfC-Ag and SiC-Ag Composite Thin Films," accepted for publication in the Fall 2002 Materials Research Society Conference Proceedings, Surface Engineering Symposium.

4. J.E. Krzanowski, J.L. Endrino and S.H. Koutzaki, "Determining the Limit of Hardness in Ternary Carbide Thin Films," in Surface Engineering 2001: Fundamentals and Applications, Materials Research Society Symposium Proceedings, vol. 697, pp. 9-14 (2002).

5. R. Obbard and T.S. Gross, "A Nano-scratch Method for Assessing Wear of Metal Carbide-Metal Nacreous Nanostructures," in Surface Engineering 2001: Fundamentals and Applications, Materials Research Society Symposium Proceedings, vol. 697, pp. 359-365 (2002).

5. J.L. Endrino, J.J. Nainaparampil, and J.E. Krzanowski, "Structural and Tribological Properties of TiC/C/Ag Coatings in Vacuum and Ambient Environments," in Surface Engineering 2001: Fundamentals and Applications, Materials Research Society Symposium Proceedings, vol. 697, pp. 273-278 (2002).

6. A.R. Phani, J.J. Nainaparampil, and J.E. Krzanowski, "The Effects of Substrate Temperature and Bias on the Structural, Mechanical and Tribological Properties of TiC Films Deposited by Magnetron Sputtering Pulsed Laser Deposition," in Surface Engineering 2001: Fundamentals and Applications, Materials Research Society Symposium Proceedings, vol. 697, pp. 409-424 (2002).

7. J.E. Krzanowski, S.H. Koutzaki, J. Nainaparampril, and J.S. Zabinski, "Phase Formation and Mechanical Properties of Multiphase Carbide Coatings," Materials Research Society Symposium Proceedings, vol. 594, pp. 181-6 (2000).

8. Factors Affecting the Amount of Carbon in Titanium Carbide Films Made By CVD. Kathryn E. Versprille, Carmela C. Amato-Wierda, and Philip Ramsey. Proceedings of the Symposium on the 15th International Conference on CVD, Electrochemical Society. In press.

9. Characterization of Ti-W-C Thin Films Deposited by CVD. Hua Xia Ji and Carmela C. Amato-Wierda. Proceedings of the Symposium on the 15th International Conference on CVD, Electrochemical Society. In press.

10. Gas Phase Analysis of TiC and TiN Plasma Enhanced CVD Processes by Molecular Beam Mass Spectrometry. Chandra M. Reddy and Carmela C. Amato-Wierda. Proceedings of the Symposium on Plasma Processing, Electrochemical Society. In press.

11. CVD of Carbide Multi-Phased Coatings. Kathryn Versprille, Hua Xia Ji, Carmela C. Amato-Wierda, and Philip J. Ramsey. Mat. Res. Soc. Symp. Proc. 581, 339-344, 2000

III.3. Papers in Preparation or Pending Review

J.J. Nainaparampil, A.R. Phani, J.E. Krzanowski and J.S. Zabinski, "Pulsed Laser Ablated MoS_2-Al Films Characterized for Friction and Wear in Humid Environments," in preparation for J. Vac. Sci. Tech. A.

III.4. Presentations

Papers presented at Conferences:

Materials Research Society Fall 2002 Meeting

J.E. Krzanowski, J.L. Endrino and K. Hirschman, "Novel Composite Coatings with 3D Coating Architectures for Tribological Applications Fabricated using Semiconductor Patterning Processes"

A.R. Phani, J.E. Krzanowski, and J.J. Nainaparampil, "Structural and Tribological Properties of Molybdenum Disulfide/Metal Multilayer Films Deposited by Pulsed Laser Deposition"

J.L. Endrino, J.J. Nainaparampil, and J.E. Krzanowski, "Microstructure Development and Mechanisms of Lubrication in Magnetron Sputtered HfC-Ag and SiC-Ag Composite Thin Films"

American Vacuum Society Annual Meeting, Fall 2002

J. J. Nainaparampil, A. R. Phani, J. E. Krzanowski and J. S. Zabinski, "Pulsed laser ablated MoS_2-Al Films characterized for friction and wear in humid conditions"

J.E. Krzanowski and J.L. Endrino, "The Effects of Si on the Mechanical Properties of WC Thin Films"

International Conference on Metallurgical Coatings and Thin Films, April 22 - 26, 2002, San Diego, California,

A. R. Phani, J. E. Krzanowski and J. J. Nainaparampil, "Study of Mechanical and Tribological Properties of WC/TiC and WC/B4C Multilayer Films Deposited by Pulsed Laser Deposition"

A. R. Phani, J. E. Krzanowski and J. J. Nainaparampil, "Structure and Tribological Properties of MoS2 Multilayer Films"

Jose L. Endrino and James E. Krzanowski, "Elastic Stresses in Nano-Composite Tribological Coatings" (Poster)

Materials Research Society Fall 2001 Meeting

R. Obbard and T.S. Gross, "A Nano-scratch Method for Determining the Wear Resistance of Thin Films"

J.E. Krzanowski, J.L. Endrino and S.H. Koutzaki, "Determining the Limit of Hardness in Ternary Carbide Thin Films," Surface Engineering Symposium

J.L. Endrino, J.J. Nainaparampil, and J.E. Krzanowski, "Structural and Tribological Properties of TiC/C/Ag Coatings in Vacuum and Ambient Environments," Surface Engineering Symposium (Poster).

A.R. Phani, J.J. Nainaparampil, and J.E. Krzanowski, "The Effects of Substrate Temperature and Bias on the Structural, Mechanical and Tribological Properties of TiC Films Deposited by Magnetron Sputtering Pulsed Laser Deposition," Surface Engineering Symposium

A.R.Phani, J.E.Krzanowski and J.J.Nainaparampil, "Structural Properties of Carbon Nitride Films Deposited by Reactive - Pulsed Laser Deposition Technique" Surface Engineering Symposium (poster presentation)

International Conference on Metallurgical Coatings and Thin Films, Spring 2001

A.R.Phani, J.E.Krzanowski and J.J.Nianparampril, "Study of Mechanical and Tribological Properties of Ti/TiC and Cr/TiC Multilayer Films Deposited by Magnetron Sputtering Assisted Pulsed Laser Deposition"

A.R.Phani, J.E.Krzanowski and J.J.Nianparampril, "The effect of microstructure on hardness enhancement in Ti-Si-C and Ti-W-C thin films deposited by MSPLD"

A.R.Phani, J.E.Krzanowski and J.J.Nianparampril, "Study of Mechanical and Tribological Properties of WC/TiC and WC/B_4C Multilayer Films Deposited by Pulsed Laser Deposition"

A.R.Phani, J.E.Krzanowski and J.J.Nianparampril, "Structure and Tribological Properties of MoS_2 Multilayer Films"

American Vacuum Society Annual Meeting, Fall 2001

A.R.Phani, J.E.Krzanowski and J.J.Nainaparampil, "Structural and Mechanical Properties of TiC/Ti and TiC/B_4C Multilayers Deposited by Pulsed Laser Deposition"

A.R.Phani, J.E.Krzanowski and J.J.Nainaparampil, "Comparison studies of structural, mechanical and tribological properties of sub and super stoichiometric TiC films deposited by Magnetron Sputtering assisted Pulsed Laser Deposition technique"

Materials Research Society Fall 2000 Meeting

J.E. Krzanowski, S.H. Koutzaki, J. Nainaparampril, and J.S. Zabinski, "Phase Formation and Mechanical Properties of Multiphase Carbide Coatings"

Electrochemical Society, Toronto, May, 2000

Factors Affecting the Amount of Carbon in Titanium Carbide Films Made By CVD. Kathryn E. Versprille, Carmela C. Amato-Wierda, and Philip Ramsey. Poster presented at the 197th Meeting of the Electrochemical Society, Toronto, May, 2000.

Characterization of Ti-W-C Thin Films Deposited by CVD. Hua Xia Ji and Carmela C. Amato-Wierda. Poster presented at the 197th Meeting of the Electrochemical Society, Toronto, May, 2000.

Gas Phase Analysis of TiC and TiN Plasma Enhanced CVD Processes by Molecular Beam Mass Spectrometry. Chandra M. Reddy and Carmela C. Amato-Wierda. Talk presented at the 197th Meeting of the Electrochemical Society, Toronto, May, 2000.

Other Presentations

J.E. Krzanowski, "Super-Hard Nano-Composite Coatings: Myth or Reality?" Seminar given at the University of Connecticut, March 12, 2002.

Dissertations

Kathryn Versprille, M.S. Thesis, "Factors Affecting the Amount of Carbon in Titanium Carbide Films Made By CVD", Advisor: Prof. Carmela C. Amato-Wierda, August 2000

Sirma Koutzaki, M.S. Thesis, "Phase Formation and Mechanical Properties of Multiphase Carbide Films", Advisor: J.E. Krzanowski, December 2000

Rachel Obbard, M.S. Thesis, "A Nano-scratch Method for Assessing Wear of Metal Carbide-Metal Nacreous Nanostructures," Advisor: T.S. Gross, September 2002

Jose L. Endrino, Ph.D. Thesis, "The Impact of Coating Architecture on the Hardness, Friction, and Wear Resistance of Ternary Carbide and Composite Lubricant Coatings," Advisor: J.E. Krzanowski, Defense Planned for April, 2003

IV. Program Personnel

Principal Investigators			
Name	**Position**	**Location**	**Department**
Prof. J.E. Krzanowski	PI	UNH	Mechanical Engineering
Prof. Todd S. Gross	Co-PI	UNH	Mechanical Engineering
Prof. C. Amato-Wierda	Co-PI	UNH	Materials Science Program
Prof. Olof Echt	Co-PI	UNH	Physics
Dr. J.J. Nainaparampil	Research Scientist	AFRL	Systran, Inc.

Professional Associates			
Name	**Position**	**Current Location**	**Dates Employed**
Dr. A.R. Phani	Post-Doc	CSEM, Switzerland	8/1999 – 8/2002
Dr. H.X. Ji	Post-Doc	Private Industry	2/2000 – 11/2000
Dr. Flora Tien	Post-Doc	U. of Texas	2/2002 – 7/2002

Graduate Students			
Name	**Degree**	**Status**	**Current Location**
Sirma Koutzaki	M.S.	Graduated, 2000	Unknown
Jose Endrino	Ph.D.	Defending 4/2003	Balzers, Inc.
Rachel Obbard	M.S.	Graduated, 2002	Dartmouth, PhD Program
Kate Versprille	M.S.	Graduated, 2000	JDS Uniphase
Matthew Treat	M.S.	Defending 5/2003	UNH

APPENDIX

1. Report of Systran, Inc. Subcontract Effort

Dr. Jeffery Zabinski and Dr. Jose Nainaparampil, Principal Investigators

Introduction

The main focus of this project was to probe into the possibilities of carbide based hardcoatings in composite as well as multilayer architectures. The proposed task was achieved by the formation of carbides of refractory metal tungsten and base metals like titanium, hafnium and zirconium and ceramics like silicon carbide. In addition to these, coatings with high temperature applications were also considered in this project by forming silver alloy of tungsten carbide and titanium carbide. In the solid lubricant area, molybdenum disulfide was studied with a novel additive like pure aluminum resulting in significantly enhanced wear life under very high humidity conditions. Overall performance of all these coatings was encouraging and created interest for further research and investigations.

Recent developments in hard coating technologies have been achieved through compositional and microstructural modifications of traditional carbide and nitride coating materials. Examples include the addition of Al to TiN in TiAlN coatings (1). Si in TiSiN, the formation of carbonitrides such as TiCN and the fabrication of heterogeneous multilayers such as TiN/NbN and TiN/CN. The incorporation of additional elements can provide solid solution strengthening, hardening due to the presence of a second phase, or an improvement in mechanical properties by Hall–Petch strengthening and crack arrest mechanisms (2-4). More recent research has focused on using nanoscale multilayers to reduce stress in the hard coatings, terminate cross-sectional cracks, and impede motion of dislocations (5-7). Compositional modifications can provide additional property improvements. For example, the addition of Al to TiN improves surface oxidation resistance, and it is also possible to form tribochemical surface films that lower friction and extend wear life, such as oxides and graphite-like transfer films. While much of the work on ternary hard coating materials has focused on nitrides, improvements in carbide coatings by alloying may also be possible. Addition of ternary elements to TiC and other B1-structured carbides to form solid solutions has shown considerable improvements in hardness (8). In our research we have attempted to alloy TiC to form multiphase carbide coatings. Research has been conducted on sputter-deposited Ti–Mo–C, Ti–W–C, and Ti–Si–C. It was found that weakly immiscible systems, such as Ti– Mo–C and Ti–W–C, tend to exhibit large super saturation and form single-phase structures when deposited in thin film form (9). In terms of hardness improvements, the most successful of these was the Ti–Si–C coatings, where the hardness increased from 12 GPa for TiC to 22 GPa for the optimal Ti–Si–C film composition. However, the low value of the TiC film indicates a less than fully dense structure, probably due to the fact that the films were deposited at a relatively low temperature 650 °C with no bias or other energetic assistance. Higher temperatures are not suitable for deposition on steel, which is the substrate of primary applications interest. Therefore a more energetic deposition method is needed. Using such a method, we can determine the extent to which Si can enhance hardness over the

accepted level for TiC, which is typically 28–30 GPa. Hardness values near that level were obtained in our previous studies of pulsed laser deposited PLD – TiC (10). In this study, the effect of Si in enhancing the mechanical property of TiC is explored. The energetic deposition is applied to bring back all the promising properties of TiC. The Ti–Si–C films are characterized for its mechanical and tribological properties. At the same time, we have also made standard PLD TiC samples for comparison.

All the TiC films were highly crystalline except the one deposited at room temperature, whereas for the Ti–Si–C films the degree of crystallinity increased with temperature, ranging from amorphous for the room temperature deposit to about 50% crystalline at 600 °C. The hardness of the TiC films was relatively constant with deposition temperature at about 25 GPa, whereas the hardness of the Ti–Si–C films increased with deposition temperature from 11 to 33 GPa. The temperature dependence of the hardness is attributed to the degree of crystallinity and the extent of phase separation in the Ti–Si–C films. The wear test data showed good results for all films up to the tested limit of 10000 cycles at 1 N load.

Another interesting work in this project was the investigation of the hardness and yield strength enhancements for multilayers with composition modulations at the nanometer scale. The mechanical properties of multilayer thin films have been the subject of numerous investigations over the past two decades. There have been reports by a number of investigators who have examined metallic, nitride, and metal/nitride9, multilayer structures (11-17). For example, TiN/VN multilayer films have shown hardness levels of up to 4800 kgf/mm2, much higher than the constituent layers. The primary strengthening mechanisms cited in these studies include coherency strengthening, modulus hardening, Hall–Petch strengthening, and the presence of slip-limiting interfaces (18-20). In general, these theories are based on mechanisms that impede dislocation motion due to multilayer interfaces or coherency stresses. Hardness enhancement has also been achieved by combining layers with very different mechanical properties, such as metal/ceramic multilayers of Ti/TiN. The mechanical properties of multilayers are closely related to their microstructural characteristics, such as grain structure, the extent of epitaxial growth, and the roughness and compositional sharpness of the interfaces as well as bilayer thickness. Therefore, characterization of multilayer structure and growth mechanisms is essential to understanding their mechanical properties. In addition to hardness enhancements, it may also be possible to obtain improvements in the toughness and wear resistance of a coating by using fine-scale multilayer structures. The interfaces in a multilayer can act to deflect cracks and increase crack path lengths. In this study we have deposited and characterized multilayers using two systems. TiC/Ti and TiC/B4C. In these systems, TiC has a B1 rocksalt structure, Ti has an HCP structure, and B4C has a complex rhombohedral lattice, although B4C forms an amorphous structure when deposited by PLD (21). These two multilayer systems represent two extremes, one having a soft metal interlayer and the other a hard carbide interlayer. In the TiC/Ti system, the choice of Ti as the metal interlayer results in a system where the two layers are both structurally and compositionally dissimilar. In the selection of a hard interlayer for the second system, it was noted that most transition metal carbides, such as ZrC and TaC, have the same B1 structure as TiC, as well as similar hardness and modulus levels.

Using one of these carbides as an interlayer would therefore be unlikely to either provide the desired structural discontinuity at the interface or provide much hardness enhancement. Therefore, B4C was selected as the carbide interlayer for the second system since it provides a structurally discontinuous layer that can impede crack propagation or dislocation motion. We have evaluated the friction and wear behavior of the deposited coatings in addition to the film composition, microstructure, and hardness. It was shown that the presence of a multilayer structure in the coatings affects the crystallinity and grain structure of the layers and can impact the wear behavior and wear failure mechanisms.

The TiC/Ti films were found to have a crystalline structure, and both (200)TiC/(100)Ti and (111)TiC/(101)Ti orientation relationships were found in these films. In the TiC/B4C films, only the sample with the largest bilayer thickness (25 nm) had significantcrystallinity and only the TiC layer was crystalline. X-ray photoelectron spectroscopy depth profiles confirmed the presence of composition modulations in these films. Nanoindentation tests of the TiC/Ti multilayers showed hardness levels exceeding that predicted by the rule-of-mixtures. The TiC/B4C multilayers showed increasing hardness with decreasing bilayer thickness but reached only 22 GPa. The pin-on-disc tests gave friction values ranging from 0.3 to 0.9 for both sets of films. These results were correlated with the degree of crystallinity and grain structure of the films.

Crystalline SiC films are typically deposited on substrates at elevated temperatures by sputtering, Pulsed Laser Ablation, thermal CVD and PACVD. However, high temperature may adversely affect the substrate, especially when metal alloys are used. To maintain substrate properties (temper, dimensional tolerance etc.) a low deposition temperature is required. In this work, silicon carbide is formed from simultaneous sputtering of silicon and laser ablation of graphite onto suitably biased substrates at room temperature. The advantage of this method lies in the independent selection of plasma characteristics of both magnetron sputtering and laser ablation to achieve the required stoichiometry and species energetics. Desirable film properties such as good adhesion and crystallinity normally requiring elevated substrate temperatures are obtained via the energetic bombardment of the growing film. In this study, films are grown on M50 steel substrates at biasing varied from 0 to -300 Volts permitting control over crystallinity, chemistry and stoichiometry. The bonding nature of species is also controlled by adjusting the Si to C ratio and by biasing the substrate. A hybrid technique combining magnetron sputtering of silicon and pulsed laser ablation of graphite was used for the deposition. This method was proven to be very effective in the Ti-C system for formation of nano-crystalline TiC amorphous C composite coatings (22). Since two independent processes (PLD and Magnetron Sputtering) are employed, individual selection and control of species may be realized. The energy of carbon atoms can be adjusted by varying either laser wavelength or fluence (23,24). At the laser fluences used in our study, (200 mJ/ 17 ns pulse) carbon ions have energies exceeding 1000eV (25). However, the fraction of C ions produced is expected to be less than 1% (26,27). A much higher fraction of Si ions are generated during the sputtering process (28). The arrival energies of these atoms may be controlled by adjusting the bias voltage applied to the substrate. Films were characterized using XPS, Raman and XRD for analytical studies,

and nanoindentation and scratch testing for mechanical properties. SEM was used to characterize the failure modes resulting from the scratch tests.

The advantages of a solid lubricant over a liquid include lower volatility, assembly cleanliness and lower torque. Solid lubricants commonly used under vacuum are MoS_2, WS_2, and Pb and Ag (29). However, the life of a solid lubricant under vacuum can be limited by wear. In contrast, hard carbide coatings exhibit excellent wear resistance (30), so a multiphase material combining a soft metal and a hard carbide phase has the potential to provide lower friction in vacuum along with good wear resistance. The present authors investigated the frictional properties of sputter-deposited WC–Ag and TiC–Ag in vacuum environments and a reduction in friction with silver content was observed (31). Friction was lower with higher Ag content, but wear was higher; the optimal Ag concentration was found to be 15%. SEM images from the surface of the films and wear tracks were obtained to understand the morphology of this type of composite ceramic coating, and revealed Ag layers in the wear track elongated in the direction of wear. Based on these results, the significance of silver as a friction-reducing agent in vacuum environments was demonstrated.

The primary focus of the work presented in this paper is to investigate two important issues: (1) whether phase separation into the desired carbide and silver phases can be achieved at a relatively low temperature by magnetron sputter co-deposition, and (2) to determine if the coatings reduce friction coefficients in vacuum environments. Furthermore, we provide preliminary results on the relative amount of silver necessary to obtain good frictional characteristics.

The role of MoS_2 as a solid lubricant in low humid conditions is a well-established fact. But, the presence of humidity act very adversely on MoS_2 films. There have been numerous attempts to increase the efficiency of MoS_2 film by various additives. Aluminum is used here as the additive because it shows more affinity for O and (OH) radical than Mo. No known molybdates exits between Al and Mo. The MoS_2 film is formed on 440C steel substrates by laser ablation along with magnetron sputtering of Al. The friction and wear studies are made on ball on disc tribometer. Films of 1- 2 micron thickness had a wear life of round 150k to 250 k in 25% humidity with ~8% aluminum. The micro Raman and X-ray photoelectron spectroscopy (XPS) are used to analyze the chemistry and scanning electron microscopy (SEM) is used to study the morphology and film cross section. Nanoindentation showed comparatively soft films. The role of Aluminum in increasing the wear life of laser-ablated MoS_2 films in humid conditions is demonstrated. Mechanism behind the increased wear life is partially explained. It was noted that Al affinity for (OH) group is high enough to have tribochemical reactions and form compounds that might help increasing the endurance and wear life. MoS_2 films are deposited using laser ablation with co-sputtering Al using magnetron. Films with different concentration of Al are deposited and tested for friction and wear on ball on disc tribotester. Chemistry of films and wear tracks were analyzed using Raman spectroscopy and X-ray photoelectron spectroscopy (XPS). Wear behavior of the wear scar and film topography are observed in a scanning electron microscope (SEM). Combining the SEM

observation with Raman data it strongly suggested that Al is gradually turned into Alumina under tribostressing in humid surroundings.

Conclusion

Most of the work planned in the begging of this project was completed with interesting results that paved the path for more work and expansion. Carbide based hard coatings of various metals were deposited with energetic process as well as ion rich process like magnetron sputtering. Substrate temperature was used to boost the energetics helping crystallization in the case of low ion methods and substrate biasing was applied in the case of ion rich methods. Both methods gave desirable results in the hardness and wear life endurance. Solid lubes with significant enhancement in lubricating characteristics were also developed under this project. High temperature coatings, coating that give lubrication and wear life enhancement for applications runs at very high temperature, were also made and characterized in this project. Overall this project was an attempt to address some of the direct or indirect interests of US Air Force, which always look for novel material systems that can be applied in the new challenges of today and tomorrow.

References

1. *Handbook of Tribology: Materials, Coatings, and Surface Treatments*, edited by B. Bhushan and B. K. Gupta ~McGraw-Hill, New York, 1991

2. S. Lopez, M. S. Wong, and W. D. Sproul, J. Vac. Sci. Technol. A **13**, 1644 ~2000

3. C. Subramanian and K. N. Strafford, Wear **165**, 85 ~1993

4. M. S. Donley and J. S. Zabiniski, in *Pulsed Laser Deposition of Thin Films*, edited by D. B. Chrisey and G. K. Huber ~Wiley, New York, 1994, p. 431.

5. H. Holleck and V. Schier, Surf. Coat. Technol. **76'77**, 328 ~1995

6. A. A. Voevidin, S. D. Walck, and J. S. Zabinski, Wear **203'204**, 516 ~1997

7. J. S. Zabinski, A. A. Voevidin, and M. A. Capano, AGARD Conf. Proc. **589**, 4 ~1996

8. H. Holleck, J. Vac. Sci. Technol. A **4**, 2661 ~1986

9. J. E. Krzanowski, S. H. Koutzaki, J. Nainaparampril, and J. S. Zabinski, Mater. Res. Soc. Symp. Proc. **594**, 181 ~2000

10. J. E. Krzanowski and R. E. Leuchtner, J. Am. Ceram. Soc. **80**, 1277 ~1997

11. S.L. Lehoczky, J. Appl. Phys. **49,** 5479 (1978).

12. J.E. Krzanowski and P. Duggan, in *Thin Films: Stresses and Mechanical Properties*

V, edited by S.P. Baker, P. Børgesen, P.H. Townsend, C.A. Ross, and C.A. Volkert (Mater. Res. Soc. Symp. Proc. **356,** Pittsburgh, PA, 1995), p. 391.

13. P. Yashar, S.A. Barnett, J. Rechner, and W.D. Sproul, J. Vac. Sci. Tech, A **16,** 2913 (1998).

14. U. Helmerson, S. Todorova, S.A. Barnett, J.E. Sundgren, L.C. Markett, and J.E. Greene, J. Appl. Phys. **62,** 481 (1987).

15. M. Shinn, L. Hultman, and S.A. Barnett, J. Mater. Res **7,** 901 (1992).

16. E. Kusano, M. Kitagawa, H. Nanto, and A. Kinbara, J. Vac. Sci. Technol., A **16,** 1272 (1998).

17. X. Wang, A. Kolitsch, and W. Mo¨ller, Appl. Phys. Lett. **71,** 1951 (1997).

18. J.E. Krzanowski, in *Thin Films: Stress and Mechanical Properties III,* edited by W.D. Nix, J.C. Brauman, E. Arzt, and L.B. Freund (Mater. Res. Soc. Symp. Proc. **239,** Pittsburgh, PA, 1992), p. 509.

19. J.E. Krzanowski, Scr. Met. Mater. **25,** 1465 (1991).

20. X. Chu and S.A. Barnett, J. Appl. Phys. **77,** 4403 (1995).

21. 16. A.R. Phani and J.E. Krzanowski, University of New Hampshire (Unpublished research).

22. A. A. Voevodin, S. V. Prasad and J. S. Zabinski, J. Appl. Phys. 82(2) 855

23. J. T. Dikinson, T. S. Langford, and L. C. Jenson, *Laser Ablation: Mechanisms and Applications*, (J. C. Miller and R. F. Haglund, eds.) Springler-Verlag(1991), Heidelberg, p. 301

24. L. Wiedeman, and H. Helvajian, J. Appl. Phys. 70, (1991) 4513

25 A. A. Voevodin, , S. D. Walck, J. S. Solomon, M. S. Donley and J. S. Zabinski, J. Appl. Phys. 78(6) 4123

26. Metev, *Laser Processing and Diagnostics (II)*, European Mater. Res. Soc. Symp. Proc., Les Ulis Cedex, France, 1986 p143

27. D. B. Geohegan, Mater. Res. Soc. Symp. Proc., 201,1991 p 557

28. S. Schiller, V. Heisig and K Goedicke, Thin Solid Films, 40 (1977) 327

29. K. Miyoshi, NASA Tech. Memo. 1 (1999) 209088.

30. B.M. Kramer, J. Vac. Sci. Technol. A 4 (1986) 2870.

31. J. Endrino, J.J. Nainaparampril and J.E. Krzanowski, "Magnetron Sputter Deposition of WC-Ag and TiC-Ag Coatings and their Frictional Properties in Vacuum Environments," Scripta Mat., v 74, pp. 613-618 (2002).

PERGAMON

Scripta Materialia 47 (2002) 613–618

Scripta MATERIALIA

www.actamat-journals.com

Magnetron sputter deposition of WC–Ag and TiC–Ag coatings and their frictional properties in vacuum environments

Jose L. Endrino [a,*], Jose J. Nainaparampil [b], James E. Krzanowski [a,*]

[a] *Department of Mechanical Engineering and Materials Program, University of New Hampshire, Durham, NH 03824, USA*
[b] *Air Force Research Laboratories/MBLT, Wright-Patterson AFB, OH 45433, USA*

Received 1 May 2002; received in revised form 12 June 2002; accepted 26 June 2002

Abstract

Thin films of WC–Ag and TiC–Ag were deposited by magnetron sputtering for the purpose of analyzing their tribological properties in vacuum. X-ray diffraction was used to determine structural properties, and energy dispersive X-ray analysis was used to determine the relative atomic content of silver in the films. Pin on disk friction tests were performed to obtain the coefficient of friction in vacuum. The deposited films showed a structure containing separate carbide/silver phases, as was desired for providing both high wear resistance and low friction. The tribological test results show a significant decrease in the friction coefficient for both TiC–Ag and WC–Ag, to a minimum value of 0.2, with increasing silver content.

Keywords: Sputtering; Scanning electron microscopy; Carbides; Surfaces and interfaces; Wear

1. Introduction

The use of advanced ceramics coatings based on transition metal carbides and nitrides has been proven to be very effective in improving the tribological performance of components such as ball bearings and cutting tools, where the friction and wear requirements are high [1,2]. There is also an increasing interest in the development of ceramic coatings that could provide low friction in vacuum environments [3]. One type of solid lubricant that is used in vacuum environments is a soft metal, such as silver, gold or indium. The incorporation of a soft metal within a hard transition metal carbide or nitride may therefore provide both high wear resistance and low vacuum friction. In this paper, we explore this concept using the TiC/Ag and WC/Ag composite systems.

Tungsten carbide–silver composite materials have been studied previously to examine their behavior as electrical contacts capable of providing low contact resistance and high hardness [4]. WC–Ag electrodes are commercially available and typically manufactured by sintering and pressing for use in microelectronics [5].

* Corresponding authors. Tel.: +1-603-862-2315; fax: +1-603-862-1865.
E-mail address: jamesk@cisunix.unh.edu (J.L. Endrino).

1359-6462/02/$ - see front matter
PII: S1359-6462(02)00236-1

The use of a hard metal/soft metal composite as a thin film coating for low friction applications was first investigated by Cheng et al. [6]. They studied the tribological properties of Ag–Mo and Ag–Ni films, and showed a significant reduction in friction and wear rates and reported the formation of a nano-crystalline composite structure. Additional studies were conducted on TiN/Ag composite thin films, which have also shown promising tribological properties [7]. However, friction coefficients in vacuum environments were not measured.

In our research we have examined WC–Ag and TiC–Ag composite thin films deposited by magnetron sputtering. The primary focus of the work presented in this paper is to investigate two important issues: (1) whether phase separation into the desired carbide and silver phases can be achieved at a relatively low temperature by magnetron sputter co-deposition, and (2) to determine if the coatings reduce friction coefficients in vacuum environments. Furthermore, we provide preliminary results on the relative amount of silver necessary to obtain good frictional characteristics.

2. Experimental details

Dual-target RF magnetron co-sputtering from tungsten carbide, titanium carbide and silver targets, were used to deposit WC–Ag and TiC–Ag films. For the WC–Ag films the substrates used were 1 in. diameter 440C steel hardened disks, which were first coated with a 50 nm titanium film for adhesion. For the TiC–Ag films, the same substrates were used, but with no titanium interlayer. In both cases a silicon wafer was also included as a substrate to facilitate XRD identification of phases.

The deposition chamber was evacuated to a base pressure of 6.7×10^{-5} Pa and then back filled with high purity argon to a pressure of 1.33 Pa during sputtering. A quartz crystal thickness monitor was used to measure film thickness, which was set at ~750 nm for all samples. Five WC–Ag films and five TiC–Ag films were deposited at a substrate temperature of 275 °C.

A Rigaku D-MAX/B diffractometer equipped with a Cu Kα X-ray tube was used to perform XRD analysis on the samples and identify the phases formed. An Amray 3300FE field emission SEM equipped with a Princeton Gamma-Tech EDX system was used to obtain both elemental composition analysis and scanning electron microscopy (SEM) images of the surfaces.

Room temperature friction and wear data from coated specimens were generated with a vacuum ($\approx 1.33 \times 10^{-6}$ Pa) ball-on-flat tribometer. A 6.25 mm diameter 440C steel ball was used as the counterface. For each friction track, the rotational speed was adjusted to get a constant sliding speed of 50 mm/s. The majority of the friction measurements were made at a normal load of 1 N. For steel-on-steel, a normal load of 1 N on a 6.25 mm diameter ball corresponds to a Hertzian contact pressure of 425 MPa.

3. Results and discussion

3.1. Chemical and morphological analysis

Energy dispersive X-ray spectroscopy was used to determine the relative atomic percentage of silver with respect to the total amount of the metallic component, (Ti + Ag) or (W + Ag), since it is difficult to accurately quantify the carbon concentration by the EDX method. Table 1 shows the

Table 1
Chemical composition and average vacuum friction of WC/Ag and TiC/Ag

Sample	Target #1/ RF power (W)	Target #2/ RF power (W)	Silver relative at. (%)	Average vacuum friction
#1	WC/200	Ag/0	0	0.68
#2	WC/200	Ag/10	4	0.70
#3	WC/200	Ag/15	12	0.75
#4	WC/200	Ag/20	21	0.25
#5	WC/200	Ag/40	39	0.32
#6	TiC/250	Ag/0	0	0.65
#7	TiC/250	Ag/5	7	0.50
#8	TiC/250	Ag/10	24	0.57
#9	TiC/250[a]	Ag/20	51	0.26
#10	TiC/250	Ag/20	86	0.28

[a] Distance between the gun and the substrate holder was increased by 1 in.

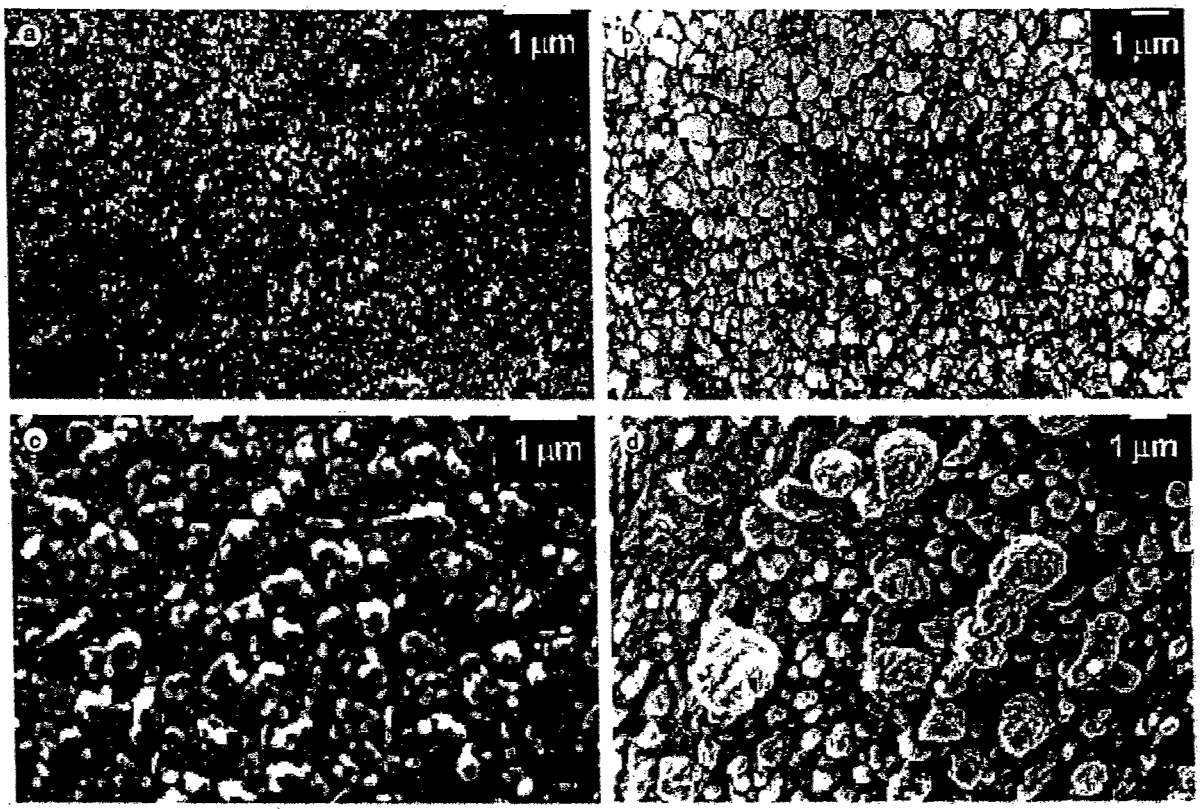

Fig. 1. Secondary electron images form the surface of the coatings. (a) WC–Ag with 4 relative at.% Ag, (b) TiC without silver, (c) WC–Ag with 21 relative at.% Ag and (d) TiC–Ag with 86 relative at.% Ag.

values for silver concentration of both WC–Ag and TiC–Ag films. Two of these films, #1 and #6, were made without silver. The WC–Ag contained up to 39% Ag, while the TiC–Ag films contained up to 86% Ag. A higher silver content was detected for the TiC–Ag samples; the reason for this was the low sputtering rate obtained for TiC compared to WC.

SEM images showed that the presence of silver in the films had a strong influence on the morphology of the coatings. Fig. 1(a) and (c) illustrate the difference between a WC–Ag film with low silver content (4%) and high silver content (35%). As the silver content of these films is increased, an increase in the number and size of the lighter colored surface particles on the surface is noted. These larger particles are believed to be silver, but they are still submicron in size, which precluded their analysis with the EDX technique.

Fig. 1(b) and (d) correspond to a pure TiC coating and one with high 86% silver content. The coating of TiC, in Fig. 1(b), showed coarse columnar grains. For the TiC/Ag coated sample in Fig. 1(d), a pattern similar to that found for WC–Ag with high silver content was observed, where silver appears to form conglomerates that become very reflective in the SEM.

3.2. XRD analysis

XRD patterns were acquired for both types of films (WC–Ag and TiC–Ag). For WC–Ag, we found that WC forms the non-stoichiometric WC_{1-x} phase, which is the phase that most commonly appears in tungsten carbide coatings deposited by magnetron sputtering [8,9]. Fig. 2(a) illustrates how silver appears in WC–Ag films as a distinct phase with FCC structure, and could be

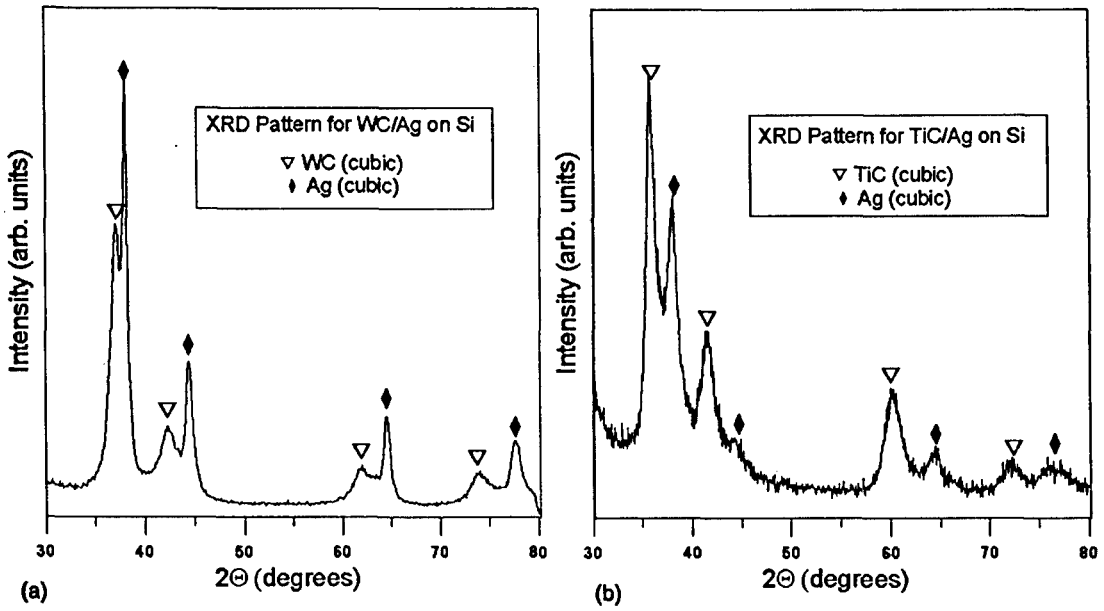

Fig. 2. XRD patterns indicating the two distinct phases formed of: (a) WC–Ag film with 39 relative at.% Ag and (b) TiC–Ag film with 24 relative at.% Ag.

quantified with respect to the carbide phase. A comparison of the pattern shown in Fig. 2(a) with previous patterns obtained for WC deposited at 275 °C show that the amount of the silver phase present does not affect the size or the orientation of the carbide crystallites.

Fig. 2(b) shows the XRD spectra of a TiC–Ag film with 24% silver (sample #8), cubic titanium carbide matches correctly with the TiC peaks that appear in our spectrum. Silver, the same as for the WC–Ag films, forms a distinct phase with an FCC structure. The lattice parameter obtained for the silver phase was 0.4084 nm, almost coincident to the expected value of 0.4086 nm.

3.3. Friction tests

Both WC–Ag and TiC–Ag coatings were analyzed using the pin-on-disk friction test under vacuum conditions to determine their friction properties. The test results for WC–Ag films are shown in Fig. 3(a). The films with 0% and 4% Ag gave high friction coefficients, as well as a high noise level, but for films with 21% and 39% Ag (samples #4 and #5), the friction coefficients were considerably reduced to values within the 0.2–0.4 range with a lower noise level. The results of the vacuum friction tests for the TiC/Ag are shown in Fig. 3(b). The films with 0%, 7% and 24% Ag showed a relatively high friction coefficient. However, the friction was reduced in films with 51% and 86% Ag. Comparing the latter two, it was noted that the friction trace was considerably smoother for the 51% Ag despite the similar friction coefficient range to the 86% Ag. The 51% Ag sample was run a second time to failure, and it maintained a low friction value for 33,000 cycles.

Table 1 shows the average value obtained for the first 10,000 cycles for WC–Ag samples and TiC–Ag films. Friction results indicate that the samples with the highest silver content do not correspond to the lowest friction observed, which suggests there is a value of silver content for which the tribological properties of these films are optimum. For the films examined, the optimum value for relative silver content is 21% for WC–Ag films and 51% for TiC–Ag. Given the adhesive friction behavior of a soft metal like silver, the mechanical properties of TiC and WC may play a significant role as counterface materials influencing the overall frictional behavior in vacuum. SEM examination of the wear track was conducted to help

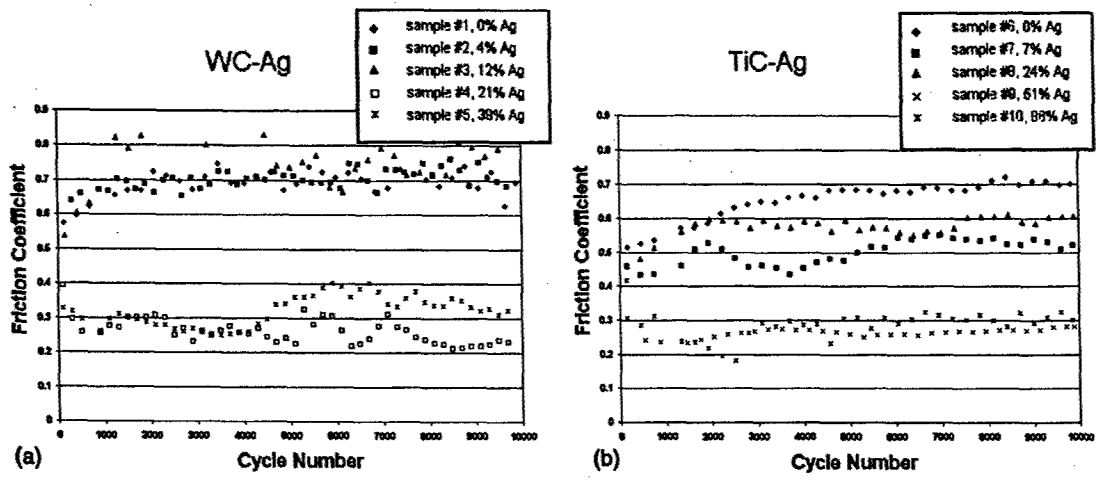

Fig. 3. Vacuum friction test results for the first 10,000 cycles: (a) WC–Ag films and (b) TiC–Ag films.

understand the role of Ag additions in these films. In general, the features observed were submicron in size, which did not allow us to conduct EDX mapping to indentify specific phases. However, we note that secondary electrons are more readily emitted from silver than carbide phases, so that in a SEM image the silver areas would appear relatively bright. Fig. 4 shows images from the wear tracks of several samples. In Fig. 4(a), the WC–Ag film (sample #3) with 12% silver content is shown after 10,000 cycles. The wear track shows rows of light particles, approximately 0.1–0.2 μm in diameter. The exact identification and source of these particles will require further study, but the fact that they are very bright compared to the background suggest they are silver particles. Fig. 4(b) show the TiC–Ag film (sample #9) deposited with 51% Ag after 33,000 cycles. Here, elongated streaks of Ag are observed covering much of the wear surface. Overall, the images in Fig. 4 suggest that the silver is present at the surface, and is smeared across the surface, providing lubrication and reducing friction.

4. Conclusions

TiC/Ag and WC/Ag thin films have been made by co-deposition of silver with titanium carbide and silver with tungsten carbide. The deposited films retain the desired carbide/metal phases forming a composite coating structure. Silver forms as agglomerates within the coating and on the surface. Friction testing in vacuum against a steel

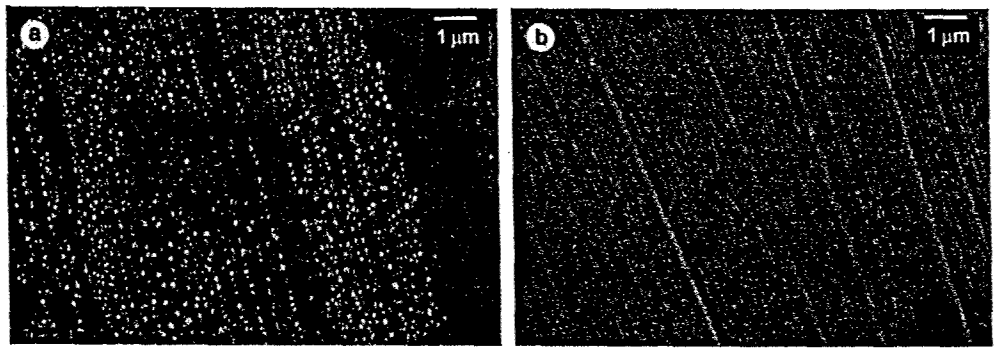

Fig. 4. SEM images of the wear track after friction tests: (a) TiC–Ag film deposited at 275 °C with 51% silver after 10,000 cycles and (b) TiC–Ag film deposited at 275 °C with 51% silver after 33,000 cycles.

counterface demonstrates that the films can exhibit a low coefficient of friction (~0.2) as a result of incorporating silver. Further tribological testing of silver–carbide films, to determine whether wear is also reduced, could lead to the design of coatings that could be optimized for vacuum tribological applications.

Acknowledgements

The financial support of the Air Force Office of Scientific Research under grant# F49620-98-1-0499, is gratefully acknowledged.

References

[1] Kramer BM. J Vac Sci Technol A 1986;4:2870–3.
[2] Bergmann E, Vogel J. J Vac Sci Technol A 1986;4:2867–9.
[3] Roller KG. J Vac Sci Technol A 1988;6:1161–5.
[4] Slade P, Bindas JA. IEEE Trans Components, Hybrids, Manufacturing Technol 1991;14:2–7.
[5] Miyoshi K. NASA Technical Memorandum, V.1, 1999-209088.
[6] Cheng Y-T, Qiu B, Tung S, Blanchard JP, Drew G. Mater Res Soc Symp Proc 1994;356:875–9.
[7] Cheng Y-T. Private communication.
[8] Gouy-Pailler Ph, Pauleau Y. J Vac Sci Technol A 1993;11:96–102.
[9] Slimani T, Goudeau Ph, Naudon A, Farges G, Derep JL. J Appl Cryst 1991;24:638–44.

Phase Formation and Microstructure in Sputter-Deposited Ti-Mo-C and Ti-W-C Thin Films

SIRMA H. KOUTZAKI, JAMES E. KRZANOWSKI, and JOSE J. NAINAPARAMPIL

Ti-Mo-C and Ti-W-C films were deposited by cosputtering from carbide targets in order to examine the phase formation, microstructure, and mechanical properties. A series of Ti-Mo-C films were deposited, with compositions ranging from TiC to Mo_2C. The X-ray diffraction (XRD) analysis showed that multiphase Ti-Mo-C films, containing the (Ti,Mo)C, Mo_2C, and Mo_3C_2 phases, were only obtained in highly Mo-rich films. The transmission electron microscopy (TEM) analysis showed a higher defect content in single-phase alloy Ti-Mo-C films in comparison to TiC alone. The hardness for most Ti-Mo-C films was in the range of 8 to 10 GPa, but even lower values were obtained in the multiphase films. Ti-W-C films deposited by cosputtering of TiC and WC formed only (Ti,W)C solid solutions. The X-ray photoelectron spectroscopy (XPS) analysis of peak positions showed that the W $4f_{7/2}$ binding energy decreased with increasing W content. The hardness of most of the Ti-W-C coatings was in the range of 15 to 17 GPa; however, a sample with 40 pct W had a hardness of 29 GPa. The TEM analysis of this sample revealed an extremely small grain size and a higher film density. The high hardness of this specimen is attributed to Hall–Petch strengthening.

I. INTRODUCTION

METAL carbides are known to have extremely high hardness levels, making them attractive candidates for wear-resistant coatings. Transition metal carbides that have been investigated as potential hard coating materials include carbides of titanium, tungsten, and zirconium.[1–6] Titanium carbide and tungsten carbide have been extensively studied to investigate both their intrinsic properties[7–13] as well as methods to deposit them as coatings.[14–17] TiC crystallizes into the rock-salt (B1) structure over a wide but substoichiometric composition range. The hardness of TiC at room temperature is 28 to 30 GPa, the highest of the transition-metal carbides,[18] although at elevated temperatures, tungsten carbide maintains a higher hardness.[18,19] Nonetheless, the hardness is substantially lower than that of diamond, which is the hardest material found in nature, with a hardness of 80 to 100 GPa.

Improving the hardness, and possibly wear resistance, of hard carbide coatings could potentially be achieved through compositional and microstructural modifications. Traditional metallurgical strengthening mechanisms such as grain refining and precipitation hardening can provide possible routes to improving the mechanical properties of these materials. In fact, recent claims by Veprek *et al.*[20,21] to have obtained nitride-based films with hardness levels higher than that of diamond are based on Hall–Petch strengthening along with a grain-boundary phase to inhibit grain-boundary sliding or microcracking. The application of these principles to carbide-based coatings, which are intrinsically harder than nitrides, therefore, has the potential to produce ultrahard coatings.

SIRMA H. KOUTZAKI, Graduate Research Assistant, and JAMES E. KRZANOWSKI, Associate Professor, are with the Mechanical Engineering Department, University of New Hampshire, Durham, NH 03824. Contact e-mail: jamesk@cisonix.unh.edu JOSE J. NAINAPARAMPIL, Visiting Scientist, is with the Air Force Research Laboratory, Wright-Patterson Air Force Base, OH 45433.

Manuscript submitted July 6, 2001.

Multiphase carbide coatings can be obtained by either multilayer deposition of the constituent carbides, or by natural phase separation during deposition. For the latter case, coating compositions will need to be based on transition-metal carbide mixtures that have limited miscibility. Most carbides that are based on the group-IVB transition metals are highly or completely miscible with those in the same group or those in group VB.[22] Examples include TiC-NbC and ZrC-TaC; these carbides all have the rock-salt structure. More structural variety is found in the group-VIB carbides of Cr, Mo, and W. Combining a group-IVB carbide, such as TiC, with a group-VIB carbide, such as Mo_2C, is more likely to produce heterogeneous multiphase carbide coatings. We have chosen to investigate this system (TiC-Mo_2C) as well as the TiC-WC system. While these are essentially ternary compounds, we can also approach these as pseudo-binary systems by depositing from dual carbide targets, as will be detailed in the following section.

The ternary Ti-Mo-C and Ti-W-C phase diagrams are shown in Figures 1(a) and (b).[23] A pseudobinary line connecting TiC and Mo_2C shows extensive solubility of Mo in TiC, a two-phase (Ti,Mo)/$(Mo,Ti)_2C$ region, and some solubility of Ti in Mo_2C. An additional nearby phase is labeled Mo_3C_2, although strictly speaking, this is a ternary phase containing both Mo and Ti. The Ti-W-C phase diagram (Figure 1(b)) shows extensive solubility of W in TiC, and it is possible that two-phase structures of TiC-WC or TiC-W_2C may be obtained, depending on the carbon stoichiometry.

While these diagrams present a suitable starting point for our study, the coatings reported in the present work are sputter deposited at temperatures of 650 °C or less, which is much lower than that represented by the phase diagrams in Figures 1(a) and (b). These lower temperatures would generally be expected to result in less solid solubility and larger miscibility gaps. However, since sputter deposition is a "rapid-quench" process, metastable phases or phases exhibiting extended solubility may form.[16,24] Therefore, experimental studies need to be conducted to determine compositional regimes that may provide suitable microstructures

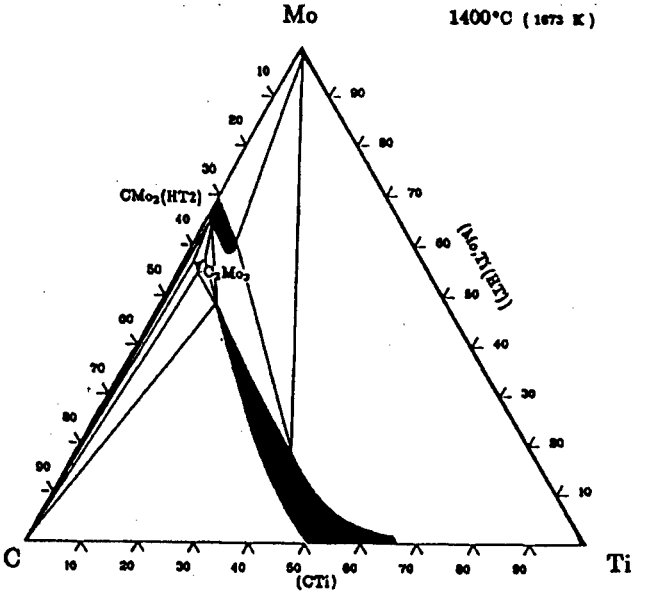

(*a*)

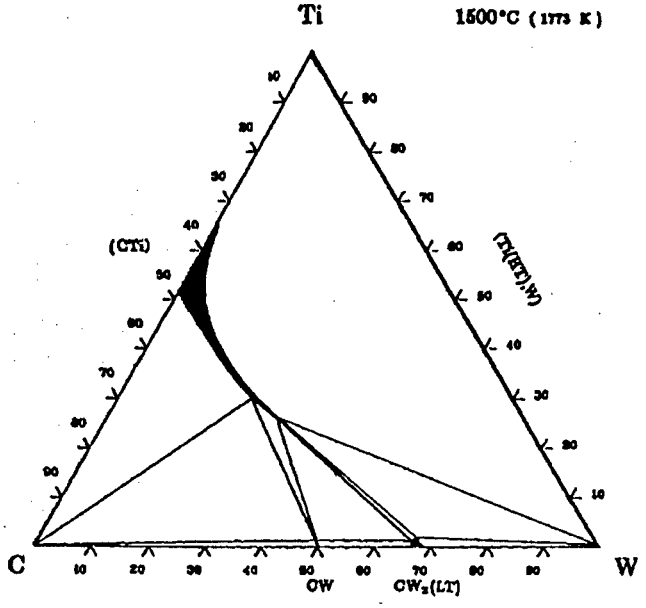

(*b*)

Fig. 1—Phase diagrams for the ternary carbide systems: (*a*) Ti-Mo-C at 1400 °C; and (*b*) Ti-W-C at 1500 °C.

for ultrahard coatings. The primary objectives of the present work are to examine the phase formation and microstructure in sputter-deposited TiC- Mo_2C and TiC-WC thin films. In addition, we have also measured the hardness of these films to determine which compositions may be promising candidates for further study.

II. EXPERIMENTAL METHODS

Film deposition was performed in a high-vacuum chamber with a base pressure of 10^{-7} Torr. During deposition, the chamber was backfilled with ultrahigh-purity argon gas to obtain working pressures of 3.5 to 8.9 mTorr. Radio frequency magnetron sputtering from dual carbide targets was chosen as the most suitable method for depositing the selected multicomponent carbide coatings. One of the sputtering guns contained the TiC target and the other gun contained the Mo_2C or WC target. While film deposition rates from carbide targets are relatively low (~3 to 6 nm/min), the use of the dual-carbide-target configuration allowed us to obtain a full range of compositions for each pseudobinary system simply by varying the relative power of the guns. The distance between the substrates and sputtering-gun targets was 10 to 12 cm. The substrates were mounted on a resistive heater during deposition. Most films discussed in this study were deposited at a temperature of 650 °C, which represents a T/T_m value of 0.28 for TiC.

The deposition rate was measured *in situ* using a quartz crystal oscillator. The film thickness was also verified by cross-sectional scanning electron microscopy (SEM) images. The thickness of the deposited films was in the range 0.35 to 0.70 μm.

The sputtering targets were obtained from commercial vendors and were fabricated by hot pressing under argon from 99.5 pct purity carbide powders. Substrates used were silicon (111) single-crystal wafers, R-plane sapphire, and INCONEL* 600. The substrates were first cleaned with a degreasing agent and distilled water and then rinsed in ethanol and dried.

*INCONEL is a trademark of INCO Alloys International, Huntington, WV.

Coating compositions were determined by X-ray photoelectron spectroscopy (XPS). The analyses were conducted on a Kratos Analytical instrument using a monochromatic Mg K_α X-ray source operating at 15 kV. The binding energies were referred to the Au $4f_{7/2}$ peak position at 84.3 eV, as measured on a clean gold thin foil. Relative peak areas were used for compositional quantification and were corrected for a spectrometer factor and X-ray cross section by using the relative sensitivity factors supplied in the Kratos software. High-resolution scans were carried out at a pass energy of 40 eV and a step of 0.1 eV, to examine the chemical bonding in the coatings by monitoring the element peak shifts.

The X-ray diffraction (XRD) technique was used for phase identification, texture, and grain-size evaluation. The analyses were performed using Cu K_α radiation in a θ-θ Rigaku D-MAX/B diffractometer operating at 45 kV and 35 mA. Patterns were obtained in the 2θ range from 20 to 80 deg at a goniometer speed of 1.8 deg/min and a step size of 0.05 deg. The Jade 5.0 computer program (Materials Data, Inc., Livermore, CA) and the database of Powder Diffraction Files[25] were used to analyze the diffraction peaks and determine the phases present in the coatings.

The coating microstructure and morphology were evaluated using transmission electron microscopy (TEM). Plan-view specimens of films deposited on silicon substrates were prepared by grinding, dimpling, and ion milling. The samples were analyzed using an Hitachi H-600 transmission electron microscope operating at 100 kV. High-resolution TEM (HRTEM) for more detailed structural analyses was conducted on a JEOL* 2010 transmission electron microscope operating at 200 kV.

*JEOL is a trademark of Japan Electron Optics Ltd., Tokyo.

The crystallite or grain size was determined from both

Table I. Deposition Parameters, Film Compositions, and Grain Sizes for Ti-Mo-C Films Deposited at 650 °C

Specimen	Gun Power (Watts)							Relative	Grain Size (nm)	
	Power, Mo_2C	Power, TiC	Power Ratio, Mo_2C/TiC	Ti, At. Pct	Mo, At. Pct	C, At. Pct	O, At. Pct	At. Pct Mo	Silicon Substrate	Sapphire Substrate
TiC	—	200	0	42.9	—	54.2	2.9	0.0	6	6
1-TM650	19	200	0.10	38.8	9.9	47.9	3.3	20.4	17	8
2-TM650	38	200	0.19	33.1	18.9	44.9	3.1	36.3	17	9
3-TM650	75	200	0.38	26.4	27.9	42.8	2.9	51.4	19	10
4-TM650	100	200	0.50	24.4	27.9	44.7	3.0	53.4	20	31
5-TM650	150	200	0.75	18.0	33.9	42.7	5.4	65.3	25	13
6-TM650	150	175	0.86	14.1	39.6	40.1	6.2	73.7	20	25
7-TM650	120	80	1.50	12.6	39.8	40.7	6.9	76.0	20	25
8-TM650	150	75	2.00	10.3	43.4	42.2	4.1	80.8	30	22
9-TM650	150	50	3.00	7.9	48.3	37.5	6.4	86.0	24	20
10-TM650	150	30	5.00	—	—	—	—	91.0*	21	21
Mo_2C	150	—	—	—	61.1	33.2	5.7	100.0	33	31

*Determined by extrapolation.

TEM and XRD experiments. In the XRD experiments, the crystallite size was determined from the full width at half-maximum of the highest peak using the Scherrer formula.[26] Application of the Scherrer formula was made after correcting for instrumental broadening. However, corrections for lattice strains generally could not be made, because the preferred orientation in the films often resulted in too few peaks to reliably apply lattice-strain correction methods. Therefore, the crystallite size calculated from XRD data may exceed the actual sizes. However, another consideration is that grain sizes formed during initial nucleation of the film are often relatively small but increase as the film grows, and a preferred orientation develops. The XRD examines the entire film thickness, while in our TEM plan-view samples, only the top ~0.1 μm thickness of the film is examined, so we would expect TEM observations of grain sizes to be larger than those obtained from XRD measurements. Based on these considerations, the XRD results can only be considered as an estimate of grain size and are most valuable when considering trends in grain size as a function of film composition.

Nanoindentation was used to measure the film hardness. The hardness values of the Ti-Mo-C films were measured with a Nano-indenter II, and the hardness of the Ti-W-C films was determined using a Hysitron nanomechanical test instrument, both equipped with Berkovich indenter. On the Hysitron instrument, films were tested using a multiple loading sequence with loads ranging from 0.2 to 5.5 mN. Typically, six to eight multiple loading measurements were used to calculate the average hardness and elastic moduli of the specimens. Values obtained at a depth of less than 20 nm were not considered reliable and, therefore, were not used. Because of roughness effects, it was found that more reliable data could be obtained by lightly polishing the film surface with a 0.3 μm colloidal solution of Al_2O_3 in distilled water.

III. RESULTS AND DISCUSSION

A. *Ti-Mo-C Films*

The results for the Ti-Mo-C films are presented in this section. A complete range of Ti-Mo-C films with compositions between pure TiC and pure Mo_2C were obtained. Table I summarizes the gun-power levels and the compositional analysis of the Ti-Mo-C films deposited on silicon substrates at 650 °C.

1. *Compositional analysis*

The XPS analyses were conducted on the Ti-Mo-C films, denoted 1-TM650 through 10-TM650, and the results are shown in Table I. The relative molybdenum concentration is given for each film, which is defined as follows:

$$\text{Relative at. pct Mo} = 100 \times (\text{at. pct Mo}/(\text{at. pct Mo} + \text{at. pct Ti}))$$

For the remainder of this article, the term "*at. pct*," for any element, shall retain its usual meaning as a percentage relative to all elements analyzed, but the term "*relative at. pct Mo*," as defined previously, will be more concisely and simply denoted "*pct Mo*."

The XPS analysis showed a nearly stoichiometric composition of the pure TiC film, with an oxygen content of less than 3 at. pct. Generally, the oxygen concentration in the Ti-Mo-C films was in the range 3 to 6 at. pct. The molybdenum carbide film consisted of 61.1 at. pct Mo, 33.2 at. pct C, and 5.7 at. pct O and was identified as Mo_2C, which was later confirmed by XRD. The Mo content of the films ranged from 20.4 to 91 pct Mo. The carbon concentration of the Ti-Mo-C films decreased gradually, approaching that of pure Mo_2C with an increasing Mo content in the films. In each deposition, sapphire substrates were also present, adjacent to the silicon substrates, and were assumed to have the same compositions as the corresponding films listed in Table I.

2. *The X-ray diffraction*

The XRD results for the Ti-Mo-C films deposited on silicon at 650 °C are shown in Figure 2. The pure TiC film exhibited a weak fcc pattern. The molybdenum carbide film was identified as Mo_2C with a hexagonal structure[25] and showed a higher degree of crystallinity than the TiC film. The Ti-Mo-C films, with compositions from 20.4 to 80.8% Mo (specimens 1-TM650 through 8-TM650), were found to be solid solutions of Mo in TiC, exhibiting the XRD pattern of the B1 crystal structure; all of these samples showed a (111) preferred orientation. Only films with 86 and 91 at. pct Mo (specimens 9-TM650 and 10-TM650) had

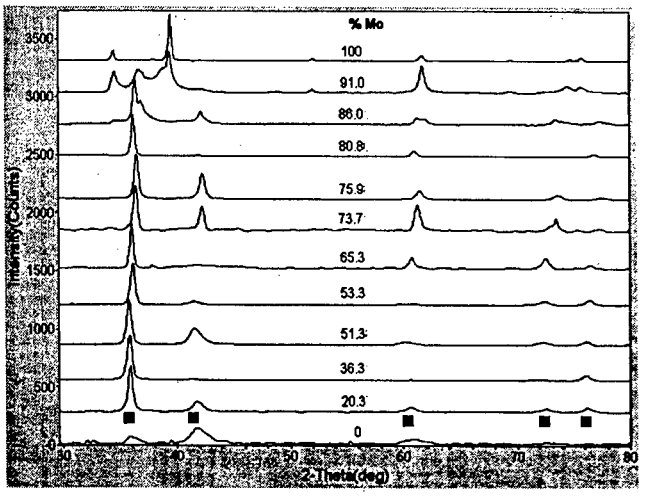

Fig. 2—XRD spectra of Ti-Mo-C films deposited on as-received Si substrates at 650 °C. Only the alloy films with the two highest Mo concentrations, 86 and 91 pct, show multiphase structures. The films with lower Mo contents show the formation a solid solution with the B1 structure. The black squares indicate the positions of the peaks for the B1-structured TiC phase. Peak positions for additional phases are shown in Fig. 3.

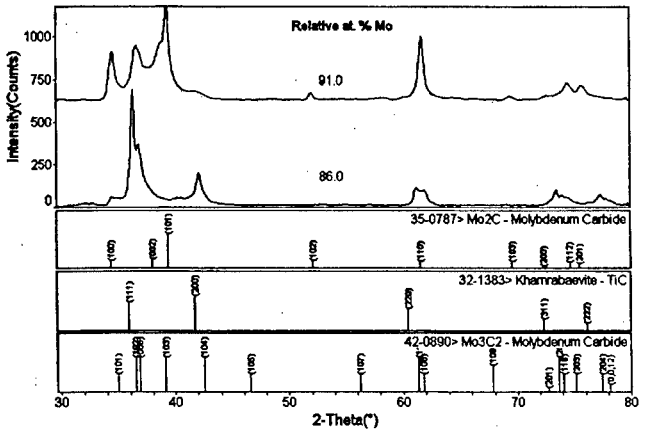

Fig. 3—XRD spectra of the two Mo-rich Ti-Mo-C films with the highest Mo content. The film with 86 pct Mo shows most lines matching with Mo_3C_2, with small amounts of (Ti,Mo)C and Mo_2C also possibly present. The 91 pct film is primarily a mixture of Mo_3C_2 and Mo_2C.

multiphase structures. Figure 3 shows the XRD results for these latter two films in greater detail. For specimen 9-TM650 with 86 pct Mo, the Mo_3C_2 phase provides an excellent match for most line positions. However, the relative intensities of the second and third peaks, the (102) and (006) lines for Mo_3C_2, are not equal in the spectrum (as the Powder Diffraction File (PDF) card indicates it should be), suggesting either a preferred orientation or that the (Ti,Mo)C phase is also present. A trace of Mo_2C is also possibly present as a minor third phase. The XRD analysis of sample 10-TM650, with 91 relative at. pct Mo, consisted mainly of two molybdenum carbide phases, Mo_2C and Mo_3C_2. In addition, the presence of small quantities of (Ti,Mo)C could not be excluded. The grain sizes for this series of films are given in Table I. There appears to be a slight trend toward increasing grain size with pct Mo, but the magnitude of this is not highly significant (compare, for example sample 1-TM650 with 17 nm and 10-TM650 with 21 nm), given the measurement uncertainty discussed in Section II.

The XRD analysis of the Ti-Mo-C films deposited on sapphire substrates at 650 °C (not shown) revealed notable differences in comparison to the corresponding films deposited on Si substrates. Films with a Mo content of up to 54.5 pct had a strong preferential (200) orientation, whereas films with between 53.4 and 86 pct Mo had a mostly mixed orientation. In addition, films with 51.4 pct Mo and below had broader peaks than those with 53.4 pct Mo and above (the one exception being the 65.3 pct Mo film), which is reflected in the grain-size measurements listed in Table I. The films with larger grain sizes had values similar to the films on Si (~20 nm), but a number of films at lower percentages of Mo on sapphire had grain sizes on the order of 10 nm. We also noted that the films with this smaller grain size had an average carbon concentration of 46.5 pct, whereas films with the larger grain size had an average carbon content of 41 pct. The films closer to the stoichiometric carbon concentration were (200) oriented, which is the most densely packed plane in the B1 structure, and the higher stoichiometry may also reduce diffusivities, resulting in smaller grain sizes. The more-substoichiometric films were of a mixed orientation. The presence of vacancies (or substitutional oxygen atoms) in carbon sites may increase the diffusivities, as well as the (200) surface energy, making other orientations more competitive. In contrast, most Ti-Mo-C films deposited on Si had a preferential (111) orientation, indicating that the film orientation was influenced by substrate orientation.

From Figure 2, as well as the films deposited on sapphire, it was observed that the (111) peak of the TiC diffraction pattern shifted to higher angles with increasing Mo content. As solid solutions of (Ti,Mo)C form with increasing Ti content, the smaller molybdenum atoms (r_{Ti} = 0.147 nm and r_{Mo} = 0.136 nm[27]) cause the TiC unit cell size to become increasingly reduced, resulting in a shifting of the Bragg reflections to higher angles.

The Mo_2C film and the Ti-Mo-C film with 91 pct Mo (sample 10-TM650) deposited on sapphire substrates at 650 °C were also examined using XRD. Both were highly oriented in the $\langle 11\bar{2}0 \rangle$ direction. In contrast to the films on the silicon substrate, no evidence for phase separation was found in the film with 91 pct Mo, indicating that a supersaturated solid solution of the type $(Mo,Ti)_2C$ had formed. The highly oriented growth on sapphire substrates appeared to have suppressed phase separation.

The ternary Ti-Mo-C phase diagram (Figure 1(a)) shows that the two-phase TiC-Mo_2C region is bound between 42 and 92 pct Mo, and many of our films fall in this compositional range. However, no films containing just these two phases were obtained. The composition range for the multiphase structures found in this work is much smaller than that indicated in the phase diagram. This can be attributed to the "rapid quenching" nature of the sputter deposition process, resulting in high degrees of supersaturation.

Table I also shows the grain size of the Ti-Mo-C films on silicon and sapphire substrates, as calculated from the XRD data. As observed from the XRD spectra, there is a trend of increasing grain size with molybdenum additions.

3. *Microstructural characterization*

The TEM analysis was first conducted on pure TiC and Mo_2C films deposited on an Si substrate at 650 °C. The TEM bright-field images of TiC and Mo_2C are shown in

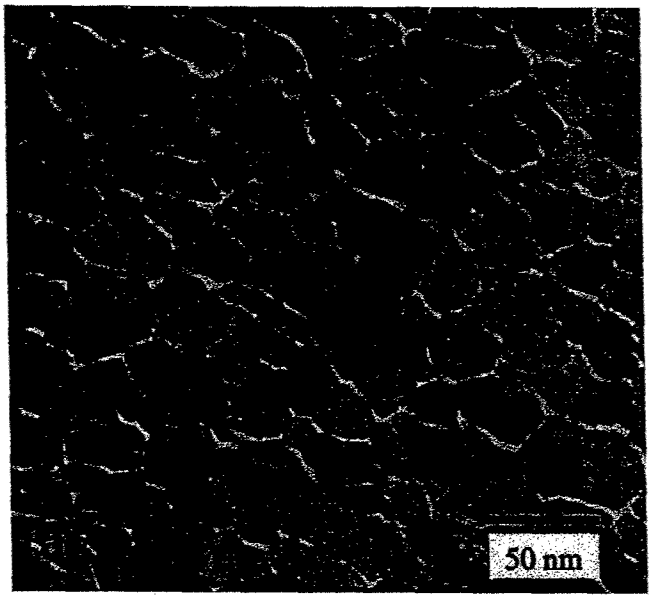

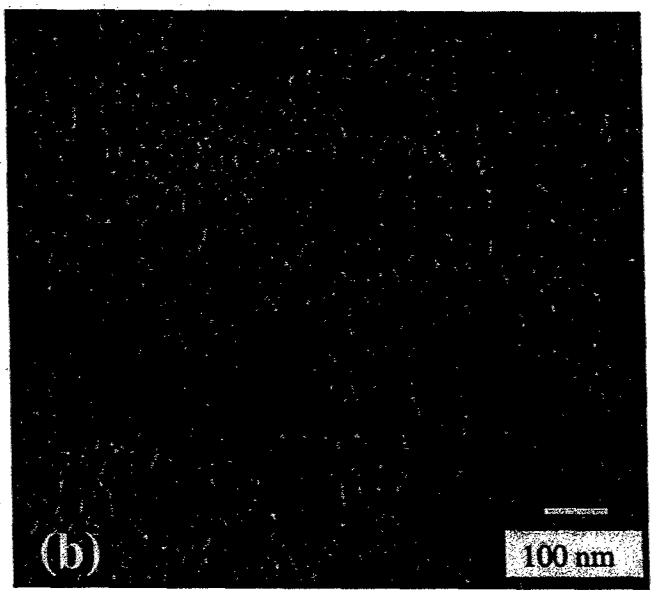

Fig. 4—Bright-field TEM plain-view images of (*a*) TiC and (*b*) Mo_2C films deposited on as-received Si substrates at 650 °C. The TiC films show a columnar grain structure with amorphous interlayers between grains, while the Mo_2C film shows a more fibrous structure, but amorphous interlayers are also present.

Figure 4. The TiC sample shows a columnar structure, which was also verified by cross-sectional SEM observations. The Mo_2C film reveals a more a fibrous morphology. In both cases, the grain size is 25 to 35 nm with intergranular layers. The nature of this intergranular region has been investigated for the TiC samples by HRTEM[28] and was found to be an amorphous material, possibly a metal oxycarbide. The electron diffraction patterns for the TiC and Mo_2C films were consistent with the fcc and hcp structures, respectively.

The Ti-Mo-C films were also examined by TEM for phase formation, microstructure, and grain morphology. Figure 5 shows a bright-field image of a solid-solution Ti-Mo-C film with 51 pct Mo (specimen 3-TM650). The selected-area electron diffraction pattern again showed only the fcc structure, indicating that there is a single phase present, *i.e.*, a (Ti,Mo)C solid solution. However, examination of this

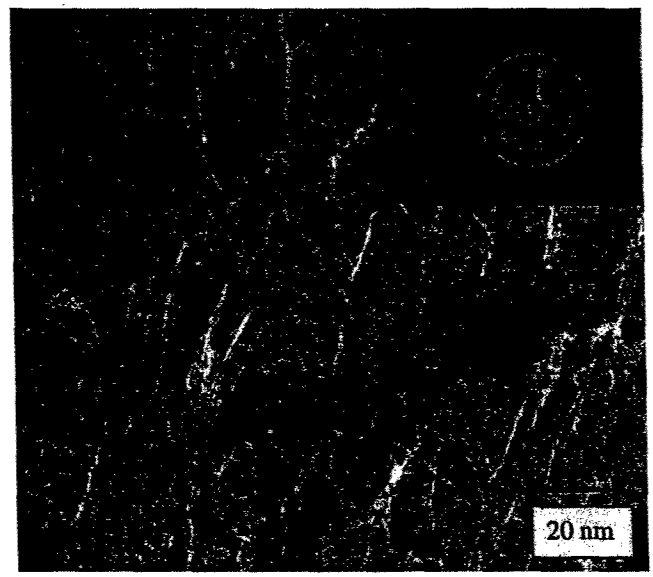

Fig. 5—TEM image of the Ti-Mo-C film with 51 relative at. pct Mo. The grain structure in this image is more elongated and a higher defect content is observed within the grains. Analysis of the diffraction pattern (inset) showed only rings due to the B1 structure, indicating the film is single phase.

specimen and similar specimens of this composition revealed a microstructure significantly different than that observed for TiC (as shown in Figure 4(a)). First, the grains appear more elongated than equiaxed; second, there is a higher defect content within the grains. The nature of these defects is not completely understood, but the observations made suggest the presence of nanotwins and nanoscale subgrain formation. Hierarchical subgrain structures of this nature are common in thin films.[29] In the present case, it is possible that the alloy Ti-Mo-C film has reduced diffusivity compared to TiC alone, and this may account for the differences in microstructure.

Figure 6(a) shows a lower-magnification image of sample 9-TM650 (86 pct Mo), where the film morphology consists of diamond-shaped crystals within a lighter-colored matrix (most clearly shown in the upper-right-hand corner of the image). The higher-magnification image (Figure 6(b)) shows that the diamond-shaped crystals are twinned, as is commonly found in materials with complex hexagonal structures. Attempts to further identify each phase by dark-field microscopy techniques was not successful due to the nearly overlapping diffraction rings, as well as the fact that the fine grain structures did not allow us to obtain single-crystal electron diffraction patterns. However, based on the XRD data, the diamond-shaped crystals were tentatively identified as Mo_3C_2, embedded in a fibrous matrix of the (Ti,Mo)C solid solution. In fact, there is a region of the Ti-Mo-C ternary-phase diagram (Figure 1(a)) where a two-phase equilibrium between Mo_3C_2 and (Ti,Mo)C exists.

Figure 7 shows bright-field TEM images of specimen 10-TM650, containing 91 pct Mo. Again, similar to Figure 6, two types of grains can be observed: (1) larger diamond-shaped grains as in specimen 9-TM650, corresponding to the Mo_3C_2 phase, and (2) smaller fibrous grains, similar in morphology to those observed in Mo_2C. In this case, the amount of fibrous Mo_2C appears in greater proportion in comparison to the sample in Figure 6, which is consistent with its higher Mo content. Figure 7(b) reveals a high density

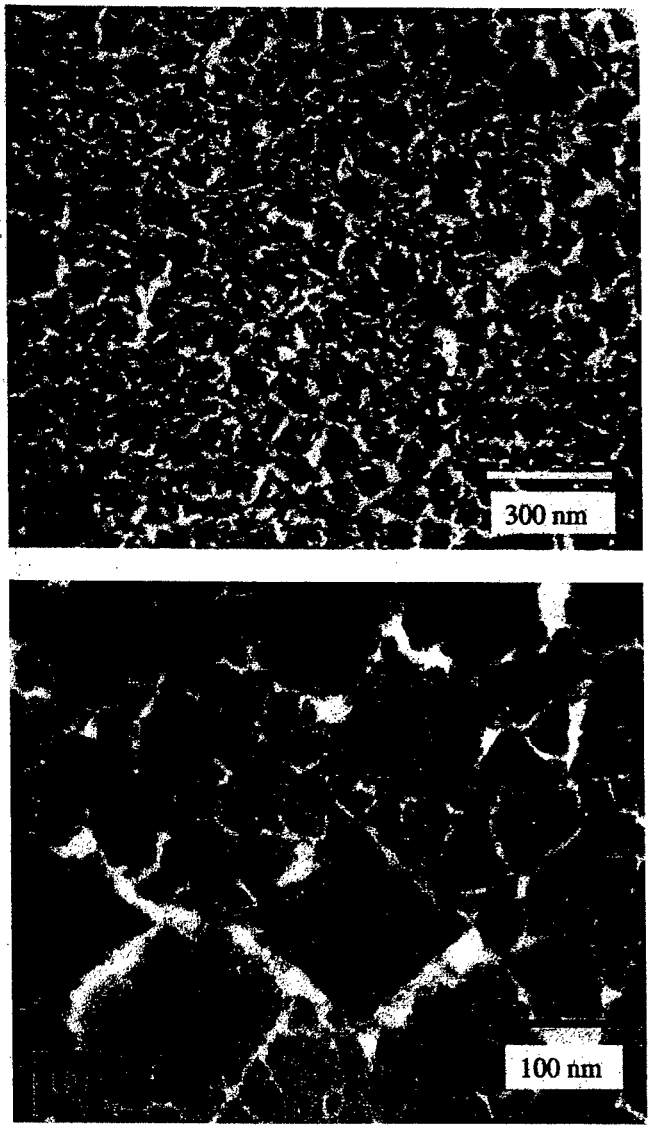

Fig. 6—TEM analysis of Ti-Mo-C film with 86 relative at. pct Mo at (*a*) lower magnification and (*b*) higher magnification. Note the two different types of grain morphologies in the upper right corner of (a).

of twins in both types of grains. Between the grains is again a lighter-colored phase, which lacks any structural features, indicating it is probably an amorphous phase containing Ti, Mo, C, and, possibly, oxygen.

4. *Ti-Mo-C film properties*

Figure 8 summarizes the results for the hardness of the Ti-Mo-C films deposited on silicon and sapphire substrates at 650 °C. The hardness is mostly in the range of 7 to 10 GPa, and no increase in hardness is evident with Mo additions. This hardness level is lower than that typically found for TiC (28 GPa) or Mo_2C (15 GPa).[18] This low hardness can be attributed to the extensive amount of amorphous material and voiding between the grains. For films in the multiphase regions, the results are scattered and the hardness is even lower. These films had a very high surface roughness, as would be expected from the coarse microstructure observed in Figures 6 and 7, which made reliable nanoindentation testing difficult and generally gives lower values. The values obtained for the reduced modulus were in the range of 55 to 200 GPa, much lower than those of the bulk (450

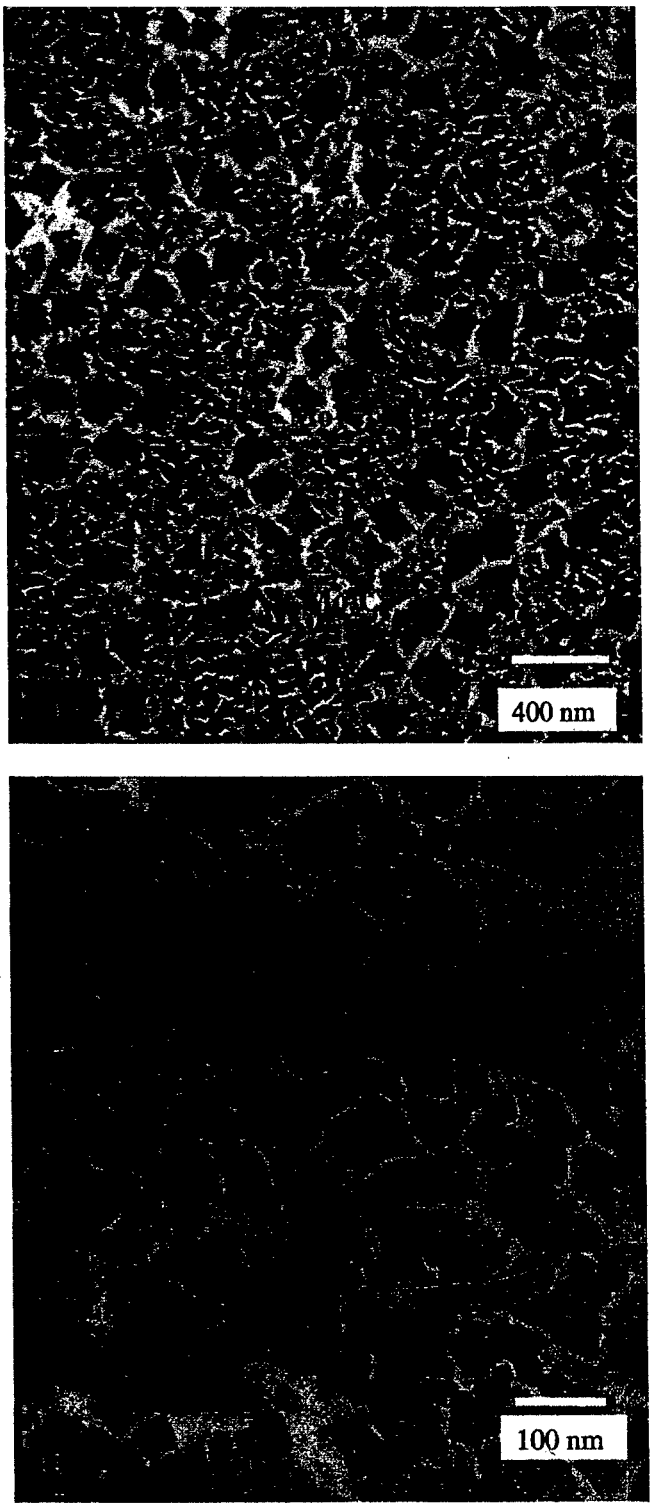

Fig. 7—TEM analysis of Ti-Mo-C film with 91 relative at. pct Mo: (*a*) bright-field image illustrating Mo_3C_2 and Mo_2C regions; and (*b*) higher magnification image showing extensive twinning within grains.

GPa for TiC and 230 GPa for Mo_2C[18]), and this is also attributed to the low film density.

B. *Results for Ti-W-C Films*

Coatings with compositions ranging from pure titanium carbide to pure tungsten carbide were deposited on silicon

and sapphire substrates by cosputtering from TiC and WC targets. The substrates were cleaned by ion sputtering prior to deposition and were heated to 650 °C for the deposition. Pure tungsten carbide films were deposited at 650 °C and room temperature.

1. *Compositional analysis of Ti-W-C films*

The film composition was analyzed by XPS using the W 4*d* peak, since the characteristic W $4f_{7/2}$ line overlapped with the Ti 3*d* peak. The results are summarized in Table II. Twelve Ti-W-C films, 1-TW through 12-TW, were in the compositional range from 3.4 relative at. pct W to 78.5 relative at. pct W. (Again, ternary film compositions will be identified by defining the relative tungsten concentration:

$$\text{Relative at. pct W} = 100 \times (\text{at. pct W}/(\text{at. pct W} + \text{at. pct Ti}))$$

For brevity, in the following discussion, this compositional variable will simply be referred to as "pct W.")

Even though a stoichiometric WC target was used, the tungsten carbide films had compositions close to the compound W_2C. This may be due to higher scattering of the lighter carbon atoms by the argon gas during the sputtering deposition process, compared to the heavier W atoms. However, XRD revealed the formation of a single phase consistent with the high-temperature nonstoichiometric B1-structured β-WC_{1-x} phase (PDF card no. 20-1316[25]). This high-temperature phase exists in equilibrium in the range of 2,525 °C to 2785 °C,[18] but has also been observed in previous studies of sputter and pulsed-laser-deposited tungsten carbide films.[16,30,31] The formation of tungsten carbide films with the B1 structure, rather than the hexagonal or orthorhombic structure, may be due to the kinetic constraints inherent in low-temperature sputter deposition that hinder the formation of the more complex structural forms. Furthermore, the high defect concentration on the carbon sublattice may promote a (111) orientation, as was suggested for the Ti-Mo-C films.

2. *The X-ray diffraction analysis*

The XRD analysis revealed that all ternary carbide Ti-W-C films (1-TW through 12-TW) formed only Ti-W-C solid solutions on both substrates. Figure 9 shows the XRD patterns of specimens 1-TW through 6-TW (3.4 to 46.5 pct W) deposited on silicon substrates. All the spectra are consistent with the TiC diffraction pattern, indicating that (Ti,W)C solid solutions formed. A strong (111) orientation was observed, similar to the pure tungsten carbide and titanium carbide films on silicon substrates. The grain size

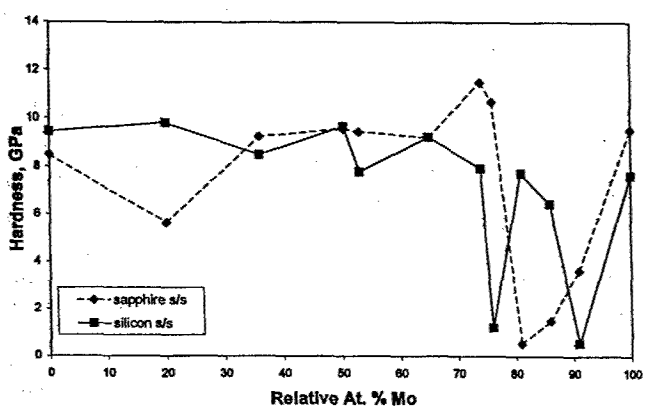

Fig. 8—Nanoidentation hardness test results for the Ti-Mo-C films deposited on silicon and sapphire substrates. The shaded region covers the compositional range where two-phase films were obtained on the silicon substrates.

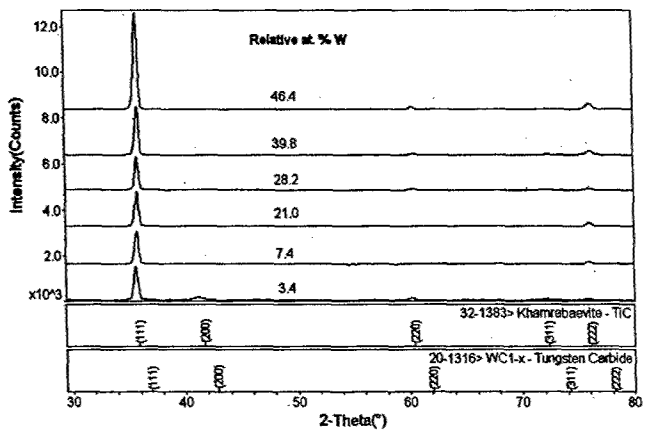

Fig. 9—XRD spectra of Ti-W-C films deposited on silicon substrates. All films showed a strong (111) reflection consistent with B1-structured (Ti,W)C. Note the shift in peak position due to alloying with tungsten.

Table II. Deposition Parameters and Film Compositions for Ti-W-C Films

Specimen	Gun Power, Watts WC	Gun Power, Watts TiC	Power Ratio, WC/TiC	Ti, At. Pct	W, At. Pct	C, At. Pct	O, At. Pct	Relative At. Pct W
WC-650	150	—	—	—	63.3	29.7	7.1	100.0
WC-RT	150	—	—	—	66.6	25.8	7.6	100.0
1-TW	5	250	0.02	48.3	1.7	46.7	3.3	3.4
2-TW	10	250	0.04	40.9	3.3	54.6	1.2	7.4
3-TW	15	250	0.06	41.9	13.4	38.4	6.3	21.1
4-TW	20	250	0.08	36.7	14.4	44.1	4.7	28.2
5-TW	25	250	0.10	33.2	21.9	35.4	9.6	39.8
6-TW	30	250	0.12	30.3	26.3	36.0	7.4	46.5
7-TW	35	250	0.14	25.7	24.3	47.1	8.0	48.6
8-TW	40	250	0.16	27.7	26.8	39.7	5.9	49.2
9-TW	45	250	0.18	26.1	29.0	40.8	4.2	52.7
10-TW	70	250	0.28	20.4	34.9	39.6	5.1	63.8
11-TW	60	250	0.24	15.7	43.5	38.4	2.5	73.5
12-TW	80	250	0.32	11.3	49.3	35.6	3.8	78.6

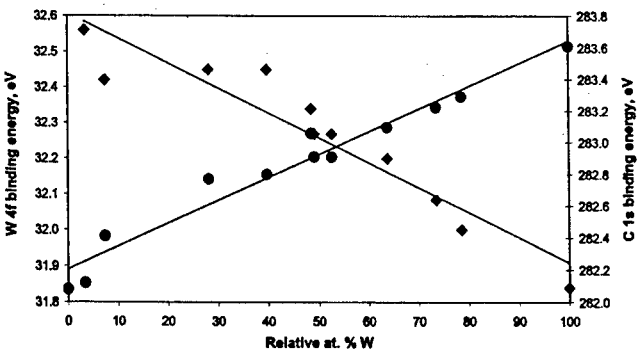

Fig. 10—XPS analysis of the peak position for the W $4f_{7/2}$ and C 1*s* binding energies in Ti-W-C coatings as a function of the tungsten content. Both the W $4f_{7/2}$ and C 1*s* positions shifted with alloy content, while the Ti $2p_{3/2}$ peak (not shown) remained constant.

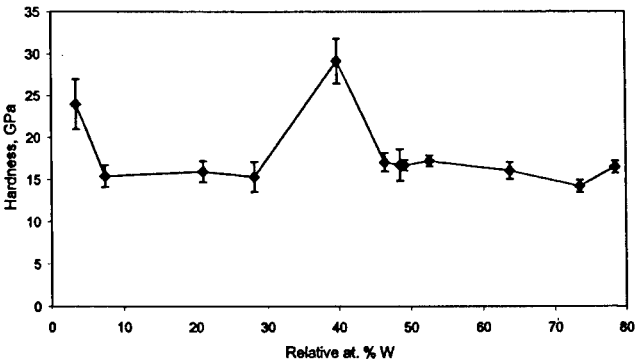

Fig. 11—Nanoindentation hardness of Ti-W-C films deposited on silicon substrates.

of the coatings, calculated from the XRD patterns, was found to be in the range of 20 to 25 nm.

The XRD analysis of the corresponding Ti-W-C films on sapphire substrates showed similar solid-solution structures. However, for Ti-rich coatings, there was a weak (200) preferred orientation, and with increasing tungsten concentration, the orientation changed from (200) to (111), matching that of tungsten carbide.

3. *Chemical bonding analysis*

Detailed XPS analysis was carried out on the Ti-W-C films in order to determine the binding energies of the elements present and to determine if any peak shifts occur due to alloying. The W $4f_{7/2}$ binding energy was determined to be 31.8 and 31.9 eV for the tungsten carbide films deposited at 650 °C and room temperature, respectively. This agrees very well with the binding energies reported by Voevodin *et al.*[16] and Pauleau and Gouy–Pailler[30] for the WC_{1-x} phase, although other researchers report lower values of 31.2 and 31.4 eV.[19,31] The C 1*s* binding energy of carbon was at 283.6 eV, which is a little higher than the 283.3 ± 0.1 eV region reported for nonstoichiometric cubic WC_{1-x}, perhaps due to the calibration of the instrument (*e.g.*, the Au $4f_{7/2}$ line was at 84.3 eV in our study, *vs* the 83.8 eV value reported by Srivastava *et al.*[31]) A second C 1*s* peak was fitted at a binding energy of 285.1 eV, identified by Pauleau and Gouy–Pailler[30] as a carbon contaminant.

A shift in the binding energy of the W 4*f* peaks was observed in the ternary Ti-W-C films with increasing tungsten concentration in the coatings. A plot of the W $4f_{7/2}$ binding energy *vs* pct W is shown in Figure 10. The binding energy is 32.6 eV for specimen 1-TW with 3.4 pct W and gradually decreases with increasing tungsten content in the films approaching the 31.8 eV binding energy of the WC_{1-x} phase. The higher W $4f_{7/2}$ binding energy of the ternary Ti-W-C films compared to that for WC_{1-x} is caused by an increase of the covalent character of the bonds in Ti-containing coatings.[30] The C 1*s* binding energy *vs* pct W is also shown in Figure 10. A shift in the binding energy for the C 1*s* peak was also observed, ranging from 282.1 eV for pure TiC to 283.6 eV for WC_{1-x}. In all of the specimens, a second type of C 1*s* bonding was observed at a binding energy of 284.5 ± 0.1 eV, which is the standard for carbon in graphite.[32] Finally, the binding energy of the Ti $2p_{3/2}$ peak was almost constant for all coatings at 454.9 to 455.0 eV. These data show that, within experimental error, there is a continuous change in binding energies for the W $4f_{7/2}$ and C 1*s* peaks, indicating that there are no discontinuous structural changes occurring with composition, but rather a continuously changing structure consistent with the formation of solid solutions.

4. *Nanoindentation hardness of Ti-W-C coatings*

The nanoindentation hardness of the Ti-W-C films was measured on a Hysitron nanomechanical test instrument. Figure 11 shows the results of the measurements for films deposited on silicon substrates. The hardness of the majority of the films is in the range of 15 to 17 GPa, comparable to the hardness of sputtered TiC, and the modulus values for these specimens were in the range of 193 to 245 GPa. However, two of the films tested showed significantly higher hardness levels, namely, specimen 1-TW (24 GPa) and specimen 5-TW (29 GPa). Interestingly, sample 1-TW had a relatively low modulus of 194 GPa, while sample 5-TW had the highest modulus measured for these samples, at 276 GPa. Hardness measurements can also be affected by the presence of a residual stress, so the residual stress in several Ti-W-C coatings was measured using XRD methods. It was found that the films have a low biaxial tensile residual stress ranging from 104 to 387 MPa. Since the measured stresses in these films were considerably low, they are not expected to affect significantly the nanoindentation measurements.

5. *Microstructural characterization*

Since the deposited Ti-W-C films all formed solid solutions, extensive microstructural characterization was not conducted on these samples. However, the microstructures of samples 3-TW (21.1 pct W, 16 GPa) and 5-TW (39.9 pct W, 29 GPa) were examined by TEM and HRTEM. Figure 12(a) shows a TEM image of sample 3-TW, revealing a grain size of 25 to 30 nm, a relatively low defect content within the grains, and voided boundaries. Figure 12(b)) is a HRTEM image of the same specimen, showing uninterrupted lattice fringes, indicative of a crystalline long-range order. The amorphous nature of the grain-boundary interlayer is also confirmed. This structure, consisting of crystalline grains with an amorphous interlayer, is nearly identical to that observed for the TiC films and is very common in thin-film structures.[33]

Figure 13(a) shows a bright-field TEM image of specimen 5-TW, with 39.9 pct W and 29 GPa hardness. An extremely small grain size of about 5 nm is observed, with a very dense film structure. The grain structure is shown in a greater detail in the HRTEM image in Figure 13(b). Microtwins

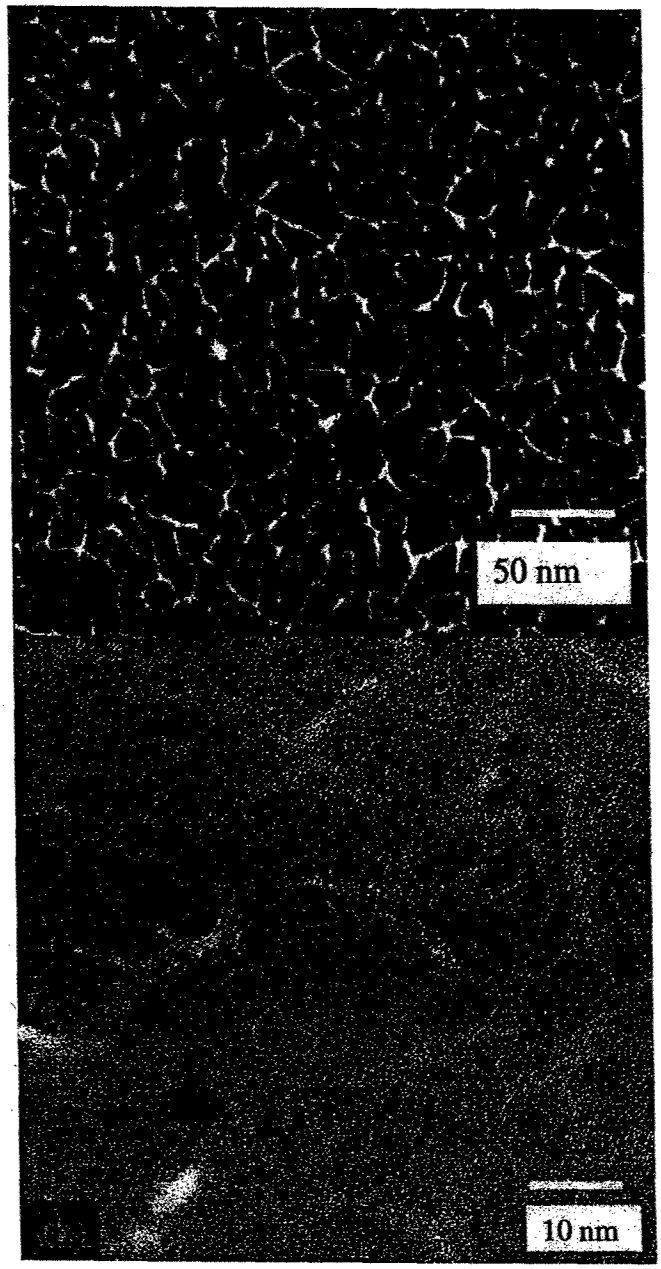

Fig. 12—TEM analysis of Ti-W-C film with 21 relative at. pct W and 16 GPa hardness (sample 3—TW): (*a*) bright-field image and (*b*) HRTEM image.

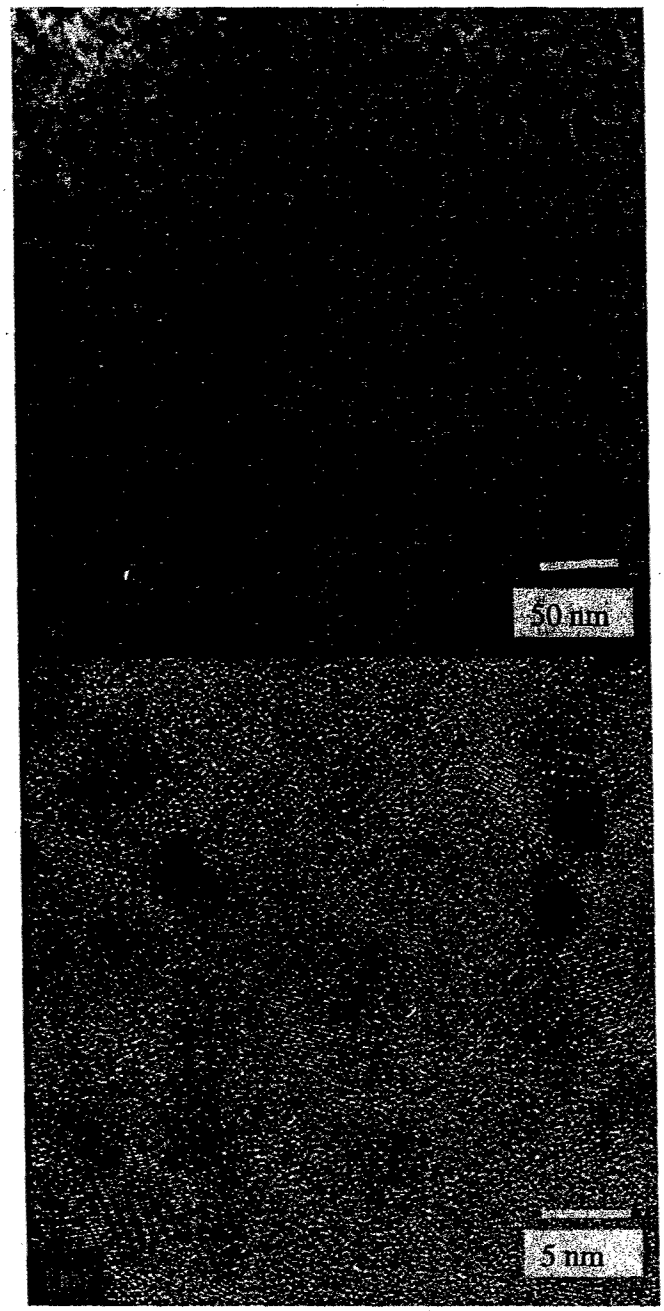

Fig. 13—TEM analysis of Ti-W-C film with 40 relative at. pct W and 29 GPa hardness (sample 5—TW): (*a*) bright-field image and (*b*) HRTEM image showing nanoscale grain size.

and subgrains were observed to subdivide the structure even further. The electron diffraction pattern had well-defined uniform rings, indicating a random in-plane orientation of the grain structure.

The foregoing TEM analyses suggest that coating hardness is related to grain size and film density. The former is a direct consequence of the Hall–Petch relationship and, as noted in the Introduction, has been proposed as a mechanism for enhancing coating hardness. Our results show that this may, in fact, be a viable approach. However, the fact that an extremely small gain size of 5 nm, which was obtained in sample 5-TW, resulted in a hardness of only 29 GPa indicates that this mechanism alone may not be sufficient to create carbide coatings with hardness levels exceeding that of diamond. In addition, further reductions in grain size may lead to grain-size softening, an effect that has been observed in materials with extremely small grain sizes.[32–35]

Another issue concerning these results is the reason for the extremely small grain size in the sample with 40 pct W. To our knowledge, the deposition conditions for this composition were not intentionally different from the other Ti-W-C samples, so it is not clear why the grain-size difference was obtained. Nonetheless, a significant difference in grain size is observed, which correlates well with the expected hardness dependence. Therefore, understanding the development of grain structure and devising methods to obtain ultrafine, equiaxed grain structures are valuable subjects for further study.

IV. SUMMARY

In this study, Ti-Mo-C and Ti-W-C films were deposited by cosputtering from carbide targets in order to examine phase formation and microstructure. A preliminary investigation of their mechanical properties was also conducted.

The XRD analysis showed that multiphase Ti-Mo-C films were only obtained in highly Mo-rich films. Alloy films on Si substrates exhibited multiphase structures at compositions only above 86 relative at. pct Mo. All films on sapphire substrates were supersaturated solid solutions. The TEM analysis showed that the defect content in Ti-Mo-C films increased with increasing molybdenum content. The multiphase films obtained were combinations of the (Ti,Mo)C fcc–solid solution phase, the Mo_2C phase, and the Mo_3C_2 phase. For the multiphase films, the microstructure was coarse and porous, yielding low hardness in the range of 8 to 10 GPa.

Ti-W-C films deposited by cosputtering of TiC and WC formed only (Ti,W)C solid solutions. High-resolution XPS showed that the W $4f_{7/2}$ binding energy decreased with increasing W content in the (Ti,W)C solid-solution films. The hardness of most of the Ti-W-C coatings was in the range of 15 to 17 GPa. A sample with 40 pct W had a high hardness of 29 GPa. The TEM analysis of this sample revealed an extremely small grain size and a higher film density. The high hardness of the Ti-W-C specimen containing 40 pct W is attributed mainly to Hall–Petch strengthening.

ACKNOWLEDGMENTS

The financial support of the Air Force Office of Scientific Research, under Grant No. F49620-98-1-0499, is gratefully acknowledged. This work made use of the MRSEC Shared Experimental Facilities at MIT supported by the National Science Foundation under award No. DMR98-008941. The assistance of Mr. Michael Frongillo with the HRTEM work is greatly appreciated.

REFERENCES

1. G. Georgiev, N. Feschiev, D. Popov, and Z. Uzunov: *Vacuum*, 1986, vol. 36, pp. 595-97.
2. J.-E. Sundgren, B.-O. Johansson, and S.-E. Karlsson: *Thin Solid Films*, 1983, vol. 105, pp. 353-66.
3. A.A. Voevodin, S.V. Prasad, and J.S. Zabinski: *J. Appl. Phys.*, 1997, vol. 82, pp. 855-58.
4. P.K. Srivastava, V.D. Vankar, and K.L. Chopra: *J. Vac. Sci. Technol. A*, 1985, vol. 3, pp. 2129-34.
5. P. Gouy-Pailler and Y. Pauleau: *J. Vac. Sci. Technol. A*, 1993, vol. 11, pp. 96-102.
6. W.F. Brock, J.E. Krzanowski, R.E. Leuchtner, L.J. Legore, and D.J. Frankel: *Mater. Res. Soc. Symp. Proc.*, 1998, vol. 505, pp. 261-66.
7. J.-E. Sundgren, B.-O. Johansson, S.-E. Karlsson, and H.T.G. Hentzell: *Thin Solid Films*, 1983, vol. 105, pp. 367-84.
8. A.A. Voevodin and J.S. Zabinski: *J. Mater. Sci.*, 1998, vol. 33, pp. 319-27.
9. J.E. Krzanowski and R.E. Leuchtner: *Mater. Res. Soc. Symp. Proc.*, 1996, vol. 410, pp. 301-06.
10. J.E. Krzanowski and R.E. Leuchtner: *J. Am. Ceram. Soc.*, 1997, vol. 80, pp. 1277-80.
11. T. Slimani, P. Goudeau, A. Naudon, G. Farges, and J.L. Derep: *J. Appl. Cryst.*, 1991, vol. 24, pp. 638-44.
12. C. Rebholz, J.M. Schneider, H. Ziegele, B. Rahle, A. Leyland, and A. Matthews: *Vacuum*, 1998, vol. 49, pp. 265-72.
13. I.N. Mihailescu, E. Gyorgy, G. Marin, M. Popescu, V.S. Teodorescu, J. Van Landuyt, G. Grivas, and A. Hatziapostolou: *J. Vac. Sci. Technol. A*, 1999, vol. 17, pp. 249-55.
14. A.A. Voevodin, M.A. Capano, A.J. Safriet, M.S. Donley, and J.S. Zabinski: *Appl. Phys. Lett.*, 1996, vol. 69, pp. 188-90.
15. L. Norin, J. Lu, U. Jansson, and J.-O. Malm: *J. Mater. Res.*, 1999, vol. 14, pp. 1589-96.
16. A.A. Voevodin, J.P. O'Neill, S.V. Prasad, and J.S. Zabinski: *J. Vac. Sci. Technol. A*, 1999, vol. 17, pp. 986-92.
17. S. Ghaisas, R.D. Vispute, S.V. Ogale, S.M. Choudhari, S.M. Kanetkar, S.K. Kulkarni, S. Mahamuni, S. Badrinarayan, and S.V. Ghaisas: *J. Mater. Res.*, 1992, vol. 7, pp. 3250-54.
18. L.E. Toth: *Transition Metal Carbides and Nitrides*, Nova Science, New York, NY, 1971.
19. A. Cavaleiro, M.T. Vieira, and G. Lemperiere: *Thin Solid Films*, 1990, vol. 185, pp. 199-217.
20. S. Veprek, P. Nesladek, A. Niederhofer, F. Glatz, M. Jilek, and M. Sima: *Surf. Coating Technol.*, 1998, vols. 108–198, pp. 138-47.
21. S. Veprek: *J. Vac. Sci. Technol. A*, 1999, vol. 17, pp. 2401-20.
22. H. Holleck: *J. Vac. Sci. Technol. A*, 1986, vol. 4, pp. 2661-69.
23. *ASM Handbook of Ternary Alloy Phase Diagrams*, ASM INTERNATIONAL, Materials Park, OH, 1995.
24. H. Holleck and H. Shulz: *Thin Solid Films*, 1987, vol. 153, pp. 11-17.
25. *Powder Diffraction File, Release 1998*, International Center of Diffraction Data, Newtown Square, PA, 1998.
26. B.D. Cullity: *Elements of X-ray Diffraction*, 2nd ed., Addison-Wesley Publishing Company, Reading, MA, 1978, pp. 447-78.
27. M. Ohring: *Engineering Materials Science*, Academic Press, Boston, MA, 1995, p. 790.
28. S.H. Koutzaki, J.E. Krzanowski, and J.J. Nainaparampril: *J. Vac. Sci. Technol. A*, 2001, vol. 19, pp. 1912-1918.
29. R. Messier, A.P. Giri, and R. Roy: *J. Vac. Sci. Technol. A*, 1984, vol. A2, p. 500.
30. Y. Pauleau and P. Gouy-Pailler: *J. Mater. Res.*, 1992, vol. 7, pp. 2070-79.
31. P.K. Srivastava, V.D. Vankar, and K.L. Chopra: *J. Vac. Sci. Technol. A*, 1986, vol. 4, pp. 2819-26.
32. *Handbook of X-ray Photoelectron Spectroscopy*, J. Chastain and R. King, Jr., eds., Physical Electronics, Inc., Eden Prarie, MN, 1995, p. 41.
33. Jakob Schiøtz, Francesco D. Di Tolla, and Karsten W. Jacobsen: *Nature*, 1998, vol. 391, p. 561.
34. A. Lasalmonie and J.L. Strudel: *J. Mater. Sci.*, 1986, vol. 21, pp. 1837-52.
35. A.H. Chokshi, A. Rosen, J. Karch, and H. Gleiter: *Scripta Met.*, 1989, vol. 23, pp. 1679-84.

journal

J. Am. Ceram. Soc., 84 [3] 672–74 (2001)

Mechanical Properties of Sputter-Deposited Titanium-Silicon-Carbon Films

James E. Krzanowski* and Sirma H. Koutzaki

Mechanical Engineering Department, University of New Hampshire, Durham, New Hampshire 03824

The effect of SiC additions on the mechanical properties of TiC films was investigated. Ti-Si-C films with varying SiC content were deposited using dual-cathode radio-frequency magnetron sputtering. The nanoindentation hardness of these films increased with SiC content to a maximum of 20–22 GPa for films in the range of 15–30 at.% SiC. The elastic modulus was also measured, and the hardness to modulus ratio (*H*/*E*) increased with SiC content, indicating that hardness increases were due to microstructural effects. The residual stress was measured in several films, but was low in magnitude, indicating that hardness measurements were not influenced by residual stress. TEM examination of several films revealed that the SiC additions altered the film microstructure in a manner that could account for the observed hardness increases.

I. Introduction

TITANIUM CARBIDE is widely used in tribological applications because of its superior hardness, wear resistance, and low friction. The hardness of bulk TiC is generally reported to be 28–30 GPa.[1,2] Numerous studies have been conducted that report property improvements in titanium-based hard coatings as a result of compositional modifications. The addition of silicon to TiN films deposited by physical and chemical vapor deposition methods has yielded coatings with high hardness levels.[3–6] The addition of silicon to TiC films has been examined in several studies,[7–12] but the hardness of these films has not greatly exceeded that of bulk TiC. Results for physical vapor deposition (PVD) films of Ti-Si-C-N recently have been reported, and they have shown hardness levels in the 15–35 GPa range, along with a highly disordered structure.[13]

Thermodynamically, the TiC compound is reported to be immiscible with SiC; therefore, phase separation during deposition may be possible and lead to higher strength levels. However, it is necessary to deposit at temperatures below which coarsening of the two-phase structure would occur, making PVD methods more suitable than chemical vapor deposition (CVD) methods. In the present work, we have deposited Ti-Si-C films by radio-frequency (rf) magnetron sputter deposition from dual TiC/SiC targets. The SiC content of these films was varied by adjusting the relative power of each sputter gun. We report here the nanoindentation hardness and residual stress in these films as a function of composition.

Investigations of compositional and microstructural effects on the mechanical properties of thin-film coatings are often complicated by the fact that the results can be strongly dependent on the deposition method and parameters used. Deposition of films at relatively low temperatures using nonenergetic deposition methods often results in films with low density and hardness; therefore, energetic ion assist or substrate bias is often used in conjunction with PVD processes. However, synergistic effects between substrate bias and compositional changes cannot be ruled out; therefore, in the present study, we have investigated purely compositional effects. Moreover, other relevant parameters—such as film thickness, gas pressure, and substrate type and condition—have been held constant for each set of films investigated.

II. Experimental Methods

Ti-Si-C films were deposited in a sputter deposition chamber with a base pressure of $\sim 10^{-7}$ torr ($\sim 1.3 \times 10^{-5}$ Pa), which was then backfilled with high-purity argon for sputtering at a pressure of 8.9 mtorr (~1.2 Pa). The films were rf cosputtered from dual targets, using targets of TiC and SiC. Targets were obtained from commercial vendors and were fabricated by hot pressing under argon from 99.5%-pure carbide powders. The film thickness was in the range of 0.35–0.7 μm, but constant for each set of films, as listed below. The substrates used were (111) silicon wafers and Inconel 600. The temperature of deposition was 650°C for the silicon substrates and 500°C for Inconel. In some cases, the substrates were ion etched in the deposition chamber just prior to deposition, using 1 keV Ar^+ ions to remove the native oxide.

Three different sets of Ti-Si-C films were deposited by cosputtering of TiC and SiC. Resulting film compositions were measured using X-ray photoelectron spectroscopy (XPS; Kratos Analytical, Inc., Chestnut Ridge, NY) to determine the absolute atomic percent of each element. For the purpose of this paper, we report the relative atomic percent of silicon, (rel.at.% Si = at.% Si/(at.% Si + at.% Ti) × 100). The carbon content for the films did not vary significantly with silicon content, and it was between 44 and 48 at.% for most films. Oxygen content was between 2 and 7 at.%. The composition ranges and deposition parameters for each set were as follows: (1) Ti-Si-C films deposited at 650°C on unetched silicon (i.e., as-received silicon with the native oxide) in the range of 0–38 rel.at.% Si, with a thickness of 0.35 μm; (2) Ti-Si-C films deposited at 650°C on ion-etched silicon substrates in the range of 0–17 rel.at.% Si (0.5 μm); and (3) Ti-Si-C films deposited at 500°C on Inconel substrates in the range of 0–21 rel.at.% Si (0.7 μm). X-ray diffractometry (XRD) analysis of these films revealed only fundamental face-centered cubic (fcc) reflections, indicative of NaCl-type TiC, ZnS-type β-SiC, or a solid-solution phase; no hexagonal α-SiC peaks were observed.[14] Further analysis of phases present was complicated by the nearly identical lattice parameters of TiC and β-SiC.[15] However, XRD studies did confirm the absence of reaction products forming between the film and substrate materials.

Film hardness was tested using a nanomechanical test instrument (Hysitron, Inc., Minneapolis, MN) equipped with a Berkovich indenter. Films were tested using a multiple-loading sequence with loads ranging from 0.3 to 3 mN. For each film, 6–8 indentations were made, with each of the multiple-loading sequences giving 10 hardness (*H*) and elastic modulus (*E*) values.

G. Pharr—contributing editor

Manuscript No. 188486. Received June 12, 2000; approved December 11, 2000.
Supported by the U.S. Air Force Office of Scientific Research under Grant No. F49620-98-1-0499.
*Member, American Ceramic Society.

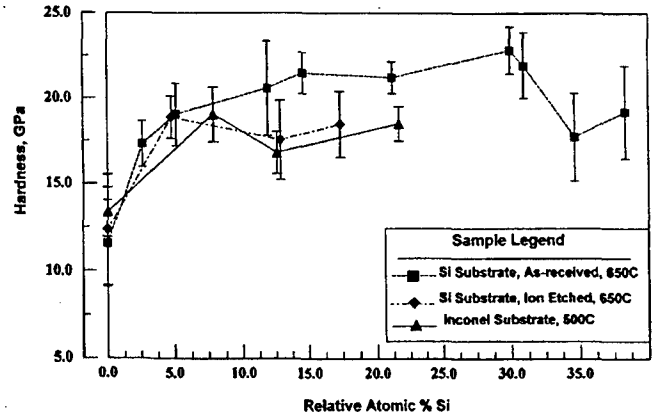

Fig. 1. Nanoindentation hardness of sputter-deposited Ti-Si-C films as a function of silicon content.

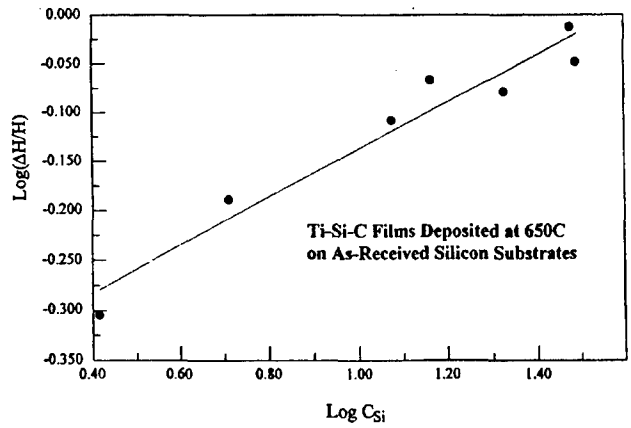

Fig. 2. Plot of the relative hardness increase, $\Delta H/H$, as a function of silicon content for films deposited at 650°C on as-received silicon substrates. Plotted line is a fit to the data and follows the equation $\Delta H/H = 0.42C_{Si}^{0.242}$.

Values obtained at depths of <20 nm were not considered reliable and, therefore, not used. Maximum indentation depths ranged from 10% to 20% of the film thickness. Indentation depths exceeding 10% of the film thickness could potentially exhibit substrate effects, and, because the substrates used here (silicon and Inconel) were softer than the coatings, the actual values may be higher than reported. However, our primary focus was to determine the change in hardness with silicon additions. Also, film hardness values for silicon versus Inconel substrates at similar silicon contents did not differ greatly, and the plots of hardness versus indentation depth did not show substantial changes with depth, indicating that substrate effects did not strongly influence our measurements. The residual stress measurements were conducted using a diffractometer (Model GADDS, Bruker/AXS Instruments, Madison, WI) equipped with an area detector and Cr$K\alpha$ radiation. Data analysis for residual stress was done using the standard $\sin^2 \psi$ method, with ψ angles ranging from 47° to 52°. Because the peaks from the films were generally broad and often weak, reliable stress measurements could be made only on a few films. Moreover, the minimum peak shift that could be reliably measured was ~0.04° 2θ, which resulted in an accuracy in the measured stress of ±200 MPa. Transmission electron microscopy (TEM) was used to examine the microstructure of several films. Planar sections were made from samples deposited on silicon substrates by dimpling and ion milling from the back side. Bright-field TEM images were obtained (Model H-600, Hitachi, Ltd., Tokyo, Japan) at 100 kV.

III. Results and Discussion

The hardness data for the Ti-Si-C films are shown in Fig. 1. The hardness values for TiC alone are in the range of 10–15 GPa, which is less than that for bulk TiC, most likely because of lower film density, as noted above. Small additions of SiC (on the order of 3–5 rel.at.% Si) significantly increase the hardness values. Higher SiC contents result in additional, but less dramatic, hardness increases, followed by a decrease in hardness at the highest silicon concentrations. Overall, hardness levels of almost two times that obtained for the sputtered TiC films are obtained, resulting in a maximum hardness in the range of 20–22 GPa. Films of SiC alone have a hardness of 9–10 GPa; therefore, the observations cannot be attributed to a rule-of-mixtures hardening.

The hardness data for films on the ion-etched substrates as well as the films deposited on Inconel appear slightly lower than the films deposited on as-received silicon at the higher silicon contents. For films on the ion-etched silicon, this may be due to a larger grain size that would be expected because of a more epitaxial growth on clean silicon. For Inconel, this may be due to lower deposition temperature or substrate effect on the hardness measurements. However, despite the fact that Inconel is considerably softer than silicon, the hardness levels are comparable, indicating that the deposition temperature is most likely the cause of the lower hardness.

Using the data for films deposited at 650°C on as-received silicon substrates, and a composition range of 0–31 at.% Si, the hardness increment above pure TiC has been fitted to the equation $\Delta H/H = 0.42C_{Si}^{0.242}$, as shown in Fig. 2. The exponent of 0.242 indicates a moderate dependence of the hardness on the silicon concentration (C_{Si}), and it shows that the most significant increases in hardness are obtained at the lower silicon contents.

Besides hardness data, the nanoindentation method provides data on elastic modulus as a reduced modulus, which is almost that of the film modulus when the values are much less than that of the diamond indenter. The elastic modulus values for the films tested here are in the range of 197–224 GPa. No systematic variation in modulus is observed with silicon content. However, these values are well below the accepted value of 460 GPa for fully dense TiC. Elastic modulus values measured for bulk carbide materials are known to be strongly dependent on the density of the sample. In many cases, full density is not obtained in sintered samples, resulting in a lower elastic modulus.[2] In thin films, full density is also often not obtained, particularly for films deposited at T/T_m values of <0.3 (T/T_m = 0.21 for the TiC films deposited at 650°C). (T_m represents the melting point of the material.)

One hypothesis for the effect of silicon on hardness might be that it increases the film density. In that case, both the modulus and hardness would increase, and the hardness to modulus ratio (H/E) would be relatively constant. However, because the modulus values for TiC and SiC are similar, if a true metallurgical-type strengthening mechanism (i.e., Hall–Petch hardening, precipitation hardening, or solid-solution hardening) is operating, the H/E ratio should increase with increasing silicon content. The values of H/E versus silicon content are shown in Fig. 3 for films deposited on as-received silicon substrates at 650°C. The value of H/E for the

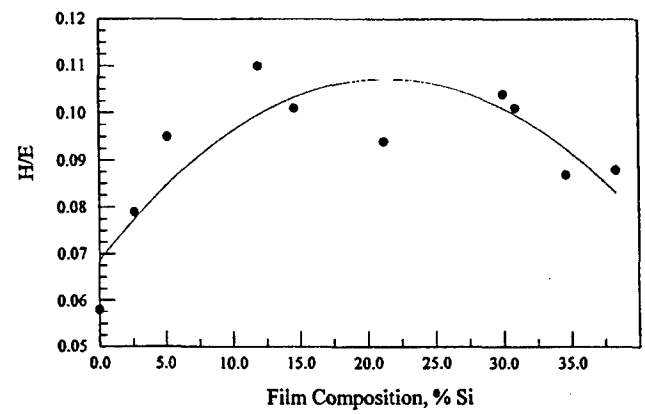

Fig. 3. Hardness relative to elastic modulus for films deposited at 650°C on as-received silicon. Plotted line serves only to guide the eye.

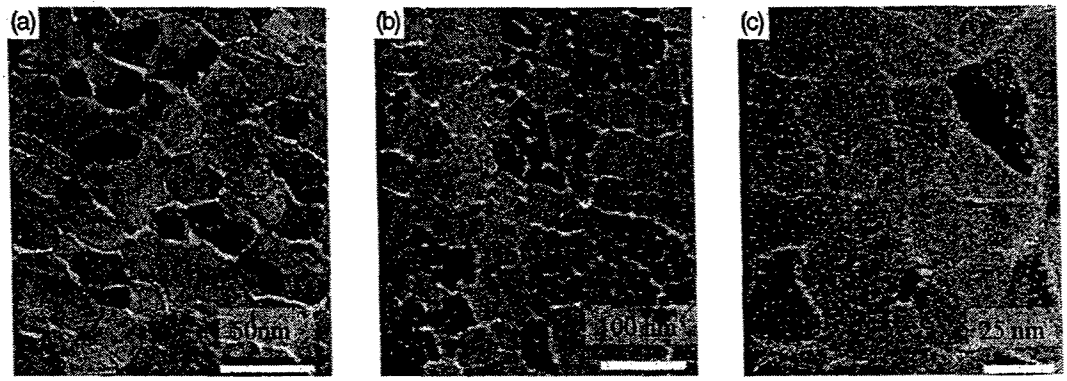

Fig. 4. Bright-field TEM images of films deposited at 650°C on silicon substrates: (a) TiC film, (b) Ti-Si-C film with 5 rel.at.% Si, and (c) Ti-Si-C film with 15 rel.at.% Si.

TiC film is 0.058, which is almost the value of 0.065 computed from bulk values for TiC. With increasing silicon content, the *H*/*E* ratio increases to larger values, with a maximum of almost 0.11. Also, the compositional trend in *H*/*E* values scales approximately with the hardness values. This result indicates that a metallurgical-strengthening mechanism, such as grain refinement or precipitation of a second phase, is the source of the hardness enhancements, because these generally do not affect the elastic modulus of the material.

Further evidence for a microstructural-strengthening mechanism is obtained from TEM images of several samples. Figure 4 shows bright-field TEM images of three specimens: pure TiC, and samples with 5 and 15 rel.at.% Si. The TiC sample has a 25 nm grain size with a relatively low defect content within the grains. At 5 rel.at.% Si, larger grains are present but are subdivided into subgrains that average 16 nm in diameter. In the sample with 15 rel.at.% Si, the grains have a mottled or grainy appearance, which may be due to fine-scale phase separation between the TiC and SiC phases. This mottled structure also is observed in the sample with 31 rel.at.% Si. The intergranular phase observed in these images has been found by high-resolution imaging to be amorphous material, explaining the low modulus values obtained. Microstructural changes with silicon content are evident, and a refined structure with reduced crystallinity develops with increased silicon content, which can be correlated with the hardness increases. A more-detailed investigation of these microstructural features is currently underway.

The film hardness also can be influenced by residual stress;[16,17] therefore, it is necessary to eliminate this as a factor in the observations. We have measured residual stress using XRD methods in a TiC film and two TiC–SiC films. The TiC film has a measured stress of −26.4 MPa (i.e., compressive) and the two TiC–SiC films measured, with rel.at.% Si of 4.78 and 17.33, have values of −284 and −173 MPa, respectively. Because the peaks are generally broad, the exact peak location is difficult to define, and, as noted above, the estimated accuracy of the measurement is ±200 MPa. These results demonstrate that the residual stresses are low (close to the measurement limit of our technique), and we conclude the hardness measurements are not influenced by the presence of a residual stress.

IV. Conclusions

(1) Additions of SiC to TiC in sputter-deposited films increased the hardness to a maximum of 20–22 GPa for films containing 15–30 rel.at.% Si, almost two times that of sputtered TiC without SiC additions.

(2) The hardness increment above pure TiC was fitted to the equation $\Delta H/H = 0.42C_{Si}^{0.242}$.

(3) The experimentally determined *H*/*E* ratios increased with the concentration of silicon in the films, and it exceeded that calculated for pure TiC. This suggested that adding SiC to the films altered the film microstructure in a manner that enhanced hardness.

(4) TEM examination of the microstructure of several films revealed a refinement of structural features and possible phase separation in films with high SiC contents.

Further characterization studies are currently underway to better understand the nature of these microstructural changes. Moreover, although it is encouraging that reasonably high hardness levels can be obtained without substrate bias, the addition of substrate bias likely enhances the hardness further, and this is also under current investigation. Nonetheless, our results show that SiC additions can strengthen TiC films when deposited under appropriate conditions (namely a suitable temperature), which is a potentially useful result for hard-coating applications. Furthermore, Ti-Si-C represents an interesting materials system that can be used to better understand strengthening mechanisms in hard coatings.

References

[1]M. Ohring, *The Materials Science of Thin Films*; pp. 551–79. Academic Press, Boston, MA, 1992.

[2]L. E. Toth, *Transition Metal Carbides and Nitrides*; pp. 6–7 and 143–46. Nova Science, New York, 1971.

[3]S. Li, Y. Shi, and H. Peng, "Ti-Si-N Films Prepared by Plasma-Enhanced Chemical Vapor Deposition," *Plasma Chem. Plasma Process.*, **12**, 287–97 (1992).

[4]F. Vaz, L. Rebouta, S. Rambos, M. F. da Silva, and J. S. Soares, "Physical, Structural, and Mechanical Characterization of $Ti_{1-x}Si_xN_y$ Films," *Surf. Coat. Technol.*, **108–109**, 236–40 (1998).

[5]M. Diserens, J. Patscheider, and F. Levy, "Improving the Properties of Titanium Nitride by Incorporation of Silicon," *Surf. Coat. Technol.*, **108–109**, 241–46 (1998).

[6]K. H. Kim and B. H. Park, "Mechanical Properties and Oxidation Behavior of Ti-Si-N Films Prepared by Plasma-Assisted CVD," *Chem. Vap. Deposition*, **5**, 275–79 (1999).

[7]M. Touanen, F. Teyssandier, M. Ducarroir, and J. L. Derep, "SiC–TiC Multiphased Materials Obtained by CVD," *Mater. Sci. Eng. A*, **147**, 239–47 (1991).

[8]C. Kawai and M. Miyake, "Fabrication and Characterization of CVD-Deposited TiC–SiC Composites," *J. Ceram. Soc. Jpn.*, **99**, 1046–52 (1991).

[9]T.-T. Lin, J.-F. Chang, and M.-H. Hon, "The Growth and Characteristics of CVD SiC–TiC *in Situ* Composites," *Ceram. Int.*, **24**, 265–72 (1998).

[10]R. Lowden, K. L. More, T. M. Besmann, and R. D. James, "Microstructural Characterization of Multiphase Coatings Produced by Chemical Vapor Deposition," *Mater. Res. Soc. Symp. Proc.*, **168**, 159–65 (1990).

[11]T. Takeuchi, H. Miyoshi, Y. Egashira, and H. Komiyama, "Chemical Vapor Deposition of Silicon Carbide/Titanium Carbide Composite Films from Dichlorodimetthylsilane, Titanium Tetrachloride, and Methane," *J. Electrochem. Soc.*, **146**, 564–69 (1999).

[12]M. Touanen, F. Teyssandier, M. Ducarroir, M. Maline, R. Hiller, and J. L. Derep, "Microcomposite and Nanocomposite Structures from Chemical Vapor Deposition in the Silicon-Titanium-Carbon System," *J. Am. Ceram. Soc.*, **76**, 1473–81 (1993).

[13]D. V. Shtansky, E. A. Levashov, A. N. Sheveiko, and J. J. Moore, "Synthesis and Characterization of Ti-Si-C-N Films," *Metall. Mater. Trans. A*, **30A**, 2439–47 (1999).

[14]J. E. Krzanowski, S. H. Koutzaki, J. Nainaparampil, and J. S. Zabinski, "Phase Formation and Mechanical Properties of Multiphase Carbide Coatings," *Mater. Res. Soc. Symp. Proc.*, **594**, 181–86 (2000).

[15]Powder Diffraction File Card Nos. 32-1383 (TiC) and 29-1129 (SiC), International Centre for Diffraction Data, Newtown Square, PA.

[16]T. Y. Tsui, W. C. Oliver, and G. M. Pharr, "Influence of Stress on the Measurement of Mechanical Properties Using Nanoindentation: Part I. Experimental Studies in an Aluminum Alloy," *J. Mater. Res.*, **11**, 752–59 (1996).

[17]A. Bolshakov, W. C. Oliver, and G. M. Pharr, "Influence of Stress on the Measurement of Mechanical Properties Using Nanoindentation: Part II. Finite-Element Simulations," *J. Mater. Res.*, **11**, 760–68 (1996). □

Structure and mechanical properties of Ti–Si–C coatings deposited by magnetron sputtering

S. H. Koutzaki and J. E. Krzanowski[a)]
Mechanical Engineering Department, University of New Hampshire, Durham, New Hampshire 03824-3591

J. J. Nainaparampril
Systran, Inc., Dayton, Ohio

(Received 8 September 2000; accepted 23 April 2001)

Nanostructured coatings consisting of mixed carbide phases can provide a potential means to developing superhard coatings. Heterogeneous nanostructured coatings can be obtained by either deposition of multilayer structures or by depositing film compositions that undergo a natural phase separation due to thermodynamic immiscibility. In the present work, we have taken the latter approach, and deposited films by radio frequency cosputtering from dual carbide targets. We have examined a number of ternary carbide systems, and here we report the results obtained on Ti–Si–C films with a nominal $(Ti_{1-x}Si_x)C$ stoichiometry and with $x \leq 0.31$. It was found that the nanoindentation hardness increased with Si content, and the maximum hardness achieved was nearly twice that of sputter-deposited TiC. We further analyzed these films using high-resolution transmission electron microscopy (TEM), x-ray photoelectron spectroscopy (XPS), and x-ray diffraction. Since cubic SiC has an x-ray pattern almost identical to that of TiC, the extent of phase separation could not be determined by that method. However, XRD did demonstrate a general disordering of the films with increasing SiC content. In addition, a mottled structure was observed in high-resolution TEM images of the Si-containing films, confirming microstructural effects due to the Si additions. © *2001 American Vacuum Society.* [DOI: 10.1116/1.1379322]

I. INTRODUCTION

The protection of materials by hard coatings is one of the most important means of improving the performance of components subject to repeated rolling and sliding contacts.[1,2] Coatings that are typically used in these applications include metallic carbides and nitrides, both of which can reduce friction and wear.

The mechanical properties of hard coatings can potentially be improved by modifying the coating composition to creating multiphase nanocomposite structures.[3,4] The objective of our work is to develop nanostructured multiphase carbide coatings with mechanical and tribological properties superior to that of pure carbides. We have examined a number of candidate ternary carbide systems that exhibit miscibility gaps and compositional regions with multiple carbide phases.[5] It was found that weakly immiscible systems, such as the Ti–Mo–C and Ti–W–C, tend to exhibit large supersaturation and form single-phase structures when deposited in thin-film form.

A more promising system is the Ti–Si–C ternary carbide system, which is the subject of this article. In the Ti–Si–C system, the carbide phases TiC and SiC are essentially insoluble.[6] Phase separation is therefore likely to occur, and this could lead to strengthening of the coating. A considerable amount of research has been carried out to investigate the phase relations in the ternary Ti–Si–C system.[7–9] The main purpose of this research was to find the optimal conditions for creating ceramic composites with improved fracture toughness.[10–14] The formation of Ti–Si–C deposits by chemical vapor deposition (CVD) has been studied in detail by Touanen *et al.*[8,15,16] The microhardness of the nanocomposite Ti–Si–C samples was lower than that of the binary compounds and was attributed to the ⟨220⟩ preferred orientation of the deposits.[16] However, no solid solution between TiC and SiC were detected in any of the studies.

In the present study we have fabricated Ti–Si–C films by radio frequency (rf) magnetron cosputtering from dual TiC/SiC targets, thus allowing us to maintain a nominal $(Ti_{1-x}Si_x)C$ stoichiometry. We report on the microstructural, mechanical, and electrical properties of these films. Probably the most important advantage of physical vapor deposition is that substrate lower temperatures, typically 200–600 °C, can be used, compared to 800–1200 °C required for CVD. It is expected that this lower deposition temperature will lead to phase separation on a finer scale, ultimately giving higher hardness.

II. EXPERIMENTAL METHODS

Ti–Si–C films were deposited using rf magnetron sputtering. Films were cosputtered from dual targets in a chamber with a base pressure of $\sim 10^{-7}$ Torr, which was then backfilled with high-purity Ar for sputtering to a pressure of 8.9×10^{-3} Torr. One of the sputtering guns contained the TiC target and the other gun contained the SiC target. The relative power applied to each target was varied to obtain films with a wide range of compositions. The targets were obtained from commercial vendors, and were fabricated by hot pressing under argon from 99.5% purity carbide pow-

a)Electronic mail: jamesk@cisunx.unh.edu

TABLE I. Chemical composition and hardness of Ti–Si–C films.

Specimen No.	Power ratio P_{SiC}/P_{TiC}	Ti (at. %)	Si (at. %)	C (at. %)	O (at. %)	Relative at. % Si	Hardness (GPa)
TiC film	0	47.9	0.0	50.1	2.0	0.0	11.6
SiC film	···	0.0	44.7	50.0	5.3	100.0	9.5
1-TS[a]	0.10	45.1	1.2	47.8	5.9	2.6	17.3
2-TS[a]	0.20	42.2	2.3	53.6	1.9	5.2	19.1
3-TS[a]	0.30	39.8	5.4	46.9	7.9	11.9	20.6
4-TS[a]	0.40	39.7	6.8	47.1	6.4	14.6	21.5
5-TS[a]	0.50	39.4	10.0	45.1	5.5	20.2	21.2
6-TS[a]	0.60	33.2	14.2	44.7	7.9	30.0	22.8
7-TS[a]	0.70	32.8	14.7	48.6	3.9	30.9	21.9
8-TS[a]	0.80	31.5	16.7	48.6	3.2	34.6	17.8
9-TS[a]	0.90	30.7	19.1	47.0	3.2	38.4	19.2
1-i.e.[b]	0.18	46.0	2.3	47.8	3.9	4.8	18.9
2-i.e.[b]	0.21	42.4	6.3	48.3	3.0	12.9	17.6
3-i.e.[b]	0.25	41.2	8.6	47.3	2.9	17.3	18.5
1-inco[c]	0.10	43.3	3.7	47.4	5.6	7.9	19.1
2-inco[c]	0.20	42.1	6.1	46.8	5.0	12.6	16.8
3-inco[c]	0.30	41.3	11.4	40.9	6.4	21.7	18.5

[a]Films on as-received Si substrates deposited at 650 °C.
[b]Films on ion-etched prior to deposition Si and sapphire substrates deposited at 650 °C.
[c]Films on Inconel substrates (ion-etched) deposited at 500 °C.

ders. The substrates used were (111) silicon wafers, *R*-plane sapphire, and Inconel 600 alloy. The substrate temperatures were 650 °C for the Si and sapphire substrates, and 500 °C for the Inconel. In addition, several films were deposited at 220 and 400 °C as specified in the following section. In some cases, the substrates were cleaned in the deposition chamber by ion etching with 1 keV Ar^+ ions for 15 min just prior to deposition to remove surface oxides. The deposition rate was measured *in situ* using a quartz crystal oscillator thickness rate monitor. The deposition rates were confirmed by observing fractured cross sections edge-on in the scanning electron microscope (SEM). Films were in the range 0.35–0.70 μm, but constant within each set as listed later.

Coating composition was determined by x-ray photoelectron spectroscopy (XPS) on a Kratos Analytical instrument using monochromatic Mg $K\alpha$ x-ray source operating at 15 kV. X-ray diffraction (XRD) was used for phase identification, texture and grain size evaluation. The analyses were performed using Cu $K\alpha$ radiation on a θ–θ Rigaku D-MAX/B diffractometer. Coating microstructure and morphology were evaluated using transmission electron microscopy (TEM) of planar sections. These samples were made by dimpling and ion milling from the backside of coated Si substrates. The samples were analyzed on a Hitachi H-600 TEM operating at 100 kV. High-resolution TEM (HRTEM) for more detailed structural analyses was conducted on a JEOL JEM-2010 TEM operating at 200 kV, with the objective aperture set to include both the (111) and (200) diffraction rings. The x-ray $\sin^2\psi$ method was used to measure the film stresses,[17] and is described in detail elsewhere.[5] The electrical resistivity of the Ti–Si–C films deposited on silicon substrates was measured with a four-point probe Signatone SYS-301. A correction factor was applied to account for the geometrical shape and the dimensions of the specimens. Four measurements were made on each sample, and the maximum error was found to be ±3.2%.

Nanoindentation was used to measure film hardness and was conducted on a Hysitron nanomechanical test instrument equipped with Berkovich indenter. A detailed explanation of the procedures, as well as analysis of the mechanical property results for the sputtered films, has been presented in a previous publication.[18]

III. RESULTS

A. Composition and properties of sputter deposited Ti–Si–C films

The compositions of the codeposited TiC/SiC films as determined by XPS are shown in Table I along with the relevant deposition conditions. The film compositions are shown both in terms of absolute atomic percent, as well as a relative Si concentration, defined as

$$\text{Relative at.\% Si} = [\text{at.\% Si}/(\text{at.\% Si} + \text{at.\% Ti})] \times 100.$$

The first set of films, consisting of specimens 1-TS to 9-TS, was deposited on both as-received (i.e., not cleaned by ion etching) silicon and sapphire substrates at 650 °C in the compositional range of 2.6–38.3 relative at. % Si. Additional films (not shown in the table) with a composition near 12 relative at. % Si were deposited on as-received Si and sapphire substrates at four different temperatures: room temperature, 220, 400, and 650 °C. The next set of films was deposited on silicon and sapphire substrates ion-etched (1 keV Ar^+ ions, 15 min) prior to deposition at 650 °C, and had compositions ranging from 4.8 to 17.3 relative at. % Si (specimens 1-i.e. to 3-i.e.). Films on ion-etched Inconel substrates were deposited at 500 °C and had 7.9–21.7 relative at. % Si (specimens 1-inco to 3-inco). Pure TiC and SiC

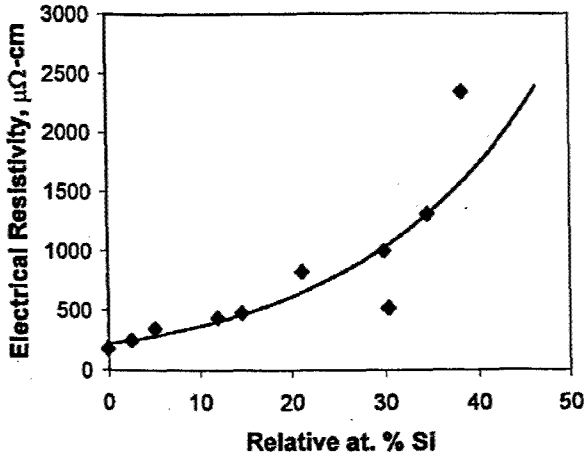

FIG. 1. Electrical resistivity of Ti–Si–C films deposited on as-received Si substrates at 650 °C.

films were also deposited with each series of films. Table I also shows results for a TiC and a SiC film deposited on silicon substrates at 650 °C. The carbon content of the films was near the stoichiometric concentration (between 45 and 50 at. %) with the exceptions of samples 2-TS (53.6%) and 3-inco (40.9%). The oxygen contents of the films ranged from 1.9% to 7.9%.

The mechanical properties of these films have been presented in detail in a previous work,[18] so the nanoindentation hardness data obtained are only summarized in Table I. The hardness value of TiC alone is 12 GPa. Small additions of SiC (on the order of 3–5 at. %) significantly increase the hardness, resulting in films in the range of 17–19 GPa. Higher SiC contents result in additional, but less dramatic hardness increases, with a maximum hardness of about 22 GPa. To ensure that the observed hardness trends in our films were not due to a residual stress effect, we measured residual stress in one TiC and two Ti–Si–C films. The TiC film had a measured stress of −26.4 MPa and the two TiC–SiC films measured had values of −284 and −173 MPa, all of which are relatively low levels of stress and unlikely to affect hardness measurements.

Limited tribological testing was also performed on several films. Friction tests of films on Inconel substrates were carried out on a ball-on-disk test machine using a $\frac{1}{4}$ in. diameter 440C steel ball. The friction coefficient of pure TiC film was 0.335, a typical value for TiC. A Ti–Si–C film with 7.9 at. % Si had a friction coefficient of 0.59, whereas the friction coefficient of a film with 21.7 at. % Si was 0.28. The lower critical load, obtained from a scratch test, was 15 N for the TiC film and 10–12 N for the Ti–Si–C films.

The variation in electrical resistivity of the Ti–Si–C films deposited on unetched Si substrates is shown in Fig. 1. The film resistivity is a strong function of the Si content in the films, ranging continuously from 182 $\mu\Omega$ cm for pure TiC film to ~2300 $\mu\Omega$ cm for the film with 38.3 at. % Si.[19–21] The resistivity of bulk TiC is about 60 $\mu\Omega$ cm,[22] whereas the value of our measurements is considerably higher (182 $\mu\Omega$ cm). This is believed to be due to a lower film density compared to the bulk.[23]

B. Structural characterization of the sputtered Ti–Si–C films

The carbide phases present in the films were identified by x-ray diffraction. XRD also provided information on the degree of crystallinity, texture and grain size. X-ray diffraction analysis was first conducted on pure TiC films. The crystallographic structure of the films was found to be consistent with the cubic B1 structure of the titanium carbide powder standard.[24] The XRD spectra of SiC films deposited at 650 °C showed a single silicon carbide phase present, identified as the cubic β-SiC phase with zinc-blende structure, with no indication of the hexagonal structure of SiC.

Figure 2 shows the XRD patterns for Ti–Si–C films deposited at 650 °C on as-received Si substrates (samples 1-TS–9-TS). Unfortunately, the x-ray patterns of TiC and β-SiC are nearly identical, hence, XRD was incapable of determining the extent of phase separation in Ti–Si–C films. However, other important film characteristics could still be obtained using XRD. The preferred orientation of films on Si substrates changes from (111) to mixed (111)/(200) with increasing the Si content. Two silicon-containing films (11.9% and 14.6% in Fig. 2) exhibited strong (311) reflections. At higher Si concentrations, the SiC additions also caused the peaks to broaden. This can be due to grain refinement or the formation of an amorphous component. Assuming it is due to grain size reductions, grain sizes were calculated from the x-ray peak broadening using the Scherrer formula and were found decrease from 35 nm for 2.6 rel. at. % Si to 6 nm for 38.3 rel. at. % Si. However, TEM results presented later will demonstrate that the broadening is due to more complex microstructural changes.

The x-ray patterns of Ti–Si–C films deposited at 650 °C on Si ion etched prior to deposition are shown in Fig. 3 (specimens 1-i.e. to 3-i.e.). All mixed carbide films deposited on ion-etched Si substrates are highly textured in the ⟨111⟩ direction and have better crystallinity than the films on unetched substrates. Ion etching the substrate promoted epitaxial growth of the film and resulted in larger grain sizes and a higher degree of crystallinity.

Film microstructure and morphology analysis was carried out first on pure TiC and SiC films using scanning and transmission electron microscopy. SEM examination of the fractured edge of a TiC film revealed a typical columnar structure. Figure 4(a) shows a bright-field TEM image of a TiC film deposited at 650 °C on an ion-etched silicon substrate. This image shows a crystalline film with a grain size of 30–40 nm, a relatively low defect content within grains and amorphous material (as later verified by HRTEM) between the grains. The selected area electron diffraction pattern shown in the inset confirms the face-centered-cubic structure of TiC.

Figure 4(b) shows a bright-field image of a SiC film deposited on Si substrate. In comparison to the TiC film, the SiC has a higher defect content within the grains, as well as

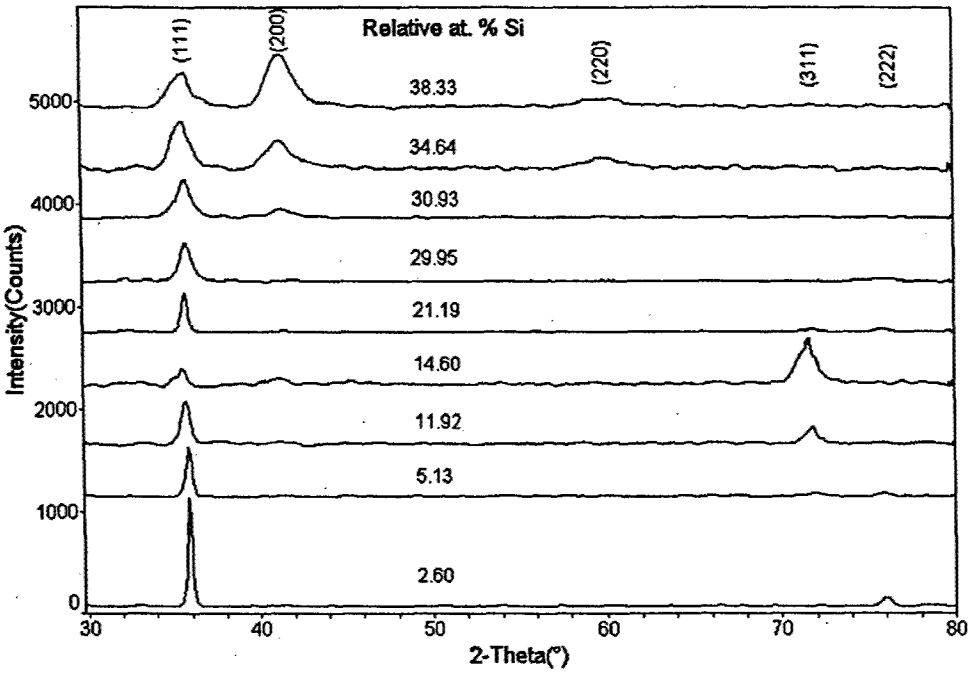

FIG. 2. XRD spectra of Ti–Si–C films deposited on as-received Si substrates at 650 °C. As the relative at. % Si is increased, the peaks become broader and a mixed orientation is obtained.

larger amount of the amorphous intergranular phase. The (111) and (200) diffraction rings of the diffraction pattern have merged into one broad uniform ring confirming the reduced crystallinity and randomly oriented grains, as also found by XRD.

TEM and HRTEM analyses were conducted on several Ti–Si–C films of different silicon concentrations. Figure 5(a) presents the TEM analysis of Ti–Si–C film with 14.6 rel. at. % Si (sample 4-TS in Table I). The grain size has not changed dramatically with the increased Si content, and an amorphous interlayer between grains is still observed. However, the grains now demonstrate a "mottled" or grainy appearance, a feature that was also observed in the samples with 30.9 at. % Si. This mottled structure is possibly due to phase separation and/or partial amorphization within the grains.

TEM analysis of a Ti–Si–C film with 17.3 relative at. % Si (sample 3-i.e., deposited on Si substrates ion-etched prior to deposition) is shown in Fig. 5(b). The grain size observed here is on the order of 50–75 nm, larger than that shown in Fig. 5(a). However, these grains, delineated by strong diffraction contrast, exhibit an internal structure that subdivides the grains into subgrains. Since the diffraction contrast is relatively constant within the grain, this suggests that the subgrains are rotated about the fiber axis. These subgrains are as small as 10 nm in diameter. A similar structure was

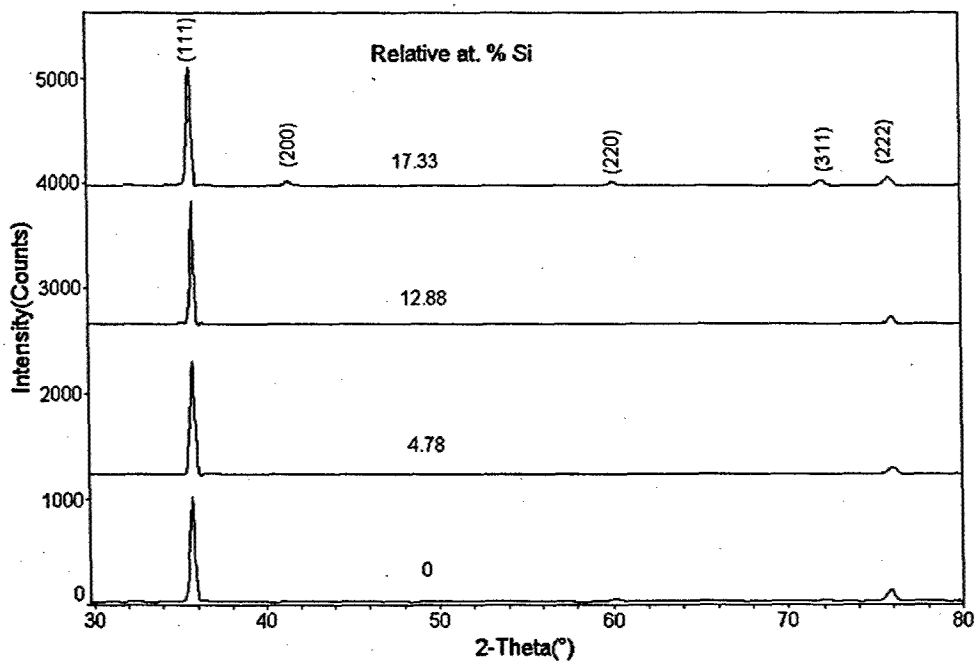

FIG. 3. XRD spectrums of Ti–Si–C films deposited on ion-etched silicon substrates at 650 °C. The peaks here are sharper and have smaller peak widths indicating a higher degree of crystallinity in comparison to the films deposited on as-received silicon.

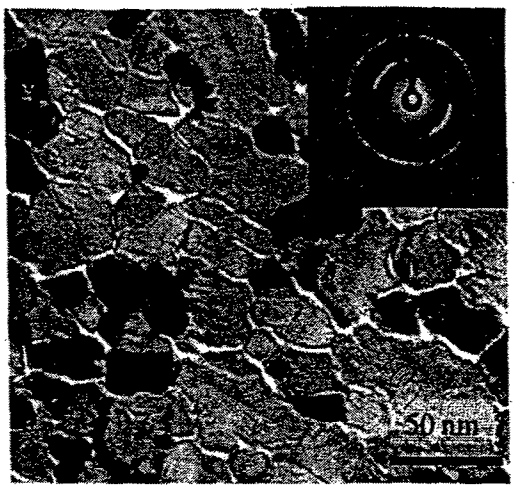

(a)

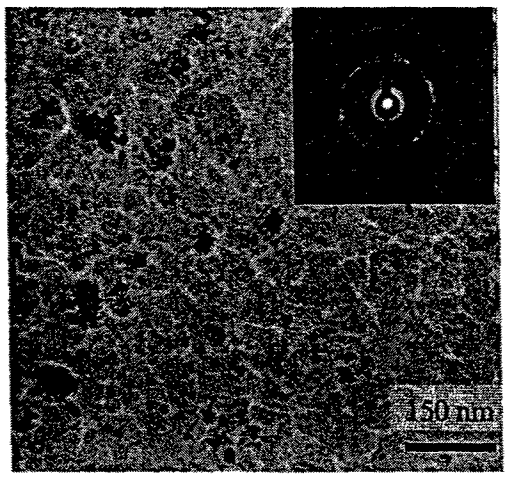

(b)

FIG. 4. Bright field TEM images and selected area diffraction patterns of (a) TiC and (b) SiC films deposited on silicon substrates at 650 °C. A higher degree of crystallinity was obtained in the TiC film.

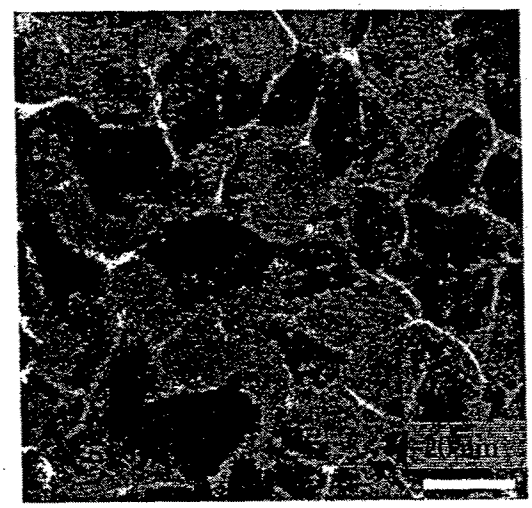

(a)

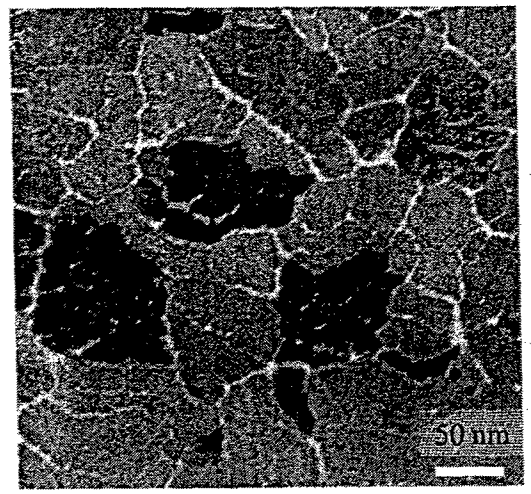

(b)

FIG. 5. Bright field TEM images of (a) Ti–Si–C film with 14.6 relative at. % Si deposited on as-received Si substrate at 650 °C showing a mottled structure within the grains; (b) Ti–Si–C film with 17.3 relative at. % Si deposited on ion-etched Si substrate at 650 °C showing subgrain divisions.

observed in specimen 2-TS with 5.1% Si deposited on as-received Si substrates.

Overall, for the samples examined here using TEM analysis, two types of structures were observed in the ternary Ti–Si–C films: (1) grains divided into subgrains, found in films with low Si content on as-received substates and in films with higher Si content deposited on ion-etched Si substrates; and (2) a mottled structure within the grains in films with higher Si content on as-received Si substrates.

High-resolution TEM was used to further investigate the structure of these films. Figure 6 shows HRTEM images of a TiC film in comparison to the Ti–Si–C film with 30.9 relative at. % Si. In the TiC grains the lattice fringes are continuous and long-range order is observed. However, in the Ti–Si–C film we observe small regions misoriented with respect to each other, rotated and curved lattice planes, and disordered regions, all of which disrupt the continuity of the lattice. This observation is similar to that made by Shtansky *et al.*[25] on Ti–Si–C–N films. An amorphous intergranular layer was observed in both types of films.

Further understanding of the mechanical properties of these films was obtained by examining the film structure near the edge of a microindentation. A sample of the 3-TS film was indented using a Vickers indenter and a load range of 0.5–1 N. Plan-view sections were made for TEM examinations, and an example is shown in Fig. 7. A crack is observed propagating away from the indent, and intergranular fracture is clearly evident. This demonstrates that the amorphous intergranular regions are the weakest part of the film, and reduction or elimination of this phase should improve the hardness.

High-resolution XPS showed no change in the binding energy of the Si $2p$ peak with increasing the Si content in the ternary Ti–Si–C films. It remained at 100.7 eV, the binding energy of the Si $2p$ peak determined for pure SiC. This value is close to the value of 100.5 eV found by Nainaparampil and Zabinski.[26] The binding energy of the Ti $2p_{3/2}$ peak was

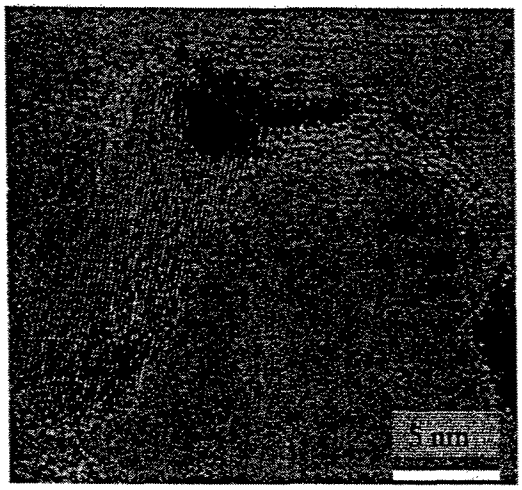

(a)

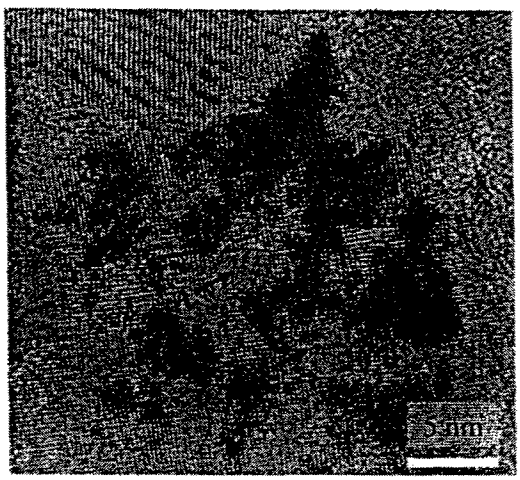

(b)

FIG. 6. High-resolution TEM images of (a) TiC film deposited on ion-etched Si substrate at 650 °C; (b) Ti–Si–C film with 30.9 relative at. % Si deposited on as-received Si substrate at 650 °C. Arrows indicated amorphous regions (A) and distorted lattice planes (along B).

found to be at 455.0 eV, which corresponds to titanium bonded in the carbidic state.[27] These results support the concept that the Si and Ti are bonding only to the carbon atoms in separate carbide phases.

IV. DISCUSSION

The alloying TiC with SiC in sputter deposited films has been found to increase the hardness of the films deposited in the range of 500–650 °C. The microstructural features responsible for the hardness increases have been investigated in this article. Thermodynamic phase diagram data indicates phase separation should occur between TiC and SiC, but kinetic limitations may inhibit phase separation leading to solid solutions or amorphous phases. Unfortunately, structural similarities between TiC and SiC as well as the fine nanoscale structures that form in these films make it difficult to assess the extent of phase separation. In addition to the work described earlier, x-ray microanalysis experiments were conducted on sample 4-TS in a Vacuum Generators HB603 field emission Scanning TEM, but the x-ray maps for Si and Ti failed to show any variation in the concentration of these elements between any grains.

X-ray diffraction analysis did show evidence for either grain refining or structural disordering as the Si content in the films increased. TEM analysis showed grain refinement in some samples, and a mottled structure in others. HRTEM showed that in samples with the mottled structure the crystal lattice was disrupted by structural interfaces, misoriented regions, and amorphous regions. These features are expected to impede dislocation slip and make plastic deformation more difficult, providing one explanation for the increased hardness of the films. Phase separation may also play an important role here, assuming that phase separation between TiC and SiC occurs on a scale smaller than the grain size, i.e., within the grains.

The maximum hardness increase observed in the Ti–Si–C films over that of pure TiC is about 10 GPa for films in the range of 12–20 relative at. % Si. Further increases in silicon content beyond what we have studied are likely to cause further amorphization of the structure, which may then lead

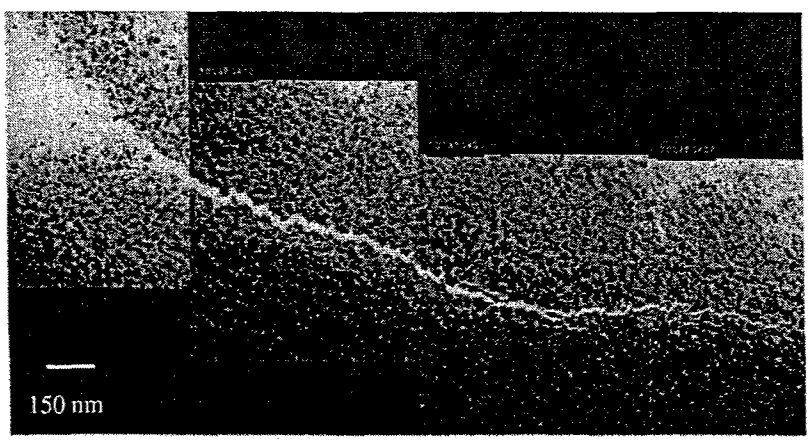

FIG. 7. TEM image of specimen 3-TS with 12 at. % Si, tested with Vickers microindenter. The original indent is at the upper left corner of the figure. The crack propagating away from the indent shows intergranular fracture.

to a decrease in hardness. In addition, if the observed microstructural features were due to phase separation between TiC and SiC, a temperature dependence on the hardness would be expected. Films deposited at low temperatures would be more highly disordered and have lower hardness. Therefore, deposition of the Ti–Si–C films needs to be carried out within a suitable temperature range in order to realize an increase in hardness.

Overall improvements in hardness values would likely be obtained if the substrates were biased, as it is well known that biasing substrates can lead to large compressive film stresses and higher film density. High bias voltages can cause structural disordering, which in our case may reduce the optimal Si concentration. Further research is currently underway to determine the effect of bias on sputtered Ti–Si–C films, and how the combined effect of Si additions and bias affect film microstructure and hardness.

V. SUMMARY AND CONCLUSIONS

The effect of Si on the structure and properties of TiC films has been examined in this article. This study has shown that Si additions can increase film hardness, and the microstructural factors responsible for this observation were investigated. The following observations and conclusions were obtained:

(1) X-ray diffraction analysis showed that the SiC additions to TiC reduced preferred orientation and created a more disordered structure, as indicated by peak broadening.

(2) TEM studies revealed that films with higher SiC content exhibited a mottled contrast within the grains, suggesting nanoscale phase separation, as well as an amorphous grain boundary layer. Lattice rotations and misorientations observed by HRTEM within the grains also suggest the presence of two different phases. In some samples, a reduced grain size was observed due to subgrain divisions.

(3) Hardening in these samples is attributed to the fact that the Si additions to TiC disorders the microstructure, but the structure still remains crystalline at the nanometer scale. This is essentially grain refining at an extremely fine scale. However, phase separation may also play a role, as a strengthening mechanism, but the extent of phase separation could not be assessed here.

(4) The electrical resistivity of the Ti–Si–C films was found to be a strong function of the Si content. The resistivity remained below 1000 $\mu\Omega$ cm for films with less than 30 at. % Si, indicating that Ti–Si–C films may be useful in diffusion barrier applications.

ACKNOWLEDGMENTS

The financial support of the Air Force Office of Scientific Research, under Grant No. F49620-98-1-0499, is gratefully acknowledged. This work made use of the MRSEC Shared Experimental Facilities at MIT supported by the National Science Foundation under Award No. DMR98-008941. The assistance of Dr. A. J. Garratt-Reed and Mike Frongillo for the HRTEM work is greatly appreciated.

[1]H. Holleck, J. Vac. Sci. Technol. A **4**, 2661 (1986).
[2]M. Ohring, *The Materials Science of Thin Films* (Academic, Boston, 1992), pp. 225, 578.
[3]S. Veprek, J. Vac. Sci. Technol. A **17**, 2401 (1999).
[4]A. A. Voevodin, S. V. Prasad, and J. S. Zabinski, J. Appl. Phys. **82**, 855 (1997).
[5]S. H. Koutzaki, M. S. thesis, Mechanical Engineering Department, University of New Hampshire, Durham, NH 03824, December 2000.
[6]*ASM Handbook of Ternary Alloy Phase Diagrams* (American Society of Metals, Metals Park, OH, 1995).
[7]S. Sambasivan and W. T. Petuskey, J. Mater. Res. **7**, 1473 (1992).
[8]M. Touanen, F. Teyssandier, and M. Ducarrior, J. Mater. Sci. Lett. **8**, 98 (1989).
[9]C. Racault, F. Langlais, and R. Naslain, J. Mater. Sci. **29**, 3384 (1994).
[10]C. Kawai and M. Miyake, J. Ceram. Sci. Jpn. **99**, 1046 (1991).
[11]T.-T. Lin, J.-F. Chang, and M.-H. Hon, Ceram. Int. **24**, 265 (1998).
[12]R. Lowden, K. L. More, T. M. Besmann, and R. James, Mater. Res. Soc. Symp. Proc. **168**, 159 (1990).
[13]G. S. Wei and P. F. Becher, J. Am. Ceram. Soc. **67**, 571 (1984).
[14]T. Takeuchi, H. Miyoshi, Y. Egashira, and H. Komiyama, J. Electrochem. Soc. **146**, 564 (1999).
[15]M. Touanen, F. Teyssandier, M. Ducarroir, and J. L. Derep, Mater. Sci. Eng., A **147**, 239 (1991).
[16]M. Touanen, F. Teyssandier, M. Ducarroir, M. Maline, R. Hiller, and J. L. Derep, J. Am. Ceram. Soc. **76**, 1473 (1993).
[17]B. D. Cullity, *Elements of X-ray Diffraction*, 2nd ed. (Addison-Wesley, Reading, MA, 1978).
[18]J. E. Krzanowski and S. H. Koutzaki, J. Am. Ceram. Soc. **84**, 672 (2001).
[19]P. M. Smith, J. S. Custer, J. G. Fleming, E. Roherty-Osmun, M. Cohn, and R. V. Jones, ISMIC Proc. **106**, 162 (1996).
[20]P. M. Smith and J. S. Custer, Appl. Phys. Lett. **70**, 3116 (1997).
[21]X. Sun, J. S. Reid, E. Kolawa, and M.-A. Nicolet, J. Appl. Phys. **81**, 656 (1997).
[22]L. E. Toth, *Transition Metal Carbides and Nitrides* (Nova Science, New York, 1971), pp. 6–7.
[23]J. E. Sundgren, B.-O. Johansson, S.-E. Karlsson, and H. T. G. Hentzell, Thin Solid Films **105**, 367 (1983).
[24]*JSPDS Data Cards* (International Center of Dffraction Data, Swarthmore, PA, 1988).
[25]D. V. Shtansky, E. A. Levashov, A. N. Sheveiko, and J. J. Moore, Metall. Mater. Trans. A **30A**, 2439 (1999).
[26]J. J. Nainaparampil and J. S. Zabinski, J. Vac. Sci. Technol. A **17**, 909 (1999).
[27]*Handbook of X-ray Photoelectron Spectroscopy*, edited by J. Chastain and R. King, Jr. (Physical Electronics, Eden Prarie, MN, 1995).

Nanostructure and mechanical properties of WC–SiC thin films

Jose L. Endrino and James E. Krzanowski
Department of Mechanical Engineering, University of New Hampshire, Durham, New Hampshire 03824

(Received 19 July 2002; accepted 16 September 2002)

The mechanical properties of WC–SiC thin films deposited by dual radio frequency magnetron sputtering were investigated. The films were characterized by x-ray photoelectron spectroscopy, x-ray diffraction (XRD), and transmission electron microscopy (TEM) to evaluate the details of the microstructure and degree of amorphization. The results indicate that small additions of SiC (<25%) can significantly increase hardness compared to a pure WC film, but higher SiC contents do not strongly affect hardness. XRD studies show the SiC had a disordering effect. TEM results showed that WC films had coarse porous structure, but films with a low silicon carbide content (approximately 10 to 25 at%) had a denser nanocrystalline structure. Samples with greater than 25% SiC were amorphous. The initial hardness increase at lower SiC contents correlated well with the observed densification, but the transition to an amorphous structure did not strongly affect hardness.

I. INTRODUCTION

Recent reports on the mechanical properties of nanocomposite ceramic thin films have claimed dramatic property enhancements, including hardness levels exceeding that of diamond and high fracture toughness.[1,2] These enhancements have been attributed to nanocomposite film structures consisting of nanocrystalline (2–5 nm) grains with amorphous interlayers between grains. In several studies,[1,3–5] these structures were obtained by adding silicon nitride to transition metal nitrides in films deposited by plasma-assisted chemical vapor deposition. Systems studied include nanocrystalline(nc)–TiN/amorphous(a)–Si_3N_4,[3] nc-W_2N/a-Si_3N_4,[4] and nc-TiN/a-Si_3N_4/nc-$TiSi_2$.[1] Detailed characterization of nc-TiN/a-Si_3N_4 by x-ray photoelectron spectroscopy (XPS) reported that the Si was bonded only to N, indicating an amorphous SiN_x phase had formed as an interlayer between nanocrystallites of the metal nitrides. High-resolution transmission electron microscopy (TEM)[5] revealed a combined amorphous/crystalline composite with a crystallite size near 4 nm. The highest hardness levels reported to date (>100 GPa) were obtained in nc-TiN/a-Si_3N_4/nc-$TiSi_2$ composite films,[1] with a microstructure of nanocrystalline TiN and $TiSi_2$ phases embedded in a Si–N phase. Additional studies on Ti–Si–N films deposited by reactive direct current (dc)[6] and radiofrequency (rf)[7] sputtering reported maximum hardness levels in the range of 43 to 47 GPa, possibly due to a solid solution hardening effect of Si[6] or phase separation between TiN, (Ti,Si)N, and an amorphous grain boundary interlayer.[7] Nanocrystalline/amorphous composite film structures have also been investigated in TiC/a-C[2] and TiC/a-C:H[8,9] films by varying the carbon content. In some cases, a hardness maxima was found at slightly superstoichiometric carbon levels.[2,9] In our recent studies on films in the Ti–Si–C system,[10–12] we have examined the effect of Si on the hardness of TiC. For sputtered films[10,11] the hardness increased with Si content, and it was proposed that phase separation between TiC and SiC within the grains was responsible for this observation. For films deposited by pulsed laser deposition (PLD),[12] film crystallinity had more effect on the hardness than did Si content, with increased crystallinity in the Ti–Si–C films (obtained at higher temperatures) yielding higher hardness levels.

The effect of Si on the phase formation and mechanical properties of early transition-metal nitride and carbide films remains a subject of considerable interest. In this article, we present results on W–Si–C films. The addition of SiC to WC disorders the structure (i.e., promotes amorphization), giving us the potential to create nanocomposite mixed crystalline/amorphous structures of high hardness.

II. EXPERIMENTAL

The films in this study were deposited by magnetron cosputtering using stoichiometric targets of WC and SiC in a dual-target rf sputter deposition system (base pressure, 6×10^{-5} Pa; sputtering pressure, 1.33 Pa). The

distance from the target to the surface of the substrate was approximately 8 cm, and the two sputter guns were oriented 15° from the substrate normal axis. The deposited films were all approximately 1-micron thick and were deposited onto Si(111) wafers at a substrate temperature of 350 °C and a negative substrate bias voltage of –50 V. The films were analyzed by XPS and x-ray diffraction (XRD). TEM of ion-milled plan-view samples was conducted on a JEOL 2000FX (Tokyo, Japan) instrument operating at 200 kV. The hardness and elastic modulus

TABLE I. Deposition parameters, composition analysis, and mechanical properties of WC–SiC thin films.

Sample no.	Sputter gun power (W) WC	SiC	W (at.%)	C (at.%)	Si (at.%)	SiC content (mol%)	*H* (GPa)	*E* (GPa)
1	175	0	54.7	45.3	0	0	10	200
2	175	25	33.1	61.2	4.8	12.6	14	220
3	175	75	38.5	50.8	10.7	21.8	28	270
4	160	100	35.8	51.7	12.5	25.9	24	270
5	160	200	26.4	47.7	25.9	49.1	21	230
6	80	200	16.7	49.7	33.6	66.9	23	240
7	50	200	10.4	59.3	30.3	74.4	25	240
8	40	200	8.3	62.5	29.2	78.0	20	220
9	30	200	4.5	55.8	39.7	89.8	23	210
10	20	200	4.6	49.5	45.9	90.8	24	195
11	7	200	1.1	47.5	45.3	97.6	27	200
12	0	175	n.t.	n.t.	n.t.	100	24	185

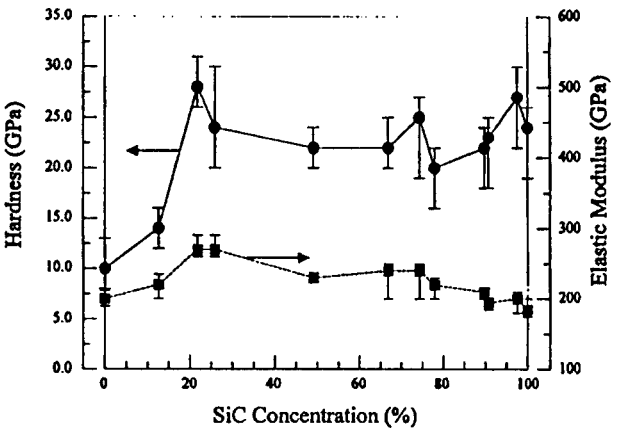

FIG. 1. Hardness and elastic modulus for WC–SiC thin films measured using the nanoindentation technique.

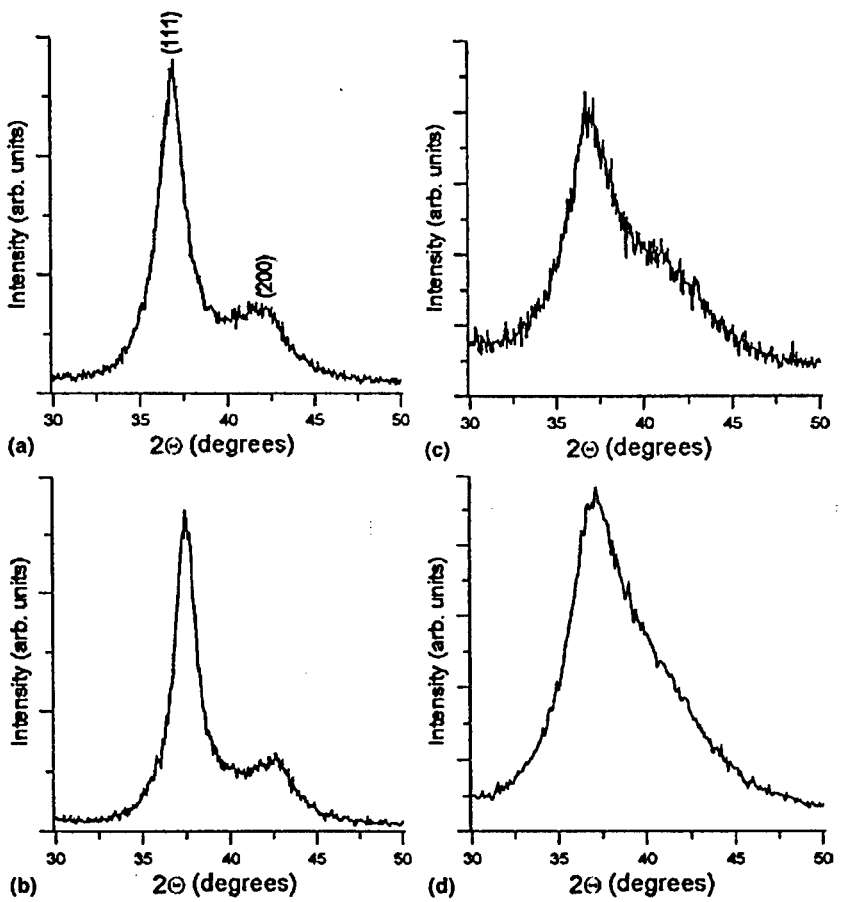

FIG. 2. XRD patterns for WC–SiC films: (a) pure WC, showing the locations of the (111) and (200) reflections for cubic WC_{1-x}; (b) WC–12.6% SiC; (c) WC–21.8% SiC; and (d) WC–25.9% SiC.

values for these films were evaluated on a Hysitron nanoindenter with a Berkovich tip using the Oliver–Pharr method.[13] For each film, 4–6 hardness measurements were made, each using a multiple indent loading procedure(up to a maximum of 8 mN) that gave ten values of hardness and reduced modulus. Values from the multiple indent sequence corresponding to contact depths ranging between 50 and 100 nm (≤10% of the film thickness) were averaged, and the average, minimum, and maximum of these hardness and reduced modulus results are reported in this paper.

By varying the power applied to the WC and SiC targets, a set of 12 films was obtained that covered the full range of compositions from pure WC to pure SiC. Table I shows the details for this set of films. The films also contained some oxygen (up to 10%), but no systematic trend of oxygen concentration with SiC/WC ratio was found, so the results in Table I are normalized to the total W, Si, and C contents. The nominal SiC concentration for each sample, based on the fraction of the Si relative to the total W and Si content, is also given in Table I.

III. RESULTS AND DISCUSSION

Figure 1 displays the mechanical properties of the deposited films versus the SiC content (error bars refer to range of values obtained). Note that neither the pure WC or pure SiC correspond to either the maximum hardness or elastic modulus. Small amounts of SiC (up to 21.8%) dramatically increase the hardness from 10 to 28 GPa and the reduced elastic modulus from 200 to 270 GPa. Further increase in SiC content has only a minor influence on the hardness of the films, which remains in the 20–27-GPa range, while the elastic modulus diminishes linearly to a value of 185 GPa for a pure SiC film. This decrease in modulus scales similarly with the lower elastic modulus of bulk SiC (480 GPa) in comparison to bulk

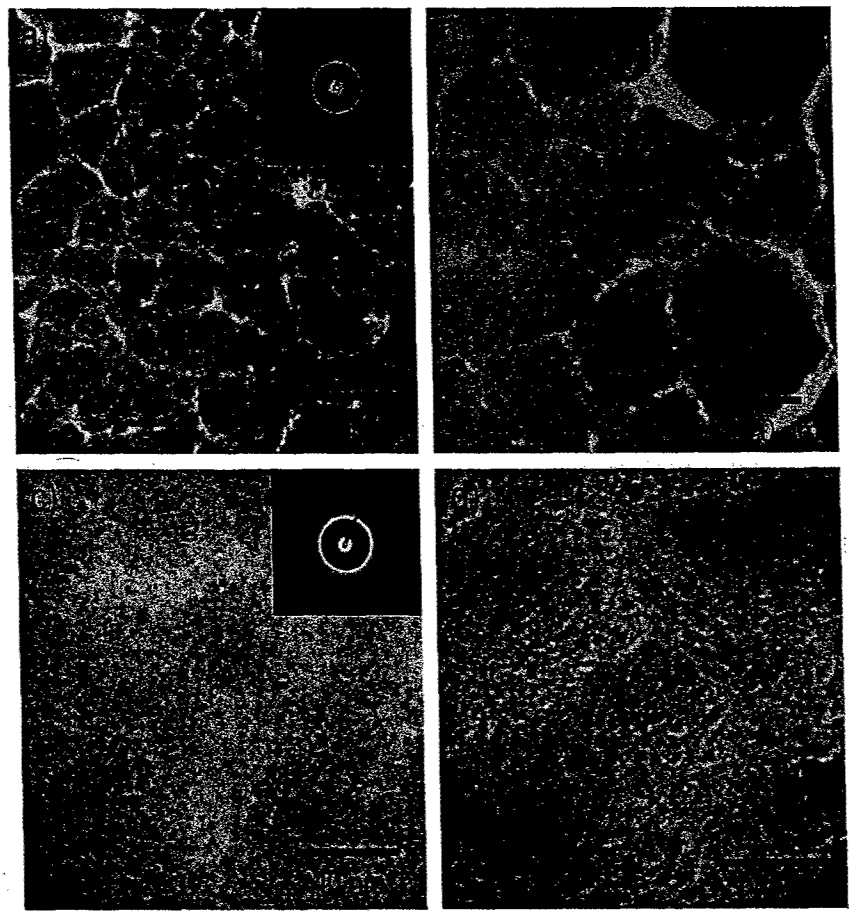

FIG. 3. (a, b) TEM images of sample no. 1 (WC): (a) Low-magnification image and electron diffraction pattern, showing the hierarchical structure with primary and secondary void networks and (b) higher magnification image, showing nanocrystalline grain structure within domains surrounded by voided regions. (c, d) TEM images of sample 3 (WC–21.8% SiC): (c) Low-magnification image, showing nanocrystalline grain structure with only weak columnar domains, and (d) intercolumnar region showing a network of a low-density phase outlining the nanocrystallites.

WC (720 GPa).[14] The values for the hardness obtained for WC–SiC films exceed the values expected by simple interpolation between SiC and WC films (for example, compare the maximum hardness of 28 GPa in film no. 3 with the rule-of-mixtures interpolated value of approximately 17 GPa). These results can be compared with our previous study of WC/TiC films,[15] where the TiC content had no systematic effect on hardness. This shows that the effect of SiC on film hardness observed here is not a geometric effect (i.e., reducing shadowing) resulting from the use of dual sources.

XRD studies revealed that increasing the SiC content in WC has a disordering effect, reducing crystallinity. Figure 2 shows the XRD patterns for the four samples with highest tungsten carbide contents. The diffraction patterns of pure WC and WC–12.6% SiC shown in Figs. 2(a) and 2(b), respectively, present the expected WC_{1-x} structure, which is a common form for tungsten carbide thin films deposited at low temperatures.[15,16] In contrast, the diffraction patterns for WC–21.8% SiC and WC–25.9% SiC, shown in Figs. 2(c) and 2(d), exhibit a single broad peak due to an increased degree of amorphization. Samples with higher SiC content did not reveal specific peaks for either WC or SiC, indicating an amorphous structure or an extremely small crystallite size.

TEM was employed for further structural characterization of the WC–SiC films. Figures 3(a) and 3(b) show TEM images and electron diffraction (ED) patterns for sample no. 1 (pure WC). The ED pattern agrees with the XRD pattern of Fig. 2(a), which corresponds to polycrystalline WC_{1-x}. Figure 3(a) illustrates a hierarchical microstructure with domains about 100-nm diameter size separated by voided regions. Within these domains a secondary void network separates microdomains (approximately 10–40-nm diameter size), which in turn consist of nanocrystallites [Fig. 3(b)]. TEM images for sample no. 3 (WC–21.8% SiC), the specimen with the highest hardness and elastic modulus, are shown in Figs. 3(c) and 3(d). The electron diffraction pattern in Fig. 3(c) still corresponds to the expected WC_{1-x} phase. However, unlike pure WC, this sample has a denser microstructure where the coarse voided regions (such as those observed in sample no. 1) are not present. Instead, we observed weakly contrasting domains (approximately 100-nm diameter) consisting of nanocrystals (approximately 2–10 nm) that were outlined by a lighter-color mesh. The regions between these domains are distinguished by a more prominent intergranular mesh. Figure 3(d) shows a more detailed image of this intergranular mesh outlining nanocrystallites that are approximately 5 nm in diameter. A TEM image of a sample with a higher SiC content (no. 7, WC–74.4% SiC) is shown in Fig. 4. A single broad diffraction ring consistent with ED patterns for amorphous materials was detected in the region of the (111) and (200) reflections of WC_{1-x}. The structure observed is common to amorphous materials.

IV. CONCLUSIONS

The compositional dependence of the hardness observed here for W–Si–C films can be summarized as an initially increasing hardness with the addition of SiC (up to approximately 20%) and thereafter remaining relatively constant. In terms of microstructure, two primary effects of the SiC additions are observed. First, the coarse primary void network observed in the WC films was eliminated in sample no. 3; this alone should improve film hardness.[17,18] Examination of Fig. 3(d) in comparison with Fig. 3(b) revealed a lighter-colored boundary mesh outlining the nanocrystallites, but the coarse voided intercolumnar regions are no longer present. The nature of the intergranular boundaries in Fig. 3(d), which are nearly subnanometer in scale, is not yet clear. One interpretation is that these are simply voided regions, and the nanocrystallites are WC–SiC solid solutions. Another is that the nanocrystallites are WC and the lighter boundary regions are amorphous SiC. If the latter is correct, then we have achieved the structure prescribed by Veprek[19,20] for ultrahard films, yet the hardness only reaches 28 GPa.

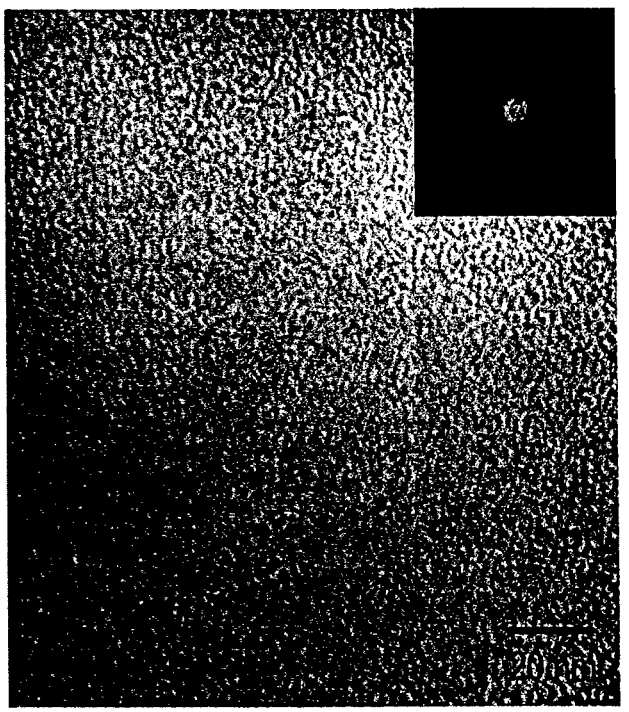

FIG. 4. TEM image and ED pattern for sample no. 7 (WC–74.4% SiC), illustrating the amorphous nature of the film. No columnar domain structure was observed in this sample.

The second primary effect of SiC additions is to cause complete amorphization of the films at >25% SiC. However, this results in only a slightly lower hardness.

Overall, the dominant effect of adding small amounts (<25%) of SiC is to alter the nature of intercolumnar void networks, either by reducing their extent or replacing them with an amorphous SiC interlayer. The latter is consistent in general with the concepts proposed by Veprek *et al.*,[19,20] in that even when an ultrafine grain structure is present, the hardness levels will depend strongly on the nature of the intercolumnar or intergranular regions. In this study, we have shown that the addition of SiC to WC can reduce intercolumnar void formation and increase hardness. The mechanism by which the SiC additions achieve this result is the subject of further study.

ACKNOWLEDGMENTS

The financial support of the Air Force Office of Scientific Research under Grant No. F49620-98-1-0499 is gratefully acknowledged. Helpful discussions with Dr. Jose J. Nainaparampil of the Air Force Research Laboratories, Wright-Patterson Air Force Base, Dayton, OH, are also appreciated.

REFERENCES

1. S. Veprek, A. Niederhofer, K. Moto, T. Bolom, H.D. Mannling, P. Nesladek, G. Dollinger, and A. Bergmaier, Surf. Coat. Technol. **133–134,** 152 (2000).
2. A.A. Voevodin and J.S. Zabinski, J. Mater. Sci. **33,** 319 (1998).
3. S. Veprek, S. Reiprich, and Li Shizhi, Appl. Phys. Lett. **66,** 2640 (1995).
4. S. Veprek, M. Haussmann, and S. Reiprich, J. Vac. Sci. Technol. A **14,** 46 (1996).
5. S. Christiansen, M. Albrecht, H.P. Strunk, and S. Veprek, J. Vac. Sci. Technol. B **16,** 19 (1998).
6. L. Rebouta, C.J. Tavares, R. Aimo, Z. Wang, K. Pischow, E. Alves, T.C. Rojas, and J.A. Odriozola, Surf. Coat. Technol. **133–134,** 234 (2000).
7. F. Vaz, L. Rebouta, P. Goudeau, J. Pacaud, H. Garem, J.P. Riviere, A. Cavaleiro, and E. Alves, Surf. Coat. Technol. **133–134,** 307 (2000).
8. W.J. Meng, R.C. Tittsworth, and L.E. Rehn, Thin Solid Films **377–378,** 222 (2000).
9. T. Zehnder and J. Patscheider, Surf. Coat. Technol. **133–134,** 138 (2000).
10. J.E. Krzanowski and S.H. Koutzaki, J. Am. Ceram. Soc. **84,** 672 (2001).
11. S.H. Koutzaki, J.E. Krzanowski, and J. Nainaparampil, J. Vac. Sci. Technol. A **19,** 1912 (2001).
12. A.R. Phani, J.E. Krzanowski, and J.J. Nainaparampil, J. Vac. Sci. Technol. A **19,** 2252 (2001).
13. W.C. Oliver and G.M. Pharr, J. Mater. Res. **7,** 1564 (1992).
14. M. Ohring, *The Materials Science of Thin Films* (Academic Press, San Diego, CA, 1992), p. 552.
15. S.H. Koutzaki, J.E. Krzanowski, and J.J. Nainaparampil, Met. Mater. Trans. **33A,** 1579 (2002).
16. A.A. Voevodin, J.P. O'Neill, S.V. Prasad, and J.S. Zabinski, J. Vac. Sci. Technol. A **17,** 986 (1999).
17. S.J. Bull and D.S. Rickerby, in *Mechanics of Coatings,* edited by D. Dowson, C.M. Taylor, and M. Godet (Institut National des Sciences Appliques, Lyon, France, 1989), pp. 337–349.
18. R. Messier, A.P. Giri, and R.A. Roy, J. Vac. Sci. Technol. A **2,** 500 (1984).
19. S. Veprek and S. Reiprich, Thin Solid Films **268,** 64 (1995).
20. S. Veprek, J. Vac. Sci. Technol. A **17,** 2401 (1999).

Reprinted from

Journal of Vacuum Science & Technology A

JVST A

Second Series
Volume 19, Number 5
September/October 2001

Structural and mechanical properties of TiC and Ti–Si–C films deposited by pulsed laser deposition

A. R. Phani and J. E. Krzanowski
Department of Mechanical Engineering, University of New Hampshire, Durham, New Hampshire 03824

J. J. Nainaparampil
Systran Inc., Dayton, Ohio

pp. 2252-2258

An official journal of the American Vacuum Society
Published for the Society by the American Institute of Physics

Structural and mechanical properties of TiC and Ti–Si–C films deposited by pulsed laser deposition

A. R. Phani and J. E. Krzanowski[a)]
Department of Mechanical Engineering, University of New Hampshire, Durham, New Hampshire 03824

J. J. Nainaparampil
Systran Inc., Dayton, Ohio

(Received 23 January 2001; accepted 7 May 2001)

TiC and Ti–Si–C films have been deposited by pulsed laser deposition at substrate temperatures ranging from room temperature to 600 °C onto (111) silicon wafers and 440C stainless steel substrates. X-ray diffraction, x-ray photoelectron spectroscopy, and electron microscopy were employed for structural and compositional evaluation of the films, and nano-indentation hardness testing and pin-on-disk wear tests were used to evaluate the mechanical and tribological properties. All the TiC films were highly crystalline except the one deposited at room temperature, whereas for the Ti–Si–C films the degree of crystallinity increased with temperature, ranging from amorphous for the room temperature deposit to about 50% crystalline at 600 °C. The hardness of the TiC films was relatively constant with deposition temperature at about 25 GPa, whereas the hardness of the Ti–Si–C films increased with deposition temperature from 11 to 33 GPa. The temperature dependence of the hardness is attributed to the degree of crystallinity and the extent of phase separation in the Ti–Si–C films. The wear test data showed good results for all films up to the tested limit of 10 000 cycles at 1 N load. © *2001 American Vacuum Society.* [DOI: 10.1116/1.1382876]

I. INTRODUCTION

Recent developments in hard coating technologies have been achieved through compositional and microstructural modifications of traditional carbide and nitride coating materials. Examples include the addition of Al to TiN in TiAlN coatings,[1] Si in TiSiN, the formation of carbonitrides such as TiCN,[2,3] and the fabrication of heterogeneous multilayers such as TiN/NbN (Ref. 4) and TiN/CN.[5,6] The incorporation of additional elements can provide solid solution strengthening, hardening due to the presence of a second phase, or an improvement in mechanical properties by Hall–Petch strengthening and crack arrest mechanisms.[7] More recent research has focused on using nanoscale multilayers to reduce stress in the hard coatings,[8,9] terminate cross-sectional cracks, and impede motion of dislocations. Compositional modifications can provide additional property improvements. For example, the addition of Al to TiN improves surface oxidation resistance, and it is also possible to form tribochemical surface films that lower friction and extend wear life, such as oxides and graphite-like transfer films.[10,11]

While much of the work on ternary hard coating materials has focused on nitrides, improvements in carbide coatings by alloying may also be possible. Addition of ternary elements to TiC and other B1-structured carbides to form solid solutions has shown considerable improvements in hardness.[12] In our research we have attempted to alloy TiC to form multiphase carbide coatings. Research has been conducted on sputter-deposited Ti–Mo–C, Ti–W–C, and Ti–Si–C.[13] It was found that weakly immisicible systems, such as Ti–Mo–C and Ti–W–C, tend to exhibit large supersaturation and form single-phase structures when deposited in thin film form. In terms of hardness improvements, the most successful of these was the Ti–Si–C coatings, where the hardness increased from 12 GPa for TiC to 22 GPa for the optimal Ti–Si–C film composition. However, the low value of the TiC film indicates a less than fully dense structure, probably due to the fact that the films were deposited at a relatively low temperature (650 °C) with no bias or other energetic assist. Higher temperatures are not suitable for deposition on steel, which is the substrate of primary applications interest. Therefore a more energetic deposition method is needed. Using such a method, we can determine the extent to which Si can enhance hardness over the accepted level for TiC, which is typically 28–30 GPa. Hardness values near that level were obtained in our previous studies of pulsed laser deposited (PLD) TiC.[14] Therefore we have investigated the use of that method for depositing Ti–Si–C films, and the results are reported here. At the same time, we have also made standard PLD TiC samples for comparison.

II. EXPERIMENTAL PROCEDURE

The films for this study were deposited by pulsed laser deposition (PLD). Deposition was carried out in an Epion model 3000 PLD system. For each deposition, the system was evacuated overnight to obtain a pressure of $\sim 3.5 \times 10^{-7}$ Torr. For depositions run at elevated temperatures, the chamber was baked at a temperature of 100 °C above the desired substrate temperature until a pressure of $< 2 \times 10^{-6}$ Torr was obtained. For each deposition, the chamber was backfilled with ultrahigh purity (99.999%) argon gas to a pressure of 5 mTorr.

Laser ablation was carried out using a KrF (248 nm) laser

a)Author to whom correspondence should be addressed; electronic mail: JamesK@cisunix.unh.edu

with a 25 ns pulse length. The energy density of the focused laser beam was optimized at 6 J/cm^2 per pulse (repetition rate 50 Hz) with the beam incident at an angle of 45°. The substrate-to-target distance was 9 cm, and both the target and the substrate were rotated during deposition to ensure good spatial uniformity. For these experiments, commercially fabricated TiC and Ti–Si–C targets were used. The targets were fabricated by hot pressing 99.5% purity carbide powders under argon cover. The nominal composition of the Ti–Si–C target was 12 mol % SiC (assuming ideal stoichiometry for TiC and SiC, the mol % SiC is equivalent to twice the absolute concentration of Si, so this corresponds to 6 at. % Si in the Ti–Si–C alloy). However, when the target was received, it was observed to be dark gray in color with numerous small light-colored areas approximately 1–3 mm in diameter. SEM analysis combined with energy dispersive x-ray spectroscopy (EDS) of the target showed the lighter areas to be primarily silicon. These areas were loosely bonded material that ablated rapidly during the early part of the deposition runs. After a few runs, the target surface was reground to regain the starting condition in order to maintain constant compositions in the films. Despite that attempts, compositional variations were observed as will be shown in the following section. However, previous studies[13] showed that while the addition of 5% SiC to TiC increased hardness by about 10 GPa over TiC alone, additions in the range of 5%–20% SiC provided further hardness increases of only 3 GPa in one sample set and no further increase was observed in the other two runs. Therefore errors in hardness assessments due to compositional variations obtained for the present studies are likely to be small.

Films were deposited in the temperature range of room temperature to 600 °C. The substrates used were (111) silicon wafers and 440C stainless steel disks. The steel substrates were cut from 2.54 cm diameter bar stock at thickness of 0.24 cm and were ground and polished, finishing with 0.05 μm alumina abrasive slurry. The film thickness was measured using a profilometer (Tencor Alpha-Step) and was in the range of 780–900 nm. The calculated deposition rate for Ti–Si–C was 1.2 Å/s.

The deposited films were characterized using x-ray diffraction (XRD), x-ray photoelectron spectroscopy (XPS), scanning and transmission electron microscopy (SEM/TEM), and nano-indentation hardness testing. XRD analyses were carried out using a Rigaku D-MAX/B system with a θ–θ goniometer and a Cu $K\alpha$ x-ray radiation source. The crystallite size of the deposited films has been calculated using the Scherrer formula. Compositional analysis of the films was carried out by XPS, performed on a Kratos Analytical instrument. The x-ray source was Mg $K\alpha$, and an Ar^+ ion beam was used for etching the surface to remove contaminants. SEM studies were conducted on an Amray 3300FE field-emission SEM. TEM was conducted on a Hitachi H-600 operating at 100 kV for general microstructural characterization, while high-resolution TEM images were obtained on a JEOL 2010 TEM operating at 200 kV. TEM samples were examined in plan-view and were prepared by back-thinning the films deposited on Si substrates by dimpling and ion milling.

Limited tribological evaluation of the samples was also carried out using a pin-on-disk apparatus. The test conditions were ambient atmosphere and temperature, a 100 g load on a $\frac{1}{4}$-in. (0.625 cm) 440C steel ball, a speed of 200 revolutions per minute, and a track diameter of 6 mm. These tests were done with the disk horizontal, and any wear debris will likely remain in the track and influence the observed friction and wear behavior. All samples were run for a total of 10 000 revolutions.

TABLE I. X-ray photoelectron spectroscopy data of TiC films deposited at different temperatures.

Sample	Substrate temperature (°C)	at. % of Ti *2p*	at. % of C *1s*	at. % of O *1s*
TiC on Si	25	52.7	35.4	11.9
TiC on Si	200	52.1	34.5	13.2
TiC on Si	400	56.0	31.8	12.2
TiC on Si	600	57.5	30.3	12.2

III. RESULTS

A. Compositional characterization

The TiC films were deposited at room temperature, 200, 400, and 600 °C. XPS analysis of TiC films deposited on Si substrates was conducted and the results are shown in Table I. In general, the films were substoichiometric with respect to carbon, and have 12 to 13 at. % oxygen. This oxygen level is consistent with previous studies of PLD TiC[14] and is believed to originate from both the target and impurities in the vacuum chamber.

The results for the Ti–Si–C films are shown in Table II. The films deposited at room temperature had a very high level of oxygen, possibly due to an initial surface oxide on the target. Subsequent runs with this target resulted in much lower oxygen levels (3.5%–9.3%). The Si content also varied, and as noted in the previous section this is attributed to difficulties encountered with the homogeneity of the target. The binding energies of Ti and C in Ti–Si–C films were 455 and 283 eV indicating the formation of the carbide phase in the deposited films. An additional Ti–Si–C film was deposited at 700 °C but the composition was not analyzed. No hydrogen analysis was carried out for the deposited films.

B. Structural characterization

Figures 1(a) and 1(b) show the typical x-ray diffraction patterns for the TiC films deposited on Si (111) and 440C steel substrates, respectively. The films deposited at room temperature were largely amorphous. At 200 °C some crystallinity was observed, and at higher temperatures the films had a strong crystalline component. Most of the films that were crystalline had a preferred (200) orientation. Both surface energy and epitaxial growth effects can play a role in determining the preferred orientations of films; in the present

TABLE II. X-ray photoelectron spectroscopy data of Ti–Si–C films deposited at different temperatures.

Sample	Substrate temperature (°C)	at. % of Ti *2p* B.E (eV)	at. % of Si *2p* B.E (eV)	at. % of C *1s* B.E (eV)	at. % of O *1s* B.E (eV)
TiSiC on Si	25	35.1 (455)	6.2 (100)	21.9 (283)	36.8 (531)
TiSiC on Si	200	42.6 (455)	11.5 (100)	36.2 (283)	9.7 (531)
TiSiC on Si	400	45.6 (455)	11.2 (100)	39.7 (283)	3.5 (531)
TiSiC on Si	600	53.7 (455)	4.6 (100)	34.5 (283)	7.2 (531)

case it appears that surface energy effects dominate, since in the TiC structure surface energy is minimized for the (200) orientation.

XRD results for the Ti–Si–C films are shown in Figs. 2(a) and 2(b) for Si and steel substrates, respectively. On Si, the films deposited at room temperature and 200 °C were essentially amorphous, while the higher deposition temperatures yielded strongly (200) oriented films. Similarly, for the films deposited on 440C steel, only the 400/600 °C samples had any significant crystallinity. An additional peak located approximately 1° 2θ below the Fe (110) peak at 44.5° 2θ could be due to the retained austenite (111) peak, or alternatively, it may represent formation of the Ti_3SiC_2 phase. The latter phase may form due to diffusion of carbon into the steel, which drives the stoichiometry to a more substoichiometric composition, where the Ti_3SiC_2 becomes a stable

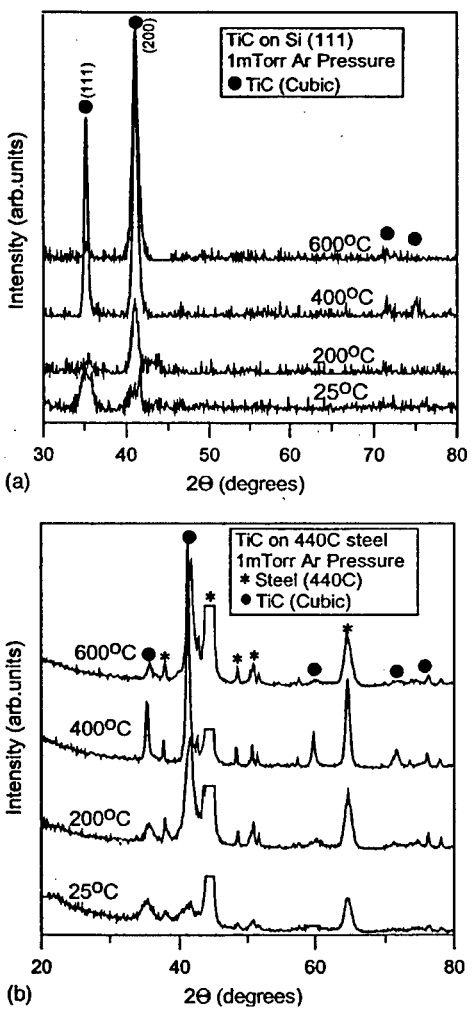

FIG. 1. X-ray diffraction patterns of TiC films deposited at various substrate temperatures: (a) Si substrates and (b) 440C steel substrates.

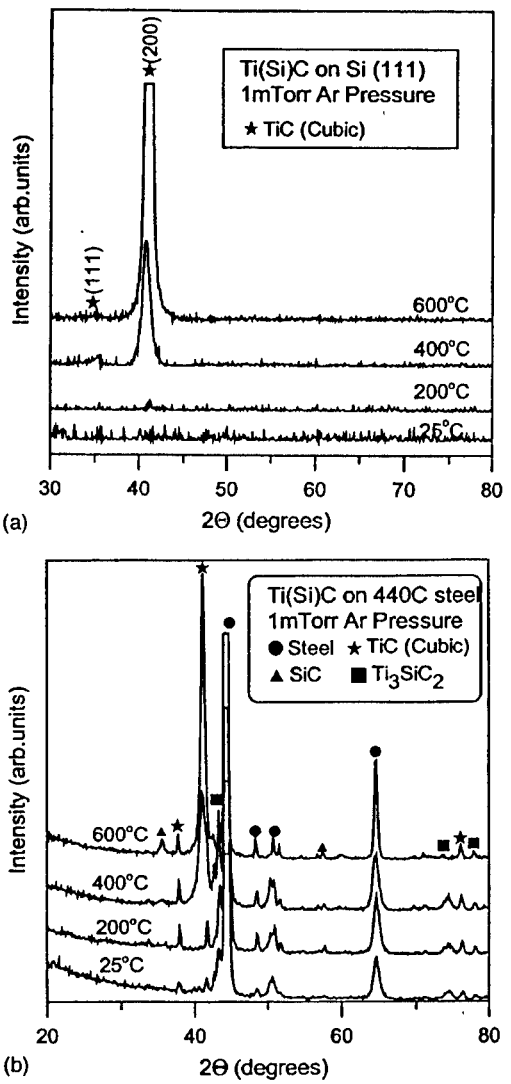

FIG. 2. X-ray diffraction patterns of Ti–Si–C films deposited at various substrate temperatures: (a) Si substrates and (b) 440C steel substrates.

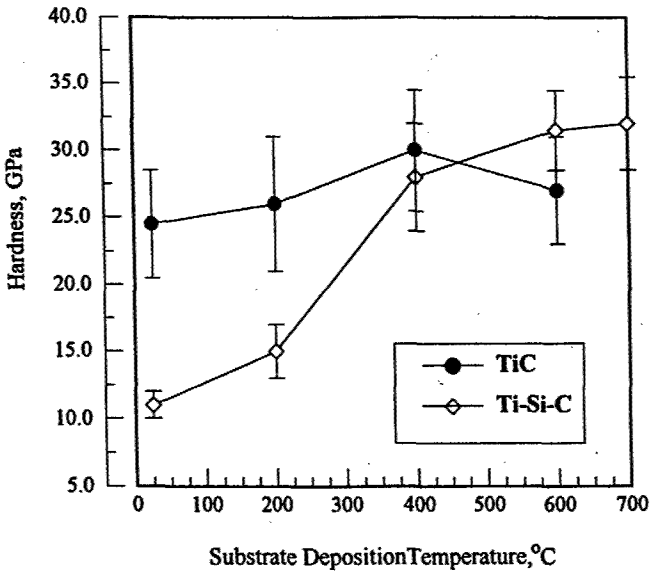

FIG. 3. Nano-indentation hardness measurements for the TiC and TiSiC films vs deposition temperature. These results are an average of data obtained on Si and steel substrates, with error bars representing the range of values obtained.

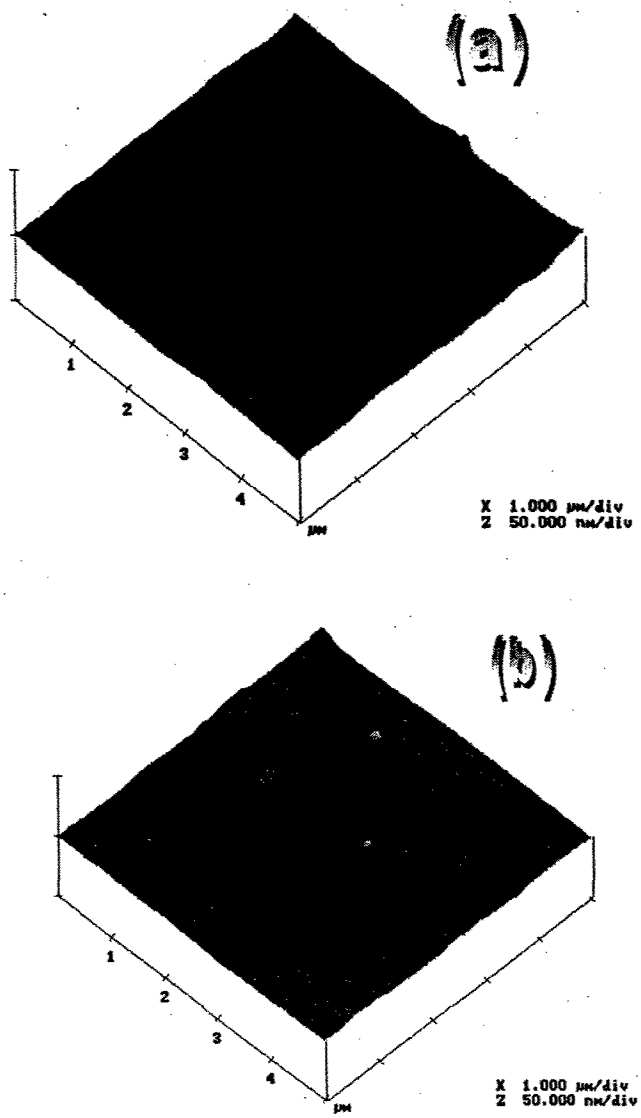

FIG. 4. AFM images of the Ti–Si–C film deposited on 440C steel at 400 °C: (a) before indentation and (b) after indentation. Note the absence of cracking near the indents.

phase. Note, however, that the peak was not present in the 600 °C spectrum, where more diffusion would be expected.

The lattice parameters of the Ti–Si–C phase were calculated for the 200, 400, and 600 °C samples using (200) reflection and found to be $a=0.430\,78$ nm, in good agreement with the literature value ($a=0.4357$ nm). As noted in our previous work, the difference in lattice parameter between TiC and SiC (cubic) is very small, and combined with the relatively broad peaks typically obtained here due to a small crystallite size, it is not possible to determine whether the individual TiC/SiC cubic phases form versus a solid solution of TiC and SiC. However, the latter case is thermodynamically unstable, providing a strong driving force for phase separation. The implications of this are further discussed in Sec. IV.

C. Hardness and wear testing results

Nano-indentation was used to measure film hardness and was conducted on a Hysitron nano-mechanical test instrument equipped with a Berkovich indenter. The films were tested using a multiple loading sequence, with loads ranging from 0.3 to 3 mN. The maximum indentation depths were 60–75 nm, generally less than 10% of the typical film thickness. For each film, approximately 3–5 multiple-loading indentations were made. Testing was done on films deposited on both the Si and steel substrates. No significant trends were observed for the two different substrate types, so an average hardness data is reported here. Figure 3 shows the hardness data for the TiC and Ti–Si–C films deposited at different substrate temperatures. For the TiC films, the hardness values for samples deposited at room temperature, 200, and 600 °C were all near 25 GPa. For the Ti–Si–C films it was observed that as the substrate temperature increased from room temperature to 600 °C there was an increase in hardness from 11 to 32 GPa. Based on this result, an additional film was deposited at 700 °C, but was only slightly higher than the 600 °C sample. The elastic modulus of these films also increased from 150 GPa at room temperature to 250 GPa at 600 °C. The surface morphology of the film deposited at 400 °C before indentation and after indentation is shown in Fig. 4. The surface roughness of the sample was around 3.5 nm. In Fig. 4 we observe that there are no microcracks after indentation even after performing two indents of close distance.

Pin-on-disk friction measurements were made on TiC and Ti–Si–C films deposited on 440C steel, and an additional set of TiC samples where a 50 nm Ti interlayer was deposited on the steel before deposition of TiC were also made. The average friction values are shown in Table III and vary between 0.20 and 0.63. This indicates that all the films survived the test for 10 000 revolutions, since steel-on-steel friction

TABLE III. Average friction data for the TiC and Ti–Si–C films deposited at different substrate temperatures.

Deposition temperature, °C	TiC only	TiC with Ti layer	Ti–Si–C only
200	Not tested	0.29	0.63
400	0.20	0.30	0.39
600	0.47	0.22	0.48

values are usually 0.8 to 0.9 under the test conditions used. Overall, the lowest friction was observed for the films deposited at 400 °C, which showed friction coefficients in the range of 0.20 to 0.39.

D. Morphological and microstructural characterization

Scanning electron microscopy was employed to examine the morphology and deposited films. Figures 5(a) and 5(b) show the surface and one of the particulates on the surface of the 400 °C film deposited on 440C steel, respectively. All the films were covered with numerous small and large size particulates as shown in Fig. 5. Aside from these particulates, the films were uniform and continuous with densely packed grains. No peeling of the film has been observed after deposition or after performing a Scotch-tape adhesion test.

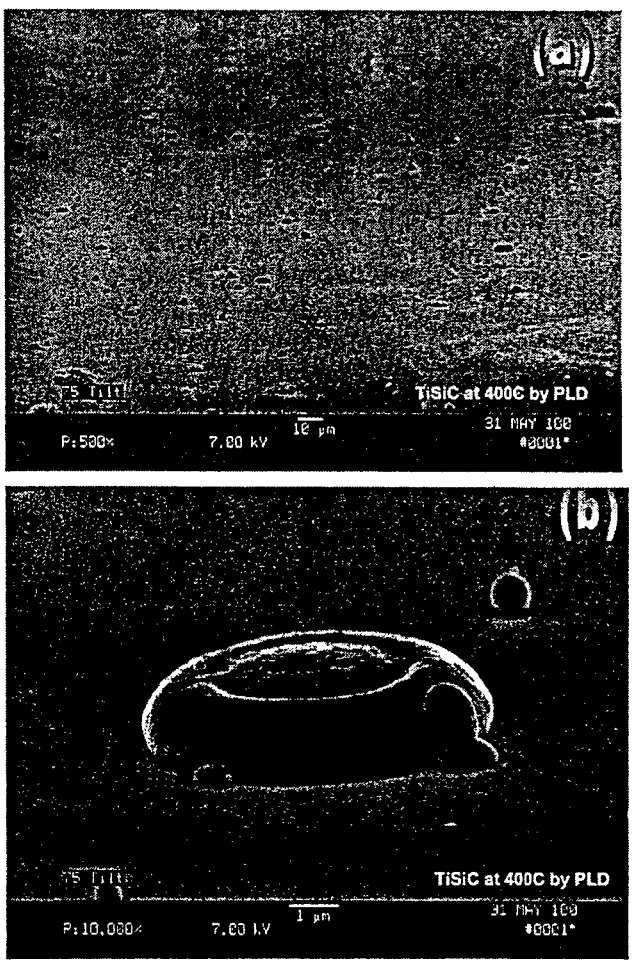

FIG. 5. SEM images of the Ti–Si–C film deposited on 440C steel at 400 °C: (a) surface image and (b) particulates on the surface.

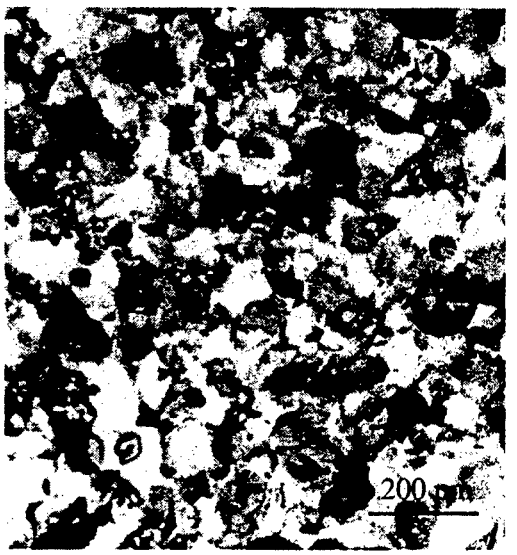

FIG. 6. TEM bright-field image of the TiC film deposited at 600 °C. Note the relatively large grain size in this sample (~100 nm).

TEM analysis was conducted on the TiC sample deposited at 600 °C, as well as the Ti–Si–C samples deposited at 200 and 600 °C. A TEM bright-field image of the TiC sample is shown in Fig. 6 and reveals a relatively dense grain structure with a grain size of ~100 nm. Since this is a plan-view specimen, it is likely that this view shows sections through columnar grains.

TEM analysis of the Ti–Si–C sample deposited at 200 °C is shown in Fig. 7. As expected from the x-ray diffraction results, this sample is completely amorphous. The 600 °C sample is shown in Fig. 8. Figure 8(a) shows a lower-magnification overall view of the structure. Two types of areas are seen, one with a darker color and mottled contrast,

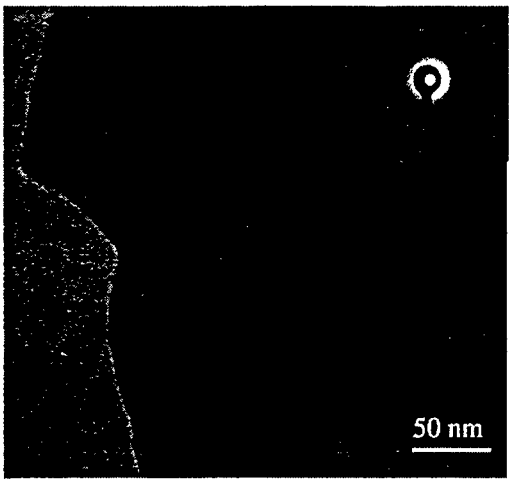

FIG. 7. TEM bright-field image of the Ti–Si–C film deposited at 200 °C, showing a nearly amorphous structure, as confirmed by the selected area diffusion pattern (inset). The edge of the hole in the TEM sample is on the left side of the image.

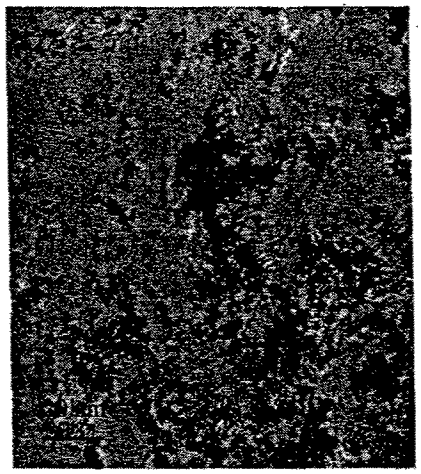

(a)

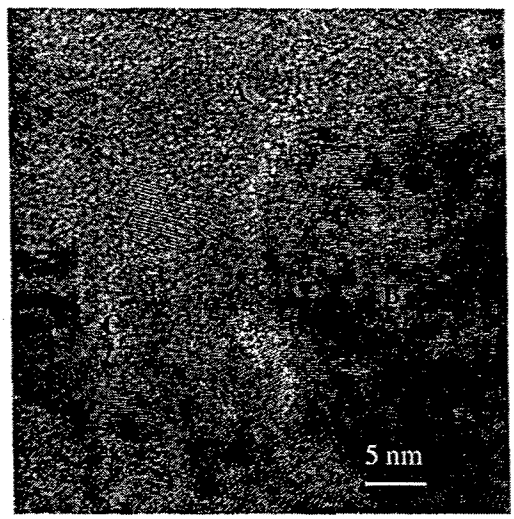

(b)

FIG. 8. TEM bright-field images of the Ti–Si–C film deposited at 600 °C: (a) lower magnification image, showing the presence of two types of phases, and (b) high-resolution (111) lattice image, showing that the lighter phase (labeled "A") is mostly amorphous, while the darker phase ("B") with the mottled structure is crystalline. The images also show that the crystalline regions are broken up into smaller domains, as shown in region "C."

and a second lighter area with little structure. Further investigation of the crystallinity in these two types of areas was carried out using high-resolution TEM, and a resulting image is shown in Fig. 8(b). Here it can be seen that the lighter areas are essentially amorphous, and constitute about 50% of the overall structure. The darker areas display a crystalline lattice. However, the lattice is not continuous across these areas, but appears broken up into smaller domains. This type of mottled structure along with smaller multiple crystalline domains was also observed in sputter-deposited Ti–Si–C films[13] and is attributed to phase separation between TiC and SiC. The implications of these microstructures on hardness are discussed below.

IV. DISCUSSION

The pulsed laser deposition technique has been used to deposit TiC and Ti–Si–C films at different substrate temperatures. The primary structural difference between TiC and the Ti–Si–C films is the degree of crystallinity. Most of the TiC films were crystalline. The Ti–Si–C films were essentially amorphous at room temperature and 200 °C, but became more crystalline at the higher temperatures; at 600 °C the films were approximately 50% crystalline. This result can have both thermodynamic and kinetic origins. The Si may reduce the mobility of the adatoms deposited on the films surface, resulting in an amorphous structure. In terms of the atomic arrangements within the film, the carbon atoms normally bond to Si in a tetrahedral bonding arrangement, whereas in TiC the carbon atoms occupy octahedral sites. In the case where Ti, Si, and C atoms are all present, but under kinetically constrained conditions that restrict phase separation, the amorphous structure may be the most thermodynamically favorable state. Overall, the effect of Si in TiC is to promote disordering of the structure; temperature, however, has the reverse effect.

The observations of the film crystallinity have interesting correlations to the measured hardness. For TiC, an average hardness of about 25 GPa was obtained, close to the bulk value for TiC. No strong temperature dependence was observed, which is notable because deposition of carbide films at lower temperatures often results in lower film densities, causing a reduction in hardness. For the Ti–Si–C films, the room temperature and 200 °C films had very low hardness values. For the room temperature film this may have been caused by the high oxygen content. However, the 200 °C film had oxygen content similar to the TiC films and higher temperature Ti–Si–C films, yet it still had a low hardness. The 200 °C film was also found to have an amorphous structure, which may contribute to the low observed hardness. The Ti–Si–C films deposited above 200 °C were significantly harder, and also increased with temperature, becoming equal to that of TiC at 400 °C and exceeding TiC at 600 and 700 °C. The hardness values are higher by an amount of about 5–10 GPa, which is reasonably consistent with the values found for sputter-deposited films.[13] In that study, the higher hardness was attributed to phase separation between TiC and SiC. In the present case it appears that the effect of increasing temperature is to first increase the degree of crystallinity, and then within the crystallized regions nano-scale phase separation may occur, which can further increase the hardness. Based on the fact that the 200 °C sample is about 15 GPa, and increases by about 17 GPa due to 50% crystallization, it may be expected that another 17 GPa increase could be obtained by complete crystallization, resulting in a hardness level near 49 GPa. However, this would require a higher deposition temperature, which is not favorable for deposition on steel substrates. If deposition temperatures become too high, phase separation of the TiC/SiC phases would result in a coarse microstructure with little benefit to hardness. In fact, chemical vapor deposition of Ti–Si–C films by Touanen *et al.*[15] in a temperature range of 950–1150 °C resulted in a coarse mixture of TiC/SiC phases with relatively low hardness (6–16 GPa). Therefore the optimal deposition conditions for fine-scale phase separation and

crystallization in Ti–Si–C film are likely to be defined by a relatively narrow window on deposition temperatures as well as film composition.

Despite this narrow window, and therefore limited utility of the Ti–Si–C films as a superhard coating material, the present set of data provide an interesting commentary on the role of crystallinity of the mechanical properties of these films. Veprek[7] has suggested that superhard and tough films can be obtained by having an ultrafine grain size and an amorphous interlayer, with an optimal amorphous content of about 10%–20%. Our results show that the amorphous material is lower in hardness, suggesting that the hardness is optimized when the structure becomes completely crystalline. However, since we have not obtained films with 10%–20% of an amorphous phase, we cannot make any conclusions about this concept without further study. In addition, since amorphous glasses typically have low toughness, examination of film toughness as well as hardness would be warranted.

As a final note, the issue of residual stress effects on hardness needs to be addressed. We measured the residual stress of the crystalline films using x-ray diffraction and the $\sin^2 \psi$ analysis method.[16] The residual stress measurements ranged from a slight tensile stress (~0.2 GPa) to about 2 GPa compressive, and generally became larger and more compressive with increasing deposition temperature. However, a strong correlation with hardness was not found for the TiC films. For example, the residual stress of the TiC/400 °C film was 0.2 GPa, and for the TiC/600 °C film it was −1.5 GPa, yet the hardness of both was about 25 GPa. Therefore it does not appear that the residual stress levels obtained here significantly affected the measured hardness values, and the observed temperature variation of hardness in the Ti–Si–C films are better attributed to film density effects and microstructural features.

V. CONCLUSIONS

Ti–Si–C films were deposited on 440C steel and silicon substrates by pulsed laser deposition (PLD) and compared to TiC PLD films. The Ti–Si–C films, in general, had lower crystallinity, indicating that Si disorders the TiC structure. Ti–Si–C films deposited at 200 °C were amorphous, and films deposited at 600 °C were about 50% crystalline. However, even within the crystalline regions, long-range order was not present, possibly due to phase separation between the TiC/SiC phases. The hardness of the TiC films showed weak temperature dependence, slightly increasing with temperature but averaging near 25 GPa. The hardness of the Ti–Si–C films increased significantly with deposition temperature, reaching a maximum of 33 GPa. The increase in hardness with temperature for the Ti–Si–C films is attributed to the increasing crystallinity. It is concluded that the presence of a significant volume fraction of an amorphous phase in the microstructure of the Ti–Si–C films reduced the film hardness.

ACKNOWLEDGMENTS

The financial support of the Air Force Office of Scientific Research, under Grant No. F49620-98-1-0499, is gratefully acknowledged. The use of the JEOL 2010 HRTEM at MIT (supported by the National Science Foundation under Award No. DMR98-008941) and the assistance of Michael Frongillo is greatly appreciated.

[1] *Handbook of Tribology: Materials, Coatings, and Surface Treatments*, edited by B. Bhushan and B. K. Gupta (McGraw-Hill, New York, 1991).
[2] K. Holmberg and A. Mathews, in *Coatings Tribology: Properties, Techniques, and Applications in Surface Engineering*, Tribology Series 28, edited by D. Dowson (Elsevier, Amsterdam, 1994).
[3] A. A. Voevidin and M. S. Donley, Surf. Coat. Technol. **82**, 199 (1996).
[4] S. Lopez, M.-S. Wong, and W. D. Sproul, J. Vac. Sci. Technol. A **13**, 1644 (2000).
[5] C. Subramanian and K. N. Strafford, Wear **165**, 85 (1993).
[6] M. S. Donley and J. S. Zabiniski, in *Pulsed Laser Deposition of Thin Films*, edited by D. B. Chrisey and G. K. Huber (Wiley, New York, 1994), p. 431.
[7] S. Verprek, J. Vac. Sci. Technol. A **17**, 2401 (1999).
[8] H. Holleck and V. Schier, Surf. Coat. Technol. **76/77**, 328 (1995).
[9] A. A. Voevidin, S. D. Walck, and J. S. Zabinski, Wear **203/204**, 516 (1997).
[10] J. S. Zabinski, A. A. Voevidin, and M. A. Capano, AGARD Conf. Proc. **589**, 4 (1996).
[11] A. A. Voevidin, A. W. Phelps, M. S. Donley, and J. S. Zabinski, Diamond Relat. Mater. **5**, 1264 (1996).
[12] H. Holleck, J. Vac. Sci. Technol. A **4**, 2661 (1986).
[13] J. E. Krzanowski, S. H. Koutzaki, J. Nainaparampril, and J. S. Zabinski, Mater. Res. Soc. Symp. Proc. **594**, 181 (2000).
[14] J. E. Krzanowski and R. E. Leuchtner, J. Am. Ceram. Soc. **80**, 1277 (1997).
[15] M. Touanen, F. Teyssandier, M. Ducarroir, M. Maline, R. Hillel, and J. L. Derep, J. Am. Ceram. Soc. **76**, 1473 (1993).
[16] B. D. Cullity, *Elements of X-Ray Diffraction*, 2nd ed. (Addison-Wesley, Reading, MA, 1978).

Structural and mechanical properties of TiC/Ti and TiC/B_4C multilayers deposited by pulsed laser deposition

A.R. Phani and J.E. Krzanowski[a)]
Mechanical Engineering Department, University of New Hampshire, Durham, New Hampshire 03824
J.J. Nainaparampil
AFRL/MBLT, Wright-Patterson Air Force Base, Ohio 45433

(Received 18 July 2001; accepted 18 March 2002)

Multilayers of TiC/Ti and TiC/B_4C have been deposited by pulsed laser deposition. Ti, B_4C, and TiC targets were used to deposit multilayer films onto 440C steel and silicon substrates at 40 °C. The structural, compositional, and mechanical properties of the multilayers were examined by x-ray diffraction, x-ray photoelectron spectroscopy, transmission electron microscopy, and nanoindentation techniques. Tribological properties were also evaluated using a pin-on-disc friction and wear test. The TiC/Ti films were found to have a crystalline structure, and both (200)TiC/(100)Ti and (111)TiC/(101)Ti orientation relationships were found in these films. In the TiC/B_4C films, only the sample with the largest bilayer thickness (25 nm) had significant crystallinity and only the TiC layer was crystalline. X-ray photoelectron spectroscopy depth profiles confirmed the presence of composition modulations in these films. Nanoindentation tests of the TiC/Ti multilayers showed hardness levels exceeding that predicted by the rule-of-mixtures. The TiC/B_4C multilayers showed increasing hardness with decreasing bilayer thickness but reached only 22 GPa. The pin-on-disc tests gave friction values ranging from 0.3 to 0.9 for both sets of films. These results were correlated with the degree of crystallinity and grain structure of the films.

I. INTRODUCTION

The mechanical properties of multilayer thin films have been the subject of numerous investigations over the past two decades. Hardness and yield strength enhancements for multilayers with composition modulations on the nanometer scale have been reported by a number of investigators who have examined metallic,[1–5] nitride,[6–8] and metal/nitride[9,10] multilayer structures. For example, TiN/VN multilayer films have shown hardness levels of up to 4800 kgf/mm^2, much higher than the constituent layers.[8] The primary strengthening mechanisms cited in these studies include coherency strengthening, modulus hardening, Hall–Petch strengthening, and the presence of slip-limiting interfaces.[11–13] In general, these theories are based on mechanisms that impede dislocation motion due to multilayer interfaces or coherency stresses. Hardness enhancement has also been achieved by combining layers with very different mechanical properties, such as metal/ceramic multilayers of Ti/TiN.[9] The mechanical properties of multilayers are closely related to their microstructural characteristics, such as grain structure, the extent of epitaxial growth, and the roughness and compositional sharpness of the interfaces as well as bilayer thickness. Therefore, characterization of multilayer structure and growth mechanisms is essential to understanding their mechanical properties.

In addition to hardness enhancements, it may also be possible to obtain improvements in the toughness and wear resistance of a coating by using fine-scale multilayer structures. The interfaces in a multilayer can act to deflect cracks and increase crack path lengths. Liu *et al.*[14] examined multilayers of TiC and various metals and claimed higher toughness compared to monolithic films. Obbard and Gross[15] conducted nanoscratch tests of TiC/Cr multilayers and found that considerable improvements in wear resistance could be obtained in films with multilayer structures.

In this study we have deposited and characterized multilayers using two systems. TiC/Ti and TiC/B_4C. In these systems, TiC has a B1 rocksalt structure, Ti has an HCP structure, and B_4C has a complex rhombohedral lattice, although B_4C forms an amorphous structure when deposited by PLD.[16] These two multilayer systems represent two extremes, one having a soft metal interlayer and the other a hard carbide interlayer. In the TiC/Ti system, the choice of Ti as the metal interlayer results

a)Address all correspondence to this author.
e-mail: jamesk@cisunix.unh.edu

in a system where the two layers are both structurally and compositionally dissimilar. In the selection of a hard interlayer for the second system, it was noted that most transition metal carbides, such as ZrC and TaC, have the same B1 structure as TiC, as well as similar hardness and modulus levels. Using one of these carbides as an interlayer would therefore be unlikely to either provide the desired structural discontinuity at the interface or provide much hardness enhancement. Therefore, B_4C was selected as the carbide interlayer for the second system since it provides a structurally discontinuous layer that can impede crack propagation or dislocation motion.

Ultimately, while it is important to understand the origins of improvements in specific properties, such as hardness and toughness, these property enhancements are most valuable to the extent that they translate into superior tribological performance of the coating in the intended application. Therefore, in this study we have evaluated the friction and wear behavior of the deposited coatings in addition to the film composition, microstructure, and hardness. It will be shown that the presence of a multilayer structure in the coatings affects the crystallinity and grain structure of the layers and can impact the wear behavior and wear failure mechanisms.

II. EXPERIMENTAL PROCEDURE

The films examined in this study were deposited by pulsed laser deposition (PLD). The PLD system used was a PVD Products model 3000 (PVD Products, Wilmington, MA). The PLD chamber incorporates a multitarget carousel that holds up to three 4-in.-diameter targets. Each target rotates about its own axis (i.e., an axis perpendicular to the target), and the targets can also be rotated into position for ablation for fixed deposition time. Target selection was computer controlled via a stepper motor and motion control software. To fabricate multilayers, a computer program was written to sequentially rotate each target into position to ablate the target for a fixed time. Substrates were also rotated during deposition, and a substrate-to-target distance of 9 cm was set by manually adjusting a linear translation stage. A programmable substrate heater was used to carry out film deposition at a substrate temperature of 400 °C. A KrF (λ = 248 nm) excimer laser (Lambda-Physik, model COMPEX 205, Fort Lauderdale, FL) was used for ablation and was operated at a laser power of 650 mJ/pulse and a repetition rate of 50 Hz. The energy density of the laser at the target was 6 J/cm^2.

Commercially manufactured titanium carbide and boron carbide targets were used to deposit the TiC and B_4C films. A background process gas (Ar, 99.999%) was present during deposition and maintained at a pressure of 5 mtorr. Si (111) and 440C stainless steel were used as substrates. After the substrates were precleaned, they were placed in the substrate holder and the system was pumped down to a base pressure of approximately 3×10^{-7} torr.

For the TiC/Ti multilayers, six sets of samples were deposited, ranging from 7 bilayers, with each layer deposited for 500 s, to 35 bilayers (100 s each), 42 (85 s), 54 (65 s), 70 (50 s), and 140 (25 s). For the TiC/B_4C multilayers, samples were deposited with 18 bilayers at 500 s for each layer, 36 (250 s), 72 (125 s), 144 (64 s), 288 (32 s), and 576 (15 s). Transmission electron microscopy (TEM) cross sections of selected samples, discussed in Sec. III.C, were used to determine the actual deposition rates, and bilayer thicknesses were calculated on the basis of these rates. The results are shown in Table I. The deposition rates obtained were 0.085 nm/s for Ti and 0.025 nm/s for TiC and B_4C. Total film thickness was 385 nm for TiC/Ti and 216 nm for TiC/B_4C.

Structural characterization of the films was carried out using x-ray diffraction (XRD) on a Rigaku D/MAX-B instrument equipped with a Cu x-ray tube (Rigaku/MSC, The Woodlands, TX). The microstructure was examined using TEM and was carried out on a Hitachi H-600 TEM operating at 100 kV (Hitachi Instruments, Inc., San Jose, CA). Samples for TEM were examined in cross section and were prepared by dimple grinding and ion thinning. Surface morphology of the films was examined using scanning electron microscopy (SEM) on an Amray 3300FE instrument.

Nanoindentation was used to measure film hardness and was conducted on a Hysitron nanomechanical test instrument (Hysitron Inc. Minneapolis, MN) equipped with a Berkovich indenter. Films were tested using a multiple loading sequence with loads ranging from 0.3 to 3 mN. Analysis of the resulting load–depth curves was carried out using the Oliver–Pharr method.[17] For each film, approximately 3–5 indents were made, with each of the multiple load sequences giving at least 10 hardness and elastic modulus values.

The film composition versus depth was determined using x-ray photoelectron spectroscopy (XPS). The XPS experiments were carried out on a Kratos Analytical

TABLE I. Parameters for TiC/Ti and TiC/B_4C multilayers.

TiC/Ti			TiC/B_4C		
No. of bilayers	Deposition time/layer (s)	Bilayer thickness (nm)	No. of bilayers	Deposition time/layer (s)	Bilayer thickness (nm)
7	500	55	18	500	25
35	100	11	36	250	12
42	85	9.4	72	125	6.2
54	65	7.2	144	64	3.2
70	50	5.5	288	32	1.6
140	25	2.3	576	15	0.8

instrument (Chestnut Ridge, NY) using a Mg K_α x-ray source. An Ar^+ ion beam was used for etching. Etch rates on the order of 15 nm/min (determined from known thickness of the bilayers) were obtained using an Ar^+ beam energy of 4 kV and a beam current of 5 μA. The incident angle of the Ar^+ beam was 45°.

Tribological studies of the samples were carried out using a pin-on-disc apparatus. The test conditions were ambient atmosphere (40% RH) and room temperature, a 100-g load on a ¼-in. (0.625 cm) 440C steel ball, a speed of 200 revolutions/min, and a track diameter of 6 mm. These tests were done with the disc horizontal. The wear debris just outside the track was examined by SEM analysis to determine the size of the wear debris particles.

III. RESULTS

A. Structural characterization

Figures 1(a) and 1(b) show x-ray diffraction patterns for the TiC/Ti and TiC/B_4C multilayers deposited on (111) Si substrates at 440 °C. For TiC/Ti multilayers, all the diffraction patterns exhibited weak Bragg reflections, indicating a low degree of crystallinity. However, it was possible to classify three types of patterns for the TiC/Ti multilayers: the first, found in the sample with 7 bilayers, exhibited primarily (100) and (101) Ti reflections; the second type, found in samples with 35, 70, and 140 bilayers, had (111) TiC and (101) Ti as the primary reflections; the third, in the 42- and 52-bilayer samples, had a strong peak intermediate between (101) Ti and (111) TiC as well as a (200) TiC reflection. For the 7-bilayer sample, the presence of the Ti metal layer is clear, but TiC reflections were not observed. Nonetheless, it will be shown in the following section describing XPS depth-profiling results that there is a layer of near-stoichiometric TiC present in these films. It is possible that the reflection is very diffuse or that the orientation of the TiC layers was not favorable for diffraction in the Bragg–Brentano geometry.

The samples with 35, 42, and 140 bilayers are consistent with known positions of the (111) TiC and (101) Ti phases. However, the (101) peaks in the 70- and 140-bilayer samples are shifted to higher angles in comparison to the 35-bilayer sample. This can be attributed to carbon diffusion into the metal layers, which is known to reduce the lattice parameter of Ti and will therefore shift the peak to higher angles.[18] In addition, the observation of more extensive interdiffusion in the samples with thinner bilayers is consistent with the kinetics of interdiffusion. The samples with 42 and 54 bilayers have a clear (200) TiC reflection, but the strongest peak lays approximately 0.4° in 2θ to the right of the (100) Ti reflection found in the 7-bilayer sample. However, the peak for the 7-bilayer sample is very broad and of low intensity, so its position cannot be used as a reliable

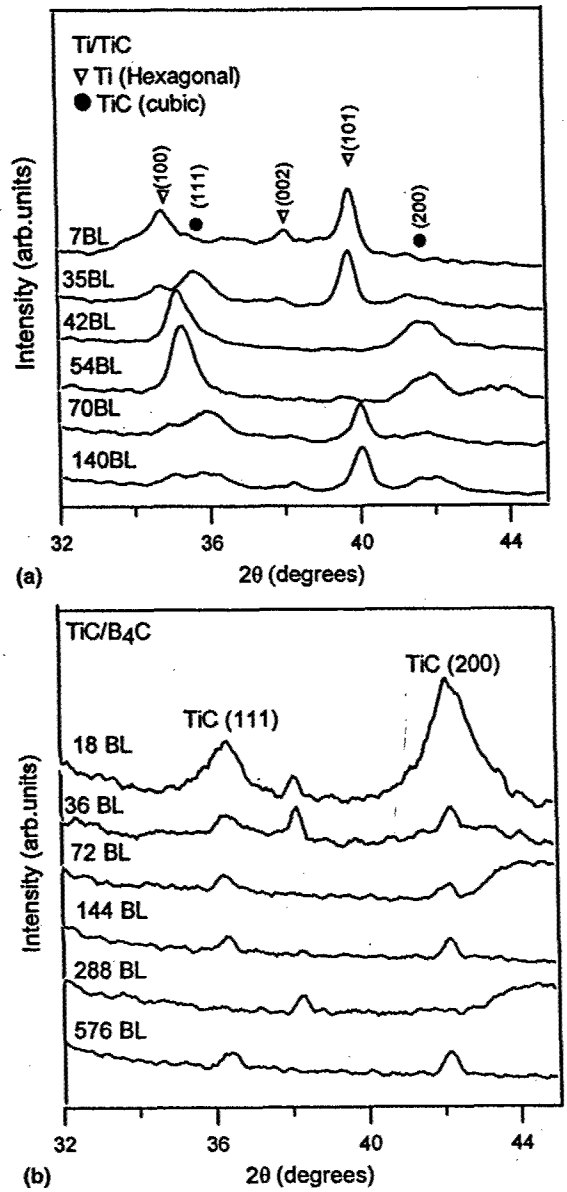

FIG. 1. X-ray diffraction patterns for multilayer films deposited at 400 °C on Si(111) substrates: (a) TiC/Ti; (b) TiC/B_4C. In the TiC/Ti multilayers, both Ti and TiC peaks are observed, but various orientations are observed depending on the bilayer thickness, as discussed in the text. For the TiC/B_4C multilayers, on the 18-bilayer sample exhibits significant crystallinity and only in the TiC layer.

standard for the (100) Ti peak position. Instead, it is noted that the accepted peak position is 35.08° in 2θ, close to the angle of 35.2° in 2θ found here. Again, the shift can be attributed to carbon diffusion into the α–Ti. Therefore, the 35-, 70-, and 140-bilayer samples had (111) TiC/(101) Ti as the primary preferred orientations while the 42- and 54-bilayer samples exhibited (200) TiC/(100) Ti orientations. The presence of a particular orientation type does not correlate with bilayer thickness, so other factors must play a role in determining which preferred orientation forms. However, it can be noted that

the observed (111) TiC/(101) relationship indicates matching between the ($\bar{1}11$) TiC planes [intersecting at 19.5° to the (111) surface normal] that continue as basal planes into the HCP-Ti layer. The latter structure can be obtained from an FCC-type structure by a displacement of a/2[$\bar{1}\bar{1}0$] of every other close-packed plane and gives a [$0\bar{1}1$]TiC ‖ [$\bar{1}2\bar{1}0$]Ti matching of directions. Lattice matching for the (200) TiC/(100) Ti combination is less favorable, with the closest in-plane matching along the [001]TiC ‖ [0001]Ti directions, which represents a 7.1% mismatch.

Films deposited on 440C steel substrates were also examined using x-ray diffraction. Analysis of the results was complicated by the fact that the steel contains both a martensitic structure and carbide phases, both of which strongly diffract. Nonetheless, the results obtained were reasonably consistent with the films on Si substrates. The 42- and 54-bilayer samples had (100) Ti reflections, whereas the 35- and 70-bilayer samples had (111) TiC and (101) Ti peaks. Verification of the (200) TiC reflections was difficult due to the nearby peaks present from the Cr carbides in the steel. The 7-bilayer sample exhibited a broad peak near 35.2°, as was observed for the films on Si substrates.

The TiC/B_4C multilayers [Fig. 1(b)] were largely amorphous, with the exception of the 18-bilayer sample, which had a crystalline TiC component. The remaining samples had very weak TiC reflections. (Note the peak-to-background ratio is much smaller than for the TiC/Ti multilayers.) We did not observe any peaks for the B_4C phase indicating these layers were always amorphous. In several cases, there is a small peak just above 38°, and this may be due to a reaction between the layers and the formation of small grains of TiB at the interface, which has a (111) peak at 38.3° in 2θ. However, the TEM observations (Sec. III.C) confirmed the mostly amorphous nature of these films, suggesting only isolated nanocrystals of TiB or crystalline TiC formed in the multilayers samples with more than 18 bilayers.

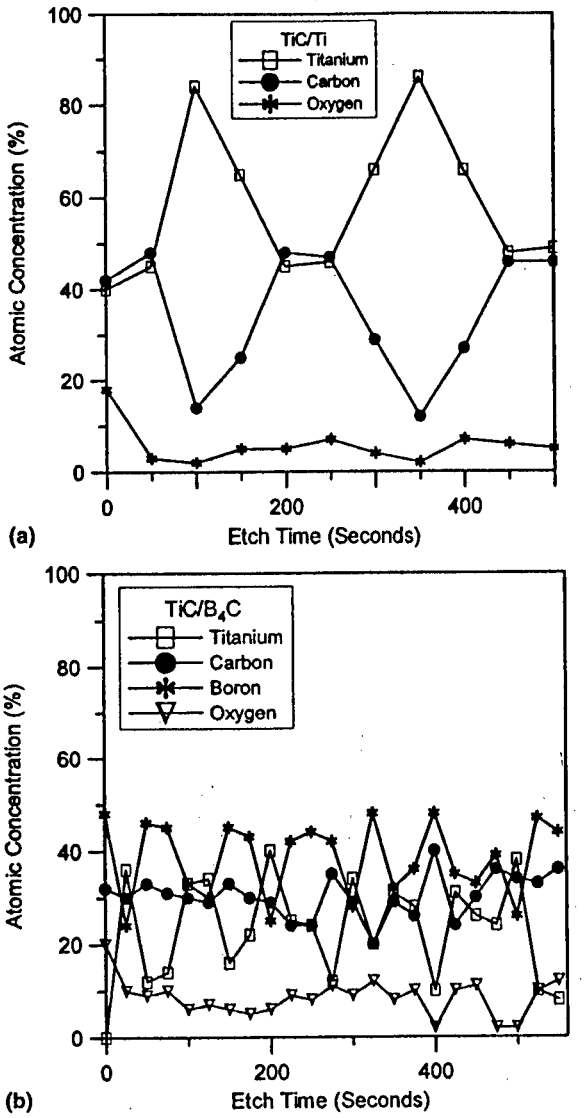

FIG. 2. XPS depth profiles of multilayer films on Si(111) deposited at 400 °C: (a) TiC/Ti (7 bilayers); (b) TiC/B_4C (18 bilayers). The observed composition modulations confirm the multilayer structure. In the TiC/Ti sample, significant diffusion of carbon into the Ti layer is observed.

B. Compositional characterization by XPS depth profiling

Compositional analysis was carried out by x-ray photoelectron spectroscopy. XPS depth profiles of the TiC/Ti (7 bilayers) and TiC/B_4C (18 bilayers) multilayers are shown in Figs. 2(a) and 2(b), respectively. Figure 2(a) shows the expected composition modulations in the TiC/Ti multilayers. The TiC layers are very close to stoichiometric TiC, and the shape of the composition profile for the Ti-rich layers indicates carbon has diffused into Ti layers, as expected on the basis of the XRD data. It is also noted that the Ti layers are considerably thicker than the TiC layers, consistent with the measured deposition rates. The binding energies of Ti and C in the TiC layers were 455 eV ($2p_{3/2}$) and 282 eV ($1s$), respectively, indicating that carbon was mostly in the carbidic state. For the TiC/B_4C multilayer [Fig. 2(b), 18-bilayer sample], a compositional modulation was also observed, but the amplitude of the modulation was small, possibly due to ion beam mixing or convolution of the layers during measurement.[19] Analysis of monolithic B_4C films deposited by PLD under the same conditions as those used for the multilayers gave a B:C ratio of approximately 7:3, indicating the PLD method provides reasonably good reproduction of the target stoichiometric in the deposited films. The depth profiles shown here also indicate the concentration of oxygen was approximately 5% in the TiC/Ti multilayer and approximately 8% in the TiC/B_4C multilayer. Previous studies of PLD TiC[20] reported similar levels of oxygen in the films, and it was

concluded that the oxygen substituted for carbon on the carbon sublattice of the B1 structure. However, the oxygen content was found to have little effect on the hardness levels.

C. Microstructural and morphological characterization

Cross-section TEM images of selected TiC/Ti and TiC/B_4C multilayers are shown in Figs. 3(a) and 3(b). Figure 3(a) shows the TiC/Ti sample deposited with 35 bilayers and 100-s deposition time/layer. (Note that not all layers are visible due to the wedge shape of the cross section created during ion thinning of the sample). The Ti layers have a thickness of 8.5 nm and TiC layers were 2.5-nm thick, for a total bilayer thickness of 11 nm. The microstructure of the multilayers shows a columnar structure, with light and dark columns appearing due to diffraction contrast. The presence of diffraction contrast indicates at least some degree of crystallinity in these layers. The continuity of the columns also indicates a degree of epitaxial growth from one layer to the next, which correlates with the XRD observations.

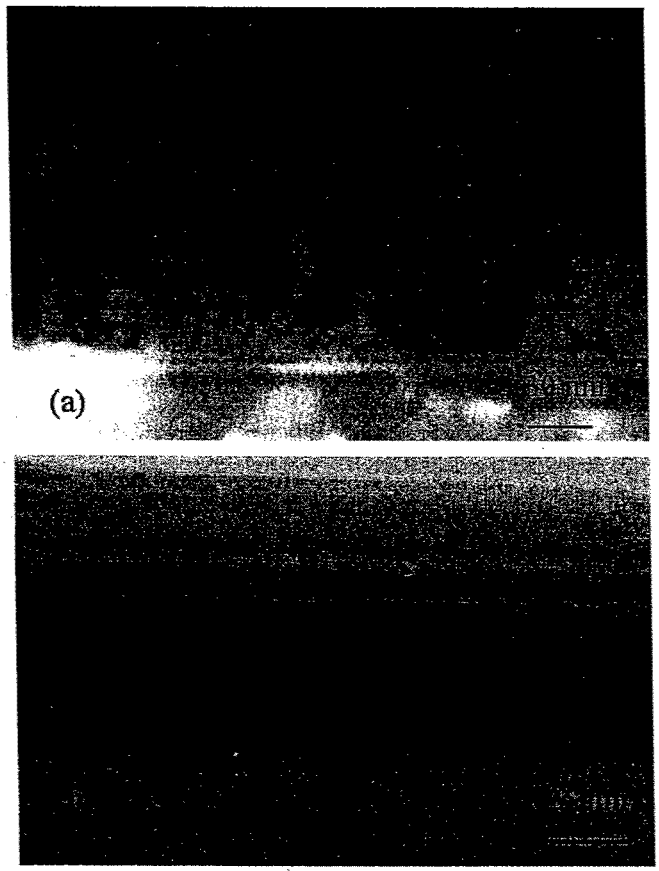

FIG. 3. TEM cross-section images of multilayer films deposited on Si(111) at 400 °C: (a) TiC/Ti (35 bilayers); (b) TiC/B_4C (36 bilayers). In the TiC/Ti sample, a columnar structure is observed. Also, note the small grains within the TiC layers (darker color) of the TiC/B_4C sample.

The deposition rate for TiC, as determined by the thickness of the TiC layers in the TiC/Ti sample, was nearly identical to the rate measured in the TiC/B_4C sample. This indicates that the extent of carbon diffusion during deposition (as discussed in Sec. III.A) was not extensive enough to modify the relative layer thickness.

The TiC/B_4C multilayer with 36 bilayers and 250 s each/layer is shown in Fig. 3(b). A distinct multilayer structure is shown with sharp interfaces between the layers. A columnar structure was not observed here, and B_4C layers (lighter color) were amorphous, as expected from the XRD data. The TiC layers show some weak nanocrystalline grain contrast, indicating slight crystallinity in these layers. However, for thinner layers, less crystallinity would be expected, as was consistent with the x-ray diffraction patterns.

Scanning electron microscopy observations of the surface morphology are shown in Figs. 4(a) and 4(b). The density of particulates for the TiC/Ti multilayer is

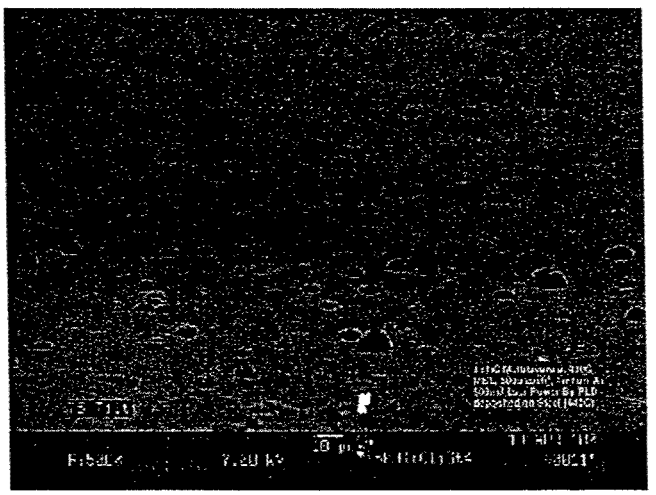

(a)

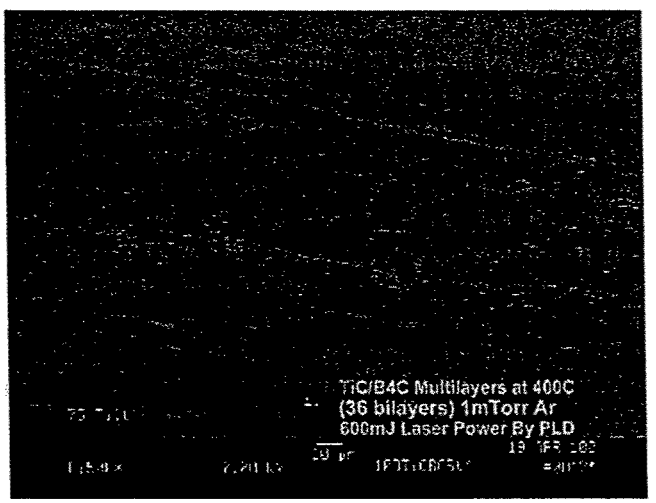

(b)

FIG. 4. SEM images of film surfaces for films deposited on Si(111) substrates: (a) TiC/Ti (7 bilayers); (b) TiC/B_4C (36 bilayers). Note the higher density of particulates on the TiC/Ti sample.

considerably higher in comparison to the TiC/B_4C. Particulates of this nature are common in PLD films, and it is expected that ablation of a metal will generate more particulates due to its lower melting point.

D. Mechanical properties

Figures 5(a) and 5(b) show the hardness and elastic modulus versus bilayer thickness (plotted as $1/\sqrt{t}$, where t = bilayer thickness) for the TiC/Ti and TiC/B_4C multilayers. For the TiC/Ti multilayers, the hardness varied between 17 and 24 GPa, but the overall trend indicated only a slight decline in hardness for the thinner bilayers. The hardness of the TiC/B_4C multilayers was generally below that of the TiC/Ti multilayers but exhibited a trend of increasing hardness with reduced bilayer thickness. These data are further discussed in the Sec. IV.

E. Tribological properties

Tribological studies were conducted on both the Ti/TiC and TiC/B_4C samples using a pin-on-disc test apparatus. The TiC/Ti samples were run for a total of 10,000 cycles under 1-N load. The results are shown in Fig. 6(a). The friction coefficients obtained in these tests exhibited a wide range of values, from 0.3 to close to 1.0. However, if the average friction values are examined (averaged from 2000 to 10^4 cycles), a bilayer-dependent trend can be observed: the lowest friction (0.3) is observed in the 7-bilayer sample. The 35-bilayer sample is considerably higher, and the 42- and 54-bilayer samples are both near 0.9. Following this, the 70- and 140-bilayer

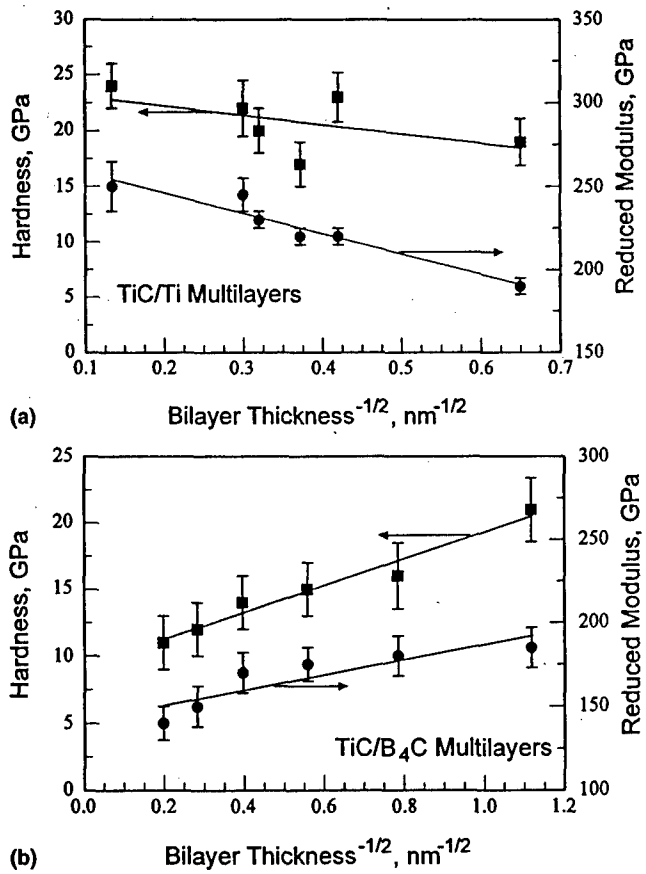

FIG. 5. Hardness and elastic modulus versus inverse square root of bilayer thickness for multilayers deposited on 440C steel substrates: (a) TiC/Ti; (b) TiC/B_4C. For TiC/Ti multilayers, the hardness values lie between those of TiC and Ti but exceed that expected from the rule of mixtures. In the TiC/B_4C multilayers the hardness is observed to increase with decreasing layer thickness.

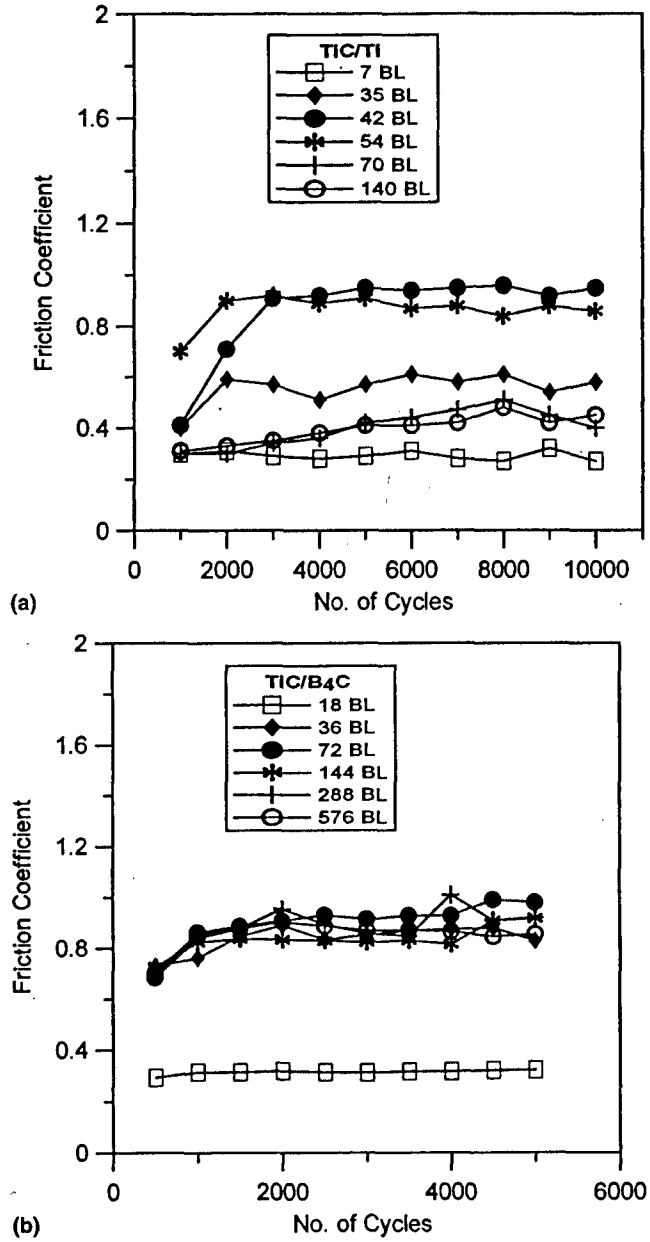

FIG. 6. Friction/wear test results for the multilayer films deposited on 440C steel: (a) TiC/Ti; (b) TiC/B_4C. In (a), the friction is lowest for the largest and smallest values of multilayer thickness; also, the 42- and 54-bilayer samples, which had a (200) TiC/(100) Ti film orientation, exhibited the highest friction. In the TiC/B_4C multilayers, only the 18-bilayer sample (the only TiC/B_4C multilayer with crystalline TiC layers) maintained low friction values.

samples exhibit reduced friction of about 0.4. Therefore, it appears that the best samples are those with either thick or very thin bilayers. However, it can also be recalled from the x-ray diffraction data that the 42- and 54-bilayer samples exhibited a crystallographic texture different from the other samples and had a (200)TiC/(100)Ti orientation. The analysis of the crystallography of this orientation relationship indicated less favorable lattice matching between layers than the other samples. Therefore, this texture difference may change the nature of crack propagation through and along the layers and cause failure of the films.

The friction data for the TiC/B_4C samples are shown in Fig. 6(b). Here, only one sample is low in friction, namely the 18-bilayer sample, while the remaining samples are all near 0.9. The latter value is obtained for steel-on-steel friction and suggests that the films exhibited rapid failure. To investigate the failure mechanisms, the wear tracks of several samples were examined in the SEM, and the results are shown in Fig. 7. Figure 7(a) shows the wear track of the 18-bilayer sample. The wear track is smooth and the film is still present in the track, as expected from the friction data. Figure 7(c) shows a 36-bilayer sample, where it is clear that the film has been removed from the track. Figures 7(b) and 7(d) show wear debris from the 18- and 36-bilayer samples, respectively. It is noted that the 18-bilayer sample has significantly smaller debris than the 36-bilayer sample. If the structural characterization is recalled, it is noted that the 18-bilayer sample was the only one with a significant degree of crystallinity, and the XRD data results indicated the formation of a nanocrystalline grain structure in the TiC layer. This fact, along with the smaller debris, suggests that the presence of the nanograin structure modifies the crack propagation path, resulting in less damage. In contrast to this, the samples that were mostly amorphous had fewer microstructural features to deflect cracks, resulting in rapid failure and large debris particles. Previous studies of PLD TiC[20] run under similar conditions reported a friction coefficient of 0.3 and a wear life of 30,000 cycles. Therefore, the layered structure in these films created by the compositionally modulating TiC and B_4C did not appear to provide improved resistance to wear failure.

IV. DISCUSSION

Pulsed laser deposition has been used to deposit multilayers of TiC/Ti and TiC/B_4C films, and the structural, compositional, mechanical, and tribological properties of these samples were reported in the previous sections. In terms of the structure of the multilayers in these two systems, the most notable difference was the formation of crystalline versus amorphous layers. The TiC/Ti multilayers were mostly nanocrystalline as determined by both XRD analysis and the TEM cross sections. The TEM images also showed a columnar structure indi-

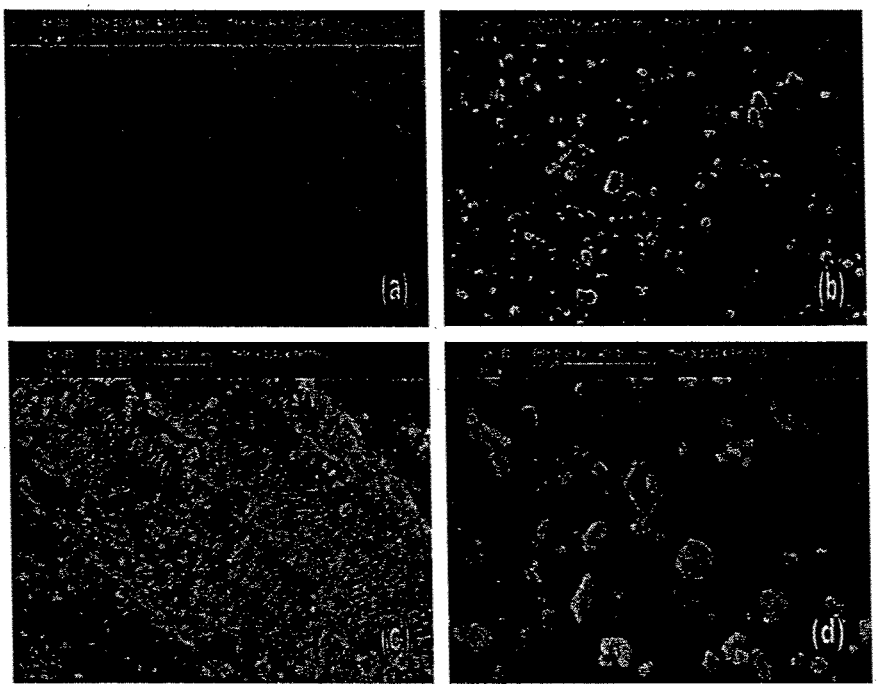

FIG. 7. SEM analysis of the wear track for two TiC/B_4C samples: (a) wear scar for the 18-bilayer sample; (b) debris outside the wear track for the 18-bilayer sample; (c) wear scar for the 36-bilayer sample; (d) debris outside the wear track for the 36-bilayer sample. Note the larger wear debris for the 36-bilayer sample.

cating some heteroepitaxy during the growth of these multilayers. The TiC/B_4C multilayers were mostly amorphous in nature, but in the TEM sample a small number of nanocrystalline grains were observed in the TiC layers. PLD of TiC at 400 °C is known to be crystalline when deposited as a single monolithic film.[20,21] The Ti and B_4C layers therefore influence the structure of deposited TiC such that Ti maintains the crystalline structure but B_4C promotes deposition of amorphous TiC. The XRD patterns for the TiC/B_4C multilayers showed significant crystallinity of TiC only at the largest bilayer thickness.

One objective of depositing fine-scale multilayer structures is to increase hardness. The TiC/Ti films had hardness values in the range of 17–24 GPa. Since the film thickness was 385 nm, and the indentation depth was typically 40 nm (10.4% of the thickness), these data should not be strongly affected by the substrate. For titanium carbide or boron carbide alone, when deposited by PLD, the hardness has been found to be in the range of 35–40 Gpa.[20,21] Unalloyed Ti typically has a yield stress of 175–500 MPa, depending on impurity content, and taking hardness as three times the yield strength gives a range of 0.5 to 1.5 GPa. Therefore, it is expected that Ti interlayers would reduce hardness. To calculate a hardness value based on the rule of mixtures, it is noted from the given deposition rates (Sec. II) that the films are 77% Ti and 23% TiC. Using these values and the maximum values for hardness of each component, we obtain a multilayer hardness of 10.4 GPa. The hardness of we obtained for the TiC/Ti multilayers is significantly higher. However, given the anisotropic nature of the multilayer structure, the linear rule of mixtures may not be valid. The fact that the softer Ti layers are constrained by the TiC layers, similar to a Hall–Petch effect grain-size hardening effect, may contribute more significantly to the measured hardness levels. In this case, we would expect that the hardness would increase with $t^{-1/2}$ (t = bilayer thickness). However, the data in Fig. 5(a) instead demonstrate a slight reduction in hardness with decreasing bilayer thickness. A possible explanation for this behavior can be found in the chemical characterization data, where XPS depth profiles showed interdiffusion taking place between the TiC and Ti layers, which would also be expected to be more extensive with thinner layers. This reduces the interface sharpness and amplitude of the composition modulations, both of which have been cited as important to obtaining high hardness levels.[11,12] Therefore, there are two competing effects, and the net effect is a slight reduction in hardness with decreasing bilayer thickness.

The TiC/B_4C multilayers had lower hardness values than the TiC/Ti films. This, in part, may be due to the lower deposition rates giving a total film thickness of only 216 nm, introducing substrate effects in the hardness measurements. Another reason for the low hardness may be due to the degree of crystallinity. In our previous studies of TiC and Ti–Si–C films,[20] it was found that amorphous Ti–Si–C films had a lower hardness value (approximately 12 GPa), whereas when the structure became 50% crystalline, the film hardness has increased to about 35 GPa. Therefore, because of the amorphous nature of the TiC/B_4C multilayers, a lower hardness would be expected. However, other explanations for the low hardness, such as interface decohesion in the multilayer structure, cannot be excluded at this point. Nonetheless, the trend of hardness versus bilayer thickness in the TiC/B_4C multilayers demonstrates interesting behavior, as it increases with decreasing bilayer thickness. When hardness versus $1/t^{1/2}$ is plotted, a reasonable fit is obtained. This is particularly noteworthy as most theories for multilayer hardening[11–13] are based on resistance to dislocation motion or coherency hardening and therefore assume a crystalline structure in the multilayers. In the present case, deformation is expected to occur by microcracking, and the presence of multilayer interfaces may force the microcracking process (i.e., the nucleation and propagation of a crack) to occur at higher stress levels.

While the hardness of the films exhibited only a modest dependence on bilayer thickness, the wear behavior of the films varied considerably. Examination of the friction and wear test results indicated that grain structure in the films can play an important role in their tribological behavior. In the TiC/B_4C samples, only the film with significant crystallinity in the TiC layer remained on the substrate for the duration of the test. The remaining films, which were largely amorphous, failed rapidly, and large debris particles were found outside the wear track. In the TiC/Ti films, the grain orientation was also found to be a factor in friction/wear behavior, with the (200) TiC/(100) Ti oriented films failing more rapidly than the remaining samples. The crystallographic orientation and texture of these coatings and their influence on grain structure and cohesion, as well as their impact on tribological properties, are subjects that warrant further investigation.

V. CONCLUSIONS

We have investigated the structural and mechanical properties of TiC/Ti and TiC/B_4C multilayers deposited by pulsed laser deposition (PLD). This investigation led to the following conclusions:

(1) Examination of the microstructure and crystallinity revealed that the TiC/B_4C multilayers were largely amorphous, whereas the TiC/Ti multilayers were crystalline with a columnar grain structure.

(2) Two types of crystallographic orientation relationships were found in the TiC/Ti films: (111) TiC/(101) Ti and (200) TiC/(100) Ti.

(3) Nanoindentation hardness tests showed that the TiC/B_4C hardness increased with decreasing bilayer thickness. The hardness scaled with the $t^{-1/2}$, but overall the hardness was lower than previously observed for the constituent layers. The hardness of the TiC/Ti sample, while exceeding values predicted by the rule of mixtures, showed a slight decrease with decreasing bilayer thickness. This was attributed to interdiffusion between the layers during deposition.

(4) Friction and wear behavior as determined by pin-on-disc wear tests showed a range of friction/wear behavior in the TiC/Ti samples. Films with the (200) TiC/(100) Ti orientations failed rapidly, while the remaining films performed significantly better. In the TiC/B_4C multilayers, only the sample with the largest bilayer thickness (and significant crystallinity) performed satisfactorily. These results indicate that the texture and grain structure can play an important role in providing wear resistance. While the presence of multilayer interfaces may impact wear behavior, the multilayer structure in these films may be more important in their role as a means to manipulate the texture and grain structure of the films.

ACKNOWLEDGMENT

The financial support of the Air Force Office of Scientific Research, under Grant No. F49620-98-1-0499, is gratefully acknowledged.

REFERENCES

1. D.M. Tench and J.Y. White, Metall. Trans. A **15A,** 2039 (1984).
2. R.F. Bunshah, R. Nimmagadda, H.J. Doerr, B.A. Movchan, N.I. Grechanuk, and E.V. Dabizha, Thin Solid Films **72,** 261 (1980).
3. R.C. Cammarata, T.E. Schlesinger, C. Kim, S.E. Qadri, and A.S. Edelstein, Appl. Phys. Lett. **56,** 1862 (1990).
4. S.L. Lehoczky, J. Appl. Phys. **49,** 5479 (1978).
5. J.E. Krzanowski and P. Duggan, in *Thin Films: Stresses and Mechanical Properties V,* edited by S.P. Baker, P. Børgesen, P.H. Townsend, C.A. Ross, and C.A. Volkert (Mater. Res. Soc. Symp. Proc. **356,** Pittsburgh, PA, 1995), p. 391.
6. P. Yashar, S.A. Barnett, J. Rechner, and W.D. Sproul, J. Vac. Sci. Tech, A **16,** 2913 (1998).
7. U. Helmerson, S. Todorova, S.A. Barnett, J.E. Sundgren, L.C. Markett, and J.E. Greene, J. Appl. Phys. **62,** 481 (1987).
8. M. Shinn, L. Hultman, and S.A. Barnett, J. Mater. Res **7,** 901 (1992).
9. E. Kusano, M. Kitagawa, H. Nanto, and A. Kinbara, J. Vac. Sci. Technol., A **16,** 1272 (1998).
10. X. Wang, A. Kolitsch, and W. Möller, Appl. Phys. Lett. **71,** 1951 (1997).
11. J.E. Krzanowski, in *Thin Films: Stress and Mechanical Properties III,* edited by W.D. Nix, J.C. Brauman, E. Arzt, and L.B. Freund (Mater. Res. Soc. Symp. Proc. **239,** Pittsburgh, PA, 1992), p. 509.
12. J.E. Krzanowski, Scr. Met. Mater. **25,** 1465 (1991).
13. X. Chu and S.A. Barnett, J. Appl. Phys. **77,** 4403 (1995).
14. C.H. Lui, W-Z. Li, and H-D. Li, J. Mater. Res. **11,** 2231 (1996).
15. R. Obbard and T. Gross, MRS Proceedings, Fall, Boston, MA (2001, unpublished).
16. A.R. Phani and J.E. Krzanowski, University of New Hampshire (unpublished research).
17. W.C. Oliver and G.M. Pharr, J. Mater. Res. **7,** 1564 (1992).
18. J-E. Sundgren, B-O. Johansson, and S-E. Karlsson, Thin Solid Films **105,** 353 (1983).
19. A. Zalar, S. Hofmann, P. Panjan, and V. Krasevec, Thin Solid Films **220,** 191 (1992).
20. J.E. Krzanowski and R.E. Leuchtner, J. Am. Ceram. Soc. **80,** 1277 (1997).
21. A.R. Phani, J.E. Krzanowski, and J.J. Nainaparampril, J. Vac. Sci. Technol., A **19,** 2252 (2001).

ELSEVIER

Applied Surface Science 174 (2001) 132–137

applied surface science

www.elsevier.nl/locate/apsusc

Preferential growth of Ti and TiN films on Si(111) deposited by pulsed laser deposition

A.R. Phani, J.E. Krzanowski*

Department of Mechanical Engineering, University of New Hampshire, Durham, NH 03824, USA

Received 25 September 2000; accepted 31 December 2000

Abstract

Ti and TiN films have been grown by pulsed laser deposition (PLD) from a titanium target in reactive gas atmospheres of 1 mTorr Ar and 10 mTorr N_2, respectively. The films were deposited onto Si(111) substrates at temperatures of 200, 400 and 600°C. X-ray diffraction (XRD) revealed that the TiN films exhibited a strong (100) orientation at all substrate temperatures. However, films deposited at 200°C showed only (100) oriented grains, while those deposited at 400 and 600°C had an additional small component of grains with alternate orientations. Ti films showed strong (100) at 200 and 400°C, but shifted to strong (002) at 600°C. The deposited films exhibited densely-packed grains, with smooth and uniform structures. X-ray photoelectron spectroscopy (XPS) analysis of the films showed 99.5% Ti in the Ti films and 50% Ti, 45% N in TiN films, indicating stoichiometric composition in the deposited films.

Keywords: Pulsed laser deposition (PLD); X-ray photoelectron spectroscopy (XPS); Scanning electron microscopy (SEM)

In recent years, extensive research has focused on metal nitrides, such as TiN, CrN, VN, and NbN, generating practical applications in the areas of protective coatings and electronic device materials. TiN has gained much interest due to its potential applications in different areas of silicon device technology, namely as diffusion barrier in metallization schemes, rectifying and ohmic contacts, and gate electrodes in field effect transistors [13]. Titanium nitride films exhibiting high hardness, enhanced wear, corrosion resistance, and excellent diffusion barrier properties have been prepared by plasma deposition methods [1–3]. On the other hand, pulsed laser deposition (PLD) is a thin film growth technique that is widely used to deposit high quality multicomponent oxide films [4,5]. These include ceramic materials such as high temperature superconductors, ferrites and ferroelectrics. Very few reports on the growth and characterization of metal nitride such as CN [6], TiN [7–9], NbN [10], TiCN [11] and multilayers of TiN/NbN [12], Ti/TiN [13], TiN/BN [14] deposited by pulsed laser and sputtering techniques have been explored.

In the present work, TiN films were grown in a high vacuum PLD chamber (Epion Corporation Model, PLD 3000, described elsewhere [15]). A pulsed (50 Hz) KrF excimer laser (248 nm) beam with a laser power of 500 mJ was focused onto a programmable rotating Ti (99.99%) target. The laser beam was rastered over a 5 cm distance on the rotating target to ensure good uniformity of the deposit. Both Ti and TiN films were deposited. For the Ti films, Ar was used as a background gas and was maintained at 1 mTorr, while TiN films, N_2 was used and maintained at a pressure of 10 mTorr. The substrates were

* Corresponding author. Tel.: +1-603-862-2315; fax: +1-603-862-1865.
E-mail address: jamesk@cisunix.unh.edu (J.E. Krzanowski).

0169-4332/01/$ – see front matter
PII: S0169-4332(01)00153-2

precleaned [14] and placed on the substrate holder and maintained at a distance of ~6.5 cm directly above the target. The substrate temperature was measured with a thermocouple mounted near the substrate holder. Film thickness was determined using profilometry (on a Tencor Alfa step instrument). After 2 h of deposition, typical films thicknesses were on the order of 1 μm. The deposited films appeared smooth and continuous were gray (Ti) and golden yellow (TiN) in color at all substrate temperatures.

The deposited films were analyzed using X-ray photoelectron spectroscopy (XPS), X-ray diffraction (XRD) and scanning electron microscopy (SEM). XRD was carried out on both a Rigaku D/MAX-B diffractometer, using a Cu X-ray tube, and a Bruker/AXS general area detector diffraction system (GADDS), which employed Cr Kα radiation.

Typical GADDS images of the Ti and TiN films deposited on Si(111) at substrate temperature of 200°C are shown in the Fig. 1(a) and (b), respectively. Both measurements have been taken at 2θ (detector) = 55, ω (sample) = 25, and detector to sample distance at 15 cm. The area detector frame provides a quick overview of the crystallinity, composition, and orientation of the film. If the observed Debye rings are smooth and continuous, then the sample is polycrystalline and fine grained. If the rings are continuous but spotty, then the material is polycrystalline and large grained. Incomplete Debye rings indicate preferred orientation or texture, and if only individual spots are observed, the material is single crystal, which can be considered the limiting case of crystallographic texture. In our case, Ti and TiN films deposited on Si(111) have shown single Debye rings indicating the deposited films are highly textured in (100) and (200) orientations, respectively, rather than single crystals. Films deposited at room temperature have shown broad peaks indicating an amorphous nature in the deposited films.

X-ray diffraction patterns collected using Rigaku θ–θ diffractometer were used to determine the lattice parameters and peak width at half maximum, with the background and $K\alpha_2$ contributions subtracted numerically before the measurements. The instrumental peak broadening was measured using a silicon standard. Fig. 2(a) and (b) represents the Ti and TiN films grown on to Si(111) at different substrate temperatures. JCPDS card No. Ti:44-1294, TiN:38-1420 were used

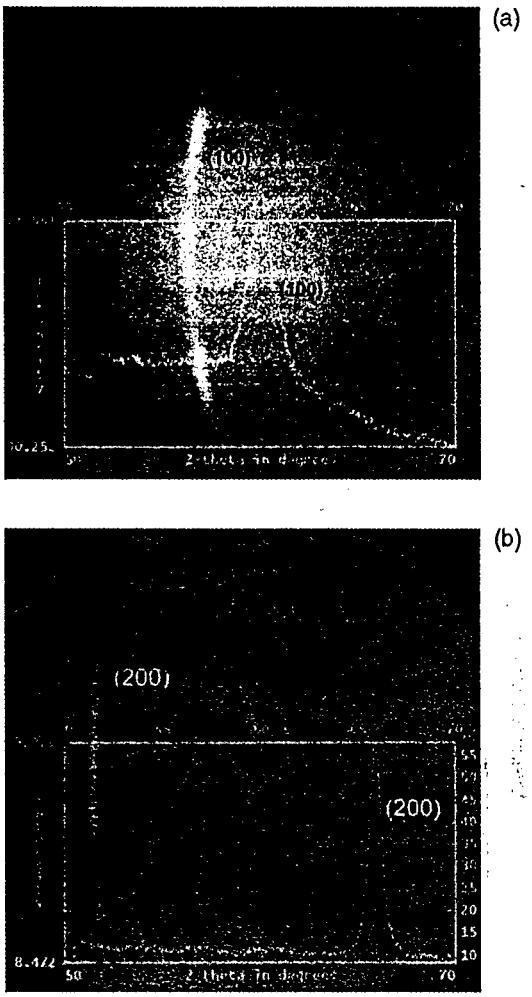

Fig. 1. A typical microdiffraction image file showing (100) diffraction discontinuous line of (a) Ti and; (b) TiN on Si(111) at 200°C.

to verify the crystalline structures for both the Ti and TiN. The TiN films are highly oriented in (100) orientation only when deposited at a substrate temperature of 200°C. As we increase the temperature, we observe additional randomly oriented grains, but the (200) peak remains the strongest line, indicating it retains the largest volume fraction. The Ti films showed a strong (100) orientation for the 200 and 400°C depositions, and then changed to polycrystalline nature with a preferred (002) orientation at 600°C. The experimental diffraction peaks, calculated lattice parameters, crystallite size of Ti and TiN on Si(111)

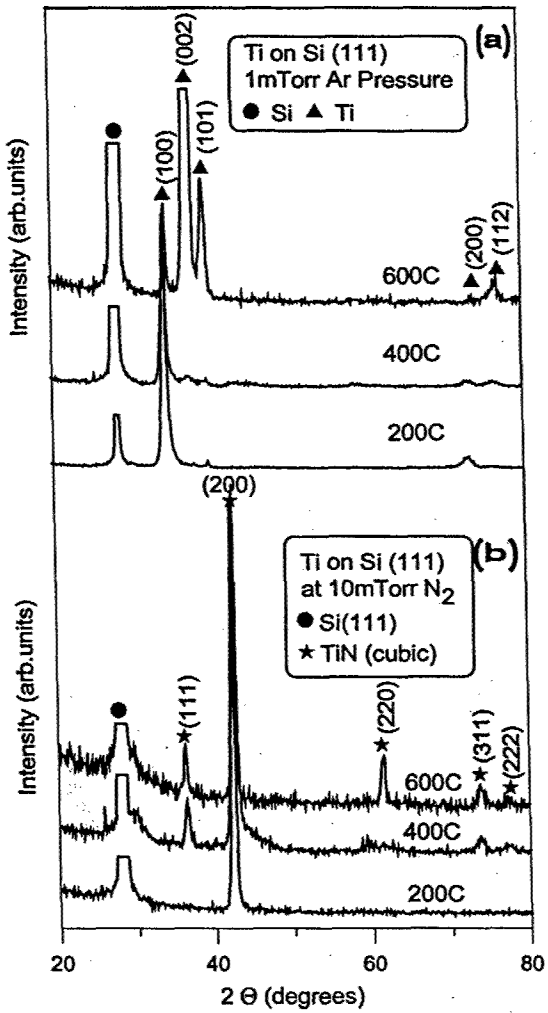

Fig. 2. X-ray diffraction pattern of (a) Ti and (b) TiN deposited on Si(111).

are tabulated in Table 1. The crystallite size of the deposited films are in the range of 28–32 nm for Ti and 21–28 nm for TiN. There is no significant change in the lattice parameters of the deposited films at different substrate temperatures compared to TiN films obtained from TiN target [8] by PLD. The crystallite size of the films are smaller (28 nm at 600°C) in our case, when compared to TiN films (67 nm at 600°C) obtained directly from TiN target by PLD [8].

The surface morphology of the deposited films was examined by scanning electron microscopy (SEM model: AMRAY 3300FE). Similar surface morphology has been observed for all the deposited films in case of Ti films with particulates (2–3 μm size) on the surface. The SEM images of Ti and TiN films deposited at 200°C are shown in Fig. 3(a) and (b), respectively. The deposited films are flat, showing very densely-packed grains. On the other hand, small particulates with a diameter of 5 μm and height of 3 μm were observed in case of Ti films on Si(111). These particulates were very much observed in case of Ti films (~40% of the surface) in comparison to the TiN films (~5% on the surface). However, the exact role played by the background gas of N_2, in case of TiN films, to make the films smooth is still to be understood. Similar behavior was also observed for the films deposited at 400 and 600°C.

Finally, the composition of the films were obtained by XPS, and showed 99.5% purity in the Ti films and 50% Ti, 45% N in the TiN films, indicating near stoichiometry of TiN in the deposited films. The adhesion of the films on to the substrates has been tested by the simple scotch tape test. No peeling or crack has been observed for the deposited films. In brief, on laser ablation area molecular nitrogen is breaking into atomic nitrogen which is further reacting with ablated titanium atoms to form TiN films. The formation of TiN is totally based on the background pressure of the N_2. In our case, we have used 10 mTorr to obtain single phase TiN structure.

The preferred orientation observed in the films here, as a function of the deposition temperatures, is contrary to the expected trend. Namely, the 200°C films showed the highest preferred orientation with other grain orientations absent. In previous studies of TiN deposition, Si(100) substrates were used [9,14]. The films were polycrystalline at low temperatures but strongly (200) oriented at higher temperatures (650°C). Our films, grown on Si(111), show a strong (200) orientation at all temperatures with additional grain orientations present at 400 and 600°C. This result can be explained by considering the competition between surface energy and epitaxy. At low temperatures, surface energy effects dominate leading to (200) oriented films, since TiN has a B1 structure with low energy (100) planes. At higher temperatures, with higher atomic mobility, there is more of a tendency for epitaxy leading to the nucleation of (111) grains. Other orientations observed, such as (220) and (311) may be due to a transition occurring from (111) to (200) during growth. However, surface energy effects

Table 1
A comparison of the experimental diffraction peaks, crystallite size, lattice parameters of Ti and TiN films deposited at 1 mTorr Ar and 10 mTorr N_2 gas pressures at 200°C on Si(111)

Ti on Si(111)	I/I_0 (%)	(hkl)	Lit. 2θ	Experimental 2θ	Lit. d (nm)	Experimental d (nm)	Crystallite size (nm)	Lit. lattice parameter (nm)	Experimental lattice parameter (nm)
Ti at 200°C (hexagonal)	25	(100)	35.09	35.1	2.555	2.556	28.5	$a = b = 0.295$, $c = 0.468$	$a = b = 0.294$, $c = 0.467$
Ti at 400°C (hexagonal)	25	(100)	35.09	35.12	2.555	2.554	31.5	$a = b = 0.295$, $c = 0.468$	$a = b = 0.293$, $c = 0.465$
Ti at 600°C (hexagonal)	25	(100)	35.09	35.14	2.555	2.552	32.9	$a = b = 0.295$, $c = 0.468$	$a = b = 0.292$, $c = 0.466$
TiN at 200°C (cubic)	100	(100)	42.59	42.55	2.121	2.136	21.4	$a = b = c = 0.424$	$a = b = c = 0.421$
TiN at 400°C (cubic)	100	(100)	42.59	42.52	2.119	2.139	25.2	$a = b = c = 0.424$	$a = b = c = 0.422$
TiN at 600°C (cubic)	100	(100)	42.59	42.51	2.120	2.137	28.7	$a = b = c = 0.424$	$a = b = c = 0.421$

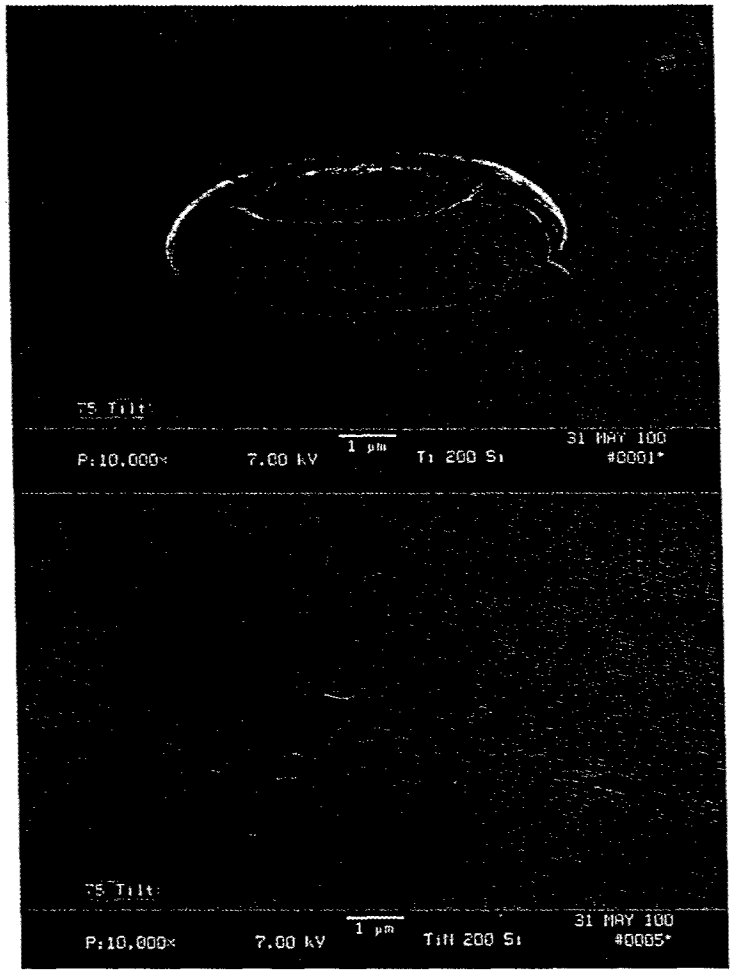

Fig. 3. SEM micrograph of (a) Ti and (b) TiN films on Si(111) at 200°C.

ultimately dominate, leading to a primary (200) orientation at all temperatures. Since the films deposited by Kools et al. [9] were on Si(100), there was no such competition between epitaxy and surface energy. The fact that they observed polycrystalline films with low crystallinity in the 225–450°C range can perhaps be attributed to their use of a lower energy XeCl laser with a pulse energy of 220 mJ, versus 600 mJ for our KrF laser.

In summary, highly textured single phase hexagonal-Ti and cubic-TiN films have been deposited by pulsed laser deposition technique on to Si(111) at substrate temperature of 200°C at 1 mTorr Ar and 10 mTorr N_2 background gas pressures, respectively. The deposited samples exhibited crack free, smooth, continuous and densely-packed grains of the films on Si(111) substrates.

Acknowledgements

The financial support of the Air Force Office of Scientific Research, under grant no. F49620-98-1-0499, is gratefully acknowledged.

References

[1] Y. Chiba, T. Omura, H. Ichimura, J. Mater. Res. 8 (1993) 1109.

[2] P. Engel, G. Schwarz, G.K. Wolf, Surf. Coat. Technol. 98 (1998) 1002.
[3] J.F. Lin, M.H. Lui, J.D. Wu, Wear 194 (1996) 1.
[4] F. Esaka, K. Furuya, H. Shimada, M. Imamura, N. Matsubayashi, H. Sato, A. Nishijima, A. Kawana, H. Ichimura, T. Kikuchi, J. Vac. Sci. Technol. A 15 (1997) 2521.
[5] R.E. Treece, J.S. Horwitz, D.B. Chrisey, Mater. Res. Proc. 327 (1994) 245.
[6] F. Quain, V. Nagabhushanam, R.K. Singh, Appl. Phys. Lett. 63 (1993) 317.
[7] P. Tiwari, T. Zheleva, J. Narayan, Mater. Res. Proc. 285 (1993) 349.
[8] R. Choudhury, R.D. Vispute, K. Jagannadham, J. Narayan, J. Mat. Res. 11 (1996) 1458.
[9] J.C.S. Kools, C.J.C.M. Nilesen, S.H. Brongersma, E. Van De Reit, J. Dieleman, J. Vac. Sci. Technol. A 10 (4) (1992) 1809.
[10] R.E. Treece, J.S. Horwitz, J.H. Claassen, D.B. Chrisey, Appl. Phys. Lett. 65 (1994) 2860.
[11] J.S. Zabinski, A. Voevodin, J. Vac. Sci. Technol. A 16 (1998) 1890, references therein.
[12] H. Ljungcrantz, C. Engstrom, L. Hultman, M. Olsson, X. Chu, M.S. Wong, W.D. Sproul, J. Vac. Sci. Technol. A 16 (1998) 3104.
[13] F. Cerio, J. drewery, E. Huang, G. Reynolds, J. Vac. Sci. Technol. A 16 (1998) 1863.
[14] T. Hara, A. Yamanoue, H. Iio, K. Inoue, G. Washidzu, S. Nakamur, Jpn. J. Appl. Phys. 30 (1991) 1447, and references therein.
[15] J.E. Krzanowski, A.R. Phani, unpublished.

ELSEVIER

Surface and Coatings Technology 148 (2001) 262–267

SURFACE & COATINGS TECHNOLOGY

www.elsevier.com/locate/surfcoat

Chemical vapor deposition of Ti–W–C thin films

Hua Xia Ji[a], Carmela C. Amato-Wierda[b,*]

[a]*2070 Route 52, Building 334, Hopewell Junction, New York, NY 12533, USA*
[b]*Materials Science Program, University of New Hampshire, Durham, NH 03824, UK*

Received 30 April 2001; accepted in revised form 23 June 2001

Abstract

Ti–W–C thin films were deposited on stainless steel substrates (440C) by chemical vapor deposition (CVD) in a horizontal hot-wall reactor from a $TiCl_4$–$W(CO)_6$–CH_4–H_2–Ar gaseous mixture, at 1323 K and at pressures ranging from 0.13 to 20.00 kPa. The structures of the Ti–W–C thin films were characterized using X-ray diffraction (XRD). The lattice constant of the Ti–W–C films shifts from that of TiC to WC_{1-x} with increasing W concentration in the thin films. A morphological analysis was carried out using scanning electron microscopy (SEM). It was found that the surface morphology varied with the W concentration and total flow. Compositional studies and binding characteristics in the Ti–W–C films were investigated by X-ray photoelectron spectroscopy (XPS). The associated hardness measured by nano-indentation ranged from 23 to 32 GPa. The studies of transmission electron microscopy (TEM) and selected area diffraction (SAD) reveal the detailed microstructure of the Ti–W–C thin films and the presence of a WC phase.

Keywords: Hard coatings; Chemical vapor deposition; Ti; WC; $TiCl_4$; $W(CO)_6$; CH_4

1. Introduction

Deposition of metal carbide films on various engineering components has attracted considerable attention in the past [1]. These films, particularly TiC based films, are primarily used for hard coating applications such as wear-resistant layers on high-speed cutting tools. However, TiC begins to oxidize at temperatures as low as 673 K, and its hardness falls quite rapidly with increasing temperature [2]. Tungsten carbide (WC) is also a hard material, and it is very stable at high temperatures [3]. Its hardness and wear resistance are maintained up to 1073 K [4,5].

The formation of novel hard coatings is of increasing interest in industrial applications in order to respond to the increasing demand for high performance materials. Composite films deposited by chemical vapor deposition (CVD) are a potential way to make thin films with a higher hardness and stability against oxidation at higher temperatures [6]. There is evidence that the use of composite films, such as Ti–Al–N and Ti–Si–C films, overcomes the disadvantages of their single phase constituents [7,8]. These composite films also show stability against oxidation up to 1073 K and demonstrate considerably higher hardness than their single-phase counterparts.

One of the significant advantages of the CVD process is that it enables the deposition of conformal coatings. In the work reported here of multi-carbide films, TiC was selected as the main phase in combination with the WC phase. These TiC/WC films are predicted to demonstrate modulus hardening, especially when a nano-structured WC in a TiC matrix is achieved, since the presence of nanostructures in the films would restrict the movement of dislocations, and enhance the hardness of films.

Herein, we describe the use of chemical vapor deposition to deposit Ti–W–C film on stainless steel (440C) substrates at low pressures using the $TiCl_4 + W(CO)_6$ precursor system. Film characterization by X-ray dif-

* Corresponding author. Tel.: +44-603-862-2526; fax: +44-603-862-4278.
E-mail address: ccaw@cisunix.unh.edu (C.C. Amato-Wierda).

0257-8972/01/$ - see front matter
PII: S0257-8972(01)01342-1

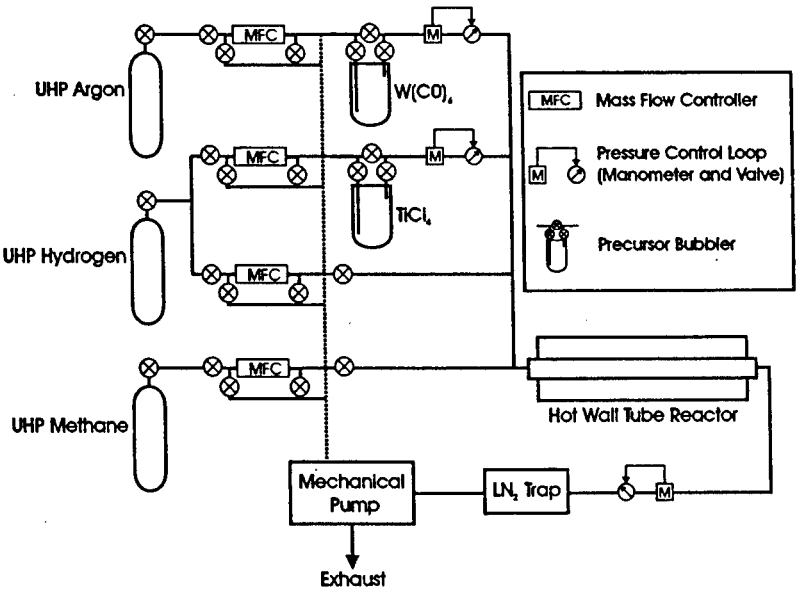

Fig. 1. Schematic representation of the tubular hot wall reactor.

fraction, X-ray photoelectron spectroscopy, nano-indentation, scanning and transmission electron microscopies are also presented.

2. Experimental

Ti–W–C films were produced by thermal CVD on stainless steel (440C) substrates. Fig. 1 is a schematic of the hot-wall CVD system used in the experiments. The hot wall reactor consists of a quartz tube inside a three-zone resistively heated furnace with a 1773-K maximum operating temperature. The reactor is connected to a gas inlet and exhaust system. Mass flow controllers delivered the reagent gases and precursors. The exhaust end was connected to a pressure control valve, followed by a liquid nitrogen trap and a mechanical pump. Titanium tetrachloride ($TiCl_4$) and tungsten hexacarbonyl [$W(CO)_6$] were contained in bubblers. The vaporized $TiCl_4$ and $W(CO)_6$ are transported to the reactor by H_2 and Ar carrier gases, respectively. Vapor pressures of liquid $TiCl_4$ and solid $W(CO)_6$ were determined by Eqs. (1) and (2):

$$\log P_{TiCl_4} = 6.8074 - (1964/T) \quad (1)$$

$$\log P_{W(CO)_6} = 10.65 - (3872/T) \quad (2)$$

where P_{TiCl_4} and $P_{W(CO)_6}$ are the vapor pressure in kPa, and T is the bubbler temperature in Kelvin [9,10]. The mass flow rates of $TiCl_4$ and $W(CO)_6$ are then calculated according to Eq. (3):

$$m = m_{carrier}[P/(P_t - P)] \quad (3)$$

where m is the mass flow of $TiCl_4$ or $W(CO)_6$ in units of standard cubic centimeter per minute (sccm), $m_{carrier}$ is the mass flow of the carrier gas (sccm), P is the vapor pressure of $TiCl_4$ or $W(CO)_6$ and P_t is the total pressure above the bubbler.

The liquid precursor $TiCl_4$ (99.8%, Strem) was handled in a dry nitrogen glove box and used as received. The $TiCl_4$ was maintained at 338 K by submerging the bubbler in a constant temperature oil bath. $W(CO)_6$ (97%, Aldrich) is an air stable solid placed in a precursor bubbler kept at 373–383 K by an oil bath. The $TiCl_4$ flow rates were between 3 and 15 sccm, and $W(CO)_6$ flow rates were between 10 and 100 sccm. Hydrogen was also used as diluent gas in order to promote the decomposition of $TiCl_4$ and $W(CO)_6$. Ti–W–C films were deposited on polished stainless steel (440C) substrate at 1323 K. The total gas flow ranged from 240 to 650 sccm.

The thickness of the deposits was determined by ball abrasion through the film, obtained by dimpling with an abrasive agent (diamond, 3 μm). The thickness values were calculated from the diameters of the ring prints measured by optical microscopy. The deposition rate was obtained by the thickness divided by the deposition time. A Rigaku Geigerflex D-Max-B X-ray diffractometer was used to characterize phase formation in the films. The composition of the films was determined by X-ray photoelectron spectroscopy (XPS) on a Kratos Analytical Axis HS system. The surface morphologies of the film were observed with scanning electron microscopy (SEM, Amray 3300FE). The sample preparation for transmission electron microscopy (TEM, Hitachi H600) was completed by using a dimpling device, followed by ion milling with argon ions at an incident angle of 11°. The hardness of the films was obtained by nano-indentation (Hysitron TriboScope Nanomechanical Test System) at loads from 4000 to 8000 μN.

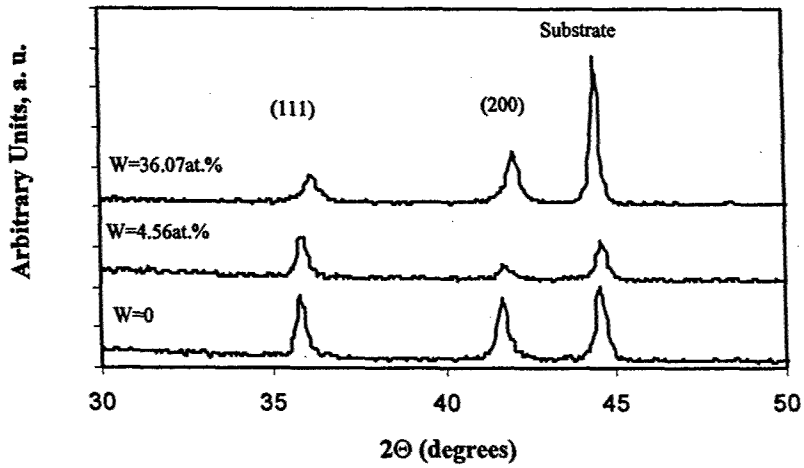

Fig. 4. Typical XRD spectra of Ti–WC films formed at 1323 K with low and high W concentrations showing the shift of (111) and (200) reflections.

parameters of the films possibly indicates the formation of WC_{1-x} phase due to the W concentration. Both TiC and WC_{1-x} have the NaCl (fcc) structure and their lattice parameters are 0.4327 and 0.4235 nm, respectively. The lattice parameters obtained from the Ti–W–C films demonstrate a slight shift from TiC to the WC_{1-x} lattice parameter with increasing the W concentration in the films.

Fig. 5 shows four typical SEM micrographs of the Ti–W–C films formed at 1323 K with different W concentrations. They reveal different surface morphologies associated with the different W concentrations. Fig. 5a shows the surface morphology of TiC films deposited at 1273 K at low pressure with no W. The faceted nodular growth of TiC films is observed. In contrast, three other types of surface morphologies for the films with W are observed: (b) faceted; (c) equiaxed; and (d) rounded particles. The faceted particles are formed as a main feature for the films with low W concentration (<3.5 at.% W). As the W concentration is increased in the films, equiaxed particles are formed and then gradually change to rounded particles.

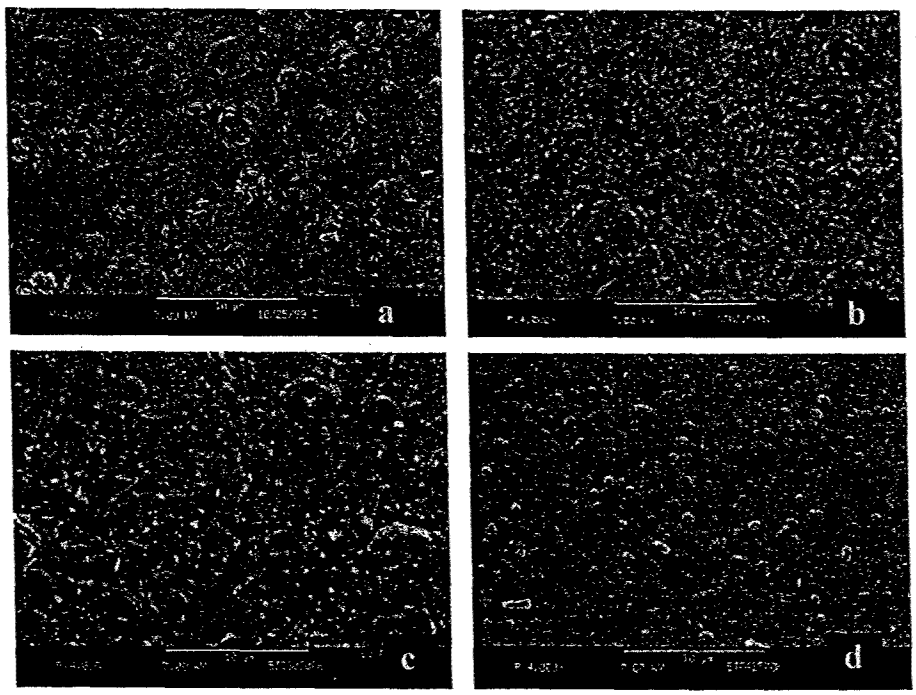

Fig. 5. SEM micrographs of Ti–W–C films formed at 1323 K showing surface morphologies as a function of W concentration (a) TiC films with 0 at.% W, (b) 3 at.% W, (c) 4 at.% W and (d) 20 at.% W.

lower residence times. The surface morphology depends on the W at.% and the total flow. The presence of a WC phase is indicated in films with higher W contents. According to preliminary results, the hardness of the Ti–W–C films ranges from 28 to 32 GPa with increasing W up to 10 at.%.

Acknowledgements

The financial support of the Air Force Office of Scientific Research, under grant no. F49620-98-1-0499, is gratefully acknowledged.

References

[1] J.E. Sundgren, H.T.G. Hentzell, J. Vac. Sci. Technol. A 4 (1986) 2259.
[2] W.-D. Munz, J. Vac. Sci. Technol. A 4 (1986) 2717.
[3] I.N. Mihailescu, E. Gyorgy, G. Marin et al., J. Vac. Sci. Technol. A 17 (1999) 249.
[4] G. Zambrano, P. Prieto, F. Perez et al., Surf. Coat. Technol. 108/109 (1998) 323.
[5] C.-W. Won, B.-S. Chun, H.Y. Sohn, J. Mater. Res. 8 (1993) 2702.
[6] S. Veprek, S. Reiprich, Thin Solid Films 268 (1995) 64.
[7] W.-D. Munz, J. Vac. Sci. Technol. 4 (1986) 2717.
[8] M. Touanen, F. Teyssandier, M. Ducarrior, M. Maline, J. Am. Ceram. Soc. 76 (1993) 1473.
[9] G. Luchinski, Russ. J. P. Chem. 40 (1966) 318.
[10] M.L. Garner, D. Chandra, J. Phase Equilibria 16 (1995) 24.
[11] H.O. Pierson, High Temp. Mater. Process 11 (1993) 239.
[12] D. Gogova, K. Gesheva, A. Veneva, Mater. Lett. 35 (1998) 351.
[13] Y. Pauleau, Ph. Gouy-Pailler, J. Mater. Res. 7 (1992) 2070.
[14] N. Chitica et al., Thin Solid Films 103 (1997) 71.
[15] E.K. Stroms, The Refractory Carbides, Academic Press, New York, 1967.
[16] B.M. Kramer, P.K. Judd, J. Vac. Sci. Technol. A 3 (1985) 2439.